UCRL-53179-82
Distribution Category UC-20,20D

UCRL--53179-82

DE84 001683

Fire-Protection Research for DOE Facilities: FY 82 Year-End Report

H. K. Hasegawa, N. J. Alvares,

A. E. Lipska-Quinn, D. G. Beason,

S. J. Priante, and K. L. Foote

Manuscript date: September 2, 1983

LAWRENCE LIVERMORE LABORATORY
University of California • Livermore, California • 94550

Available from: National Technical Information Service • U.S. Department of Commerce
5285 Port Royal Road • Springfield, VA 22161 • $10.00 per copy • (Microfiche $4.50)

Contents

Fire Protection Research for DOE Facilities: FY 82 Year-End Report

Abstract

We summarize our research in FY 82 for the DOE-sponsored project, *Fire Protection Research for DOE Facilities*. This research program was initiated in 1977 to advance fire-protection strategies for energy technology facilities to keep abreast of the unique fire problems that develop along with energy technology research. Since 1977, the program has broadened its original scope, as reflected in previous year-end reports. We are developing an analytical methodology through detailed study of fusion energy experiments at Lawrence Livermore National Laboratory (LLNL). Using these experiments as models for methodology development, we are concurrently advancing three major task areas: (1) the identification of fire hazards unique to current fusion energy facilities; (2) the evaluation of accepted fire-management measures to meet and negate hazards; and (3) the performance of unique research into problem areas we have identified to provide input into analytical fire-growth and damage-assessment models.

Introduction

We report our work performed in FY 82 for a DOE-supported study entitled *Fire Protection Research for DOE Facilities*. Previous fiscal-year reports have been published.[1-3] Note that the program title of this report has changed to a more general subject of DOE facilities. This reflects broadened programmatic goals that have evolved since 1977. We feel the logic and analytical methodologies developed for fusion facilities can be applied to a range of emerging and established energy technologies. One ultimate goal of this study is the assessment of potential fire damage in such facilities. To accomplish this, three parameters have to be evaluated: (1) fire-threat potential to the facility, (2) response and effectiveness of fire-management systems, and (3) possible fire-related damage.

The milestone chart in Fig. 1 delineates the sub-tasks (marked by bullets) which must be completed to achieve our major goals (underlined) for this program. These major goals are all necessary to the ultimate objective: a standard guide of fire-management tactics for large DOE facilities. It is appropriate here to describe the logic and significance of each milestone as to its contribution to the final result. The sub-tasks listed under *Fire Growth Parameters for Model Development* are a combination of small- and large-scale fire experiments to provide appropriate data input for our modeling efforts and is also a partial model-validation tool. Those sub-tasks supporting *Smoke Aerosol Production and Transport; Physical and Chemical Characteristics* will help define two major phenomena: (1) the potential corrosive and particulate damage to experimental components, and (2) the particulate analysis (size, distribution, etc.) that will provide insight into the response times of smoke detection systems.

The next two milestones listed in Fig. 1 (*Adaptation of Modeling Technique for Fire-Risk Assessment* and *Advanced Fire Management System Development*) integrate all results from the previous two milestones and are probably the most significant components to the program. They combine all the facets of what has been learned that can be applied to real facilities. The modeling technique will predict the rate and extent of fire development in these facilities and the work on fire-management systems will define how detection and suppression response to predicted fires will modify the degree of fire damage. The *Advanced Fire Management System Development* phase will concentrate on unique detection and suppression systems to deal with fire problems in DOE

PROJECT 6294-93 FIRE PROTECTION RESEARCH
FOR ENERGY TECHNOLOGY PROJECTS

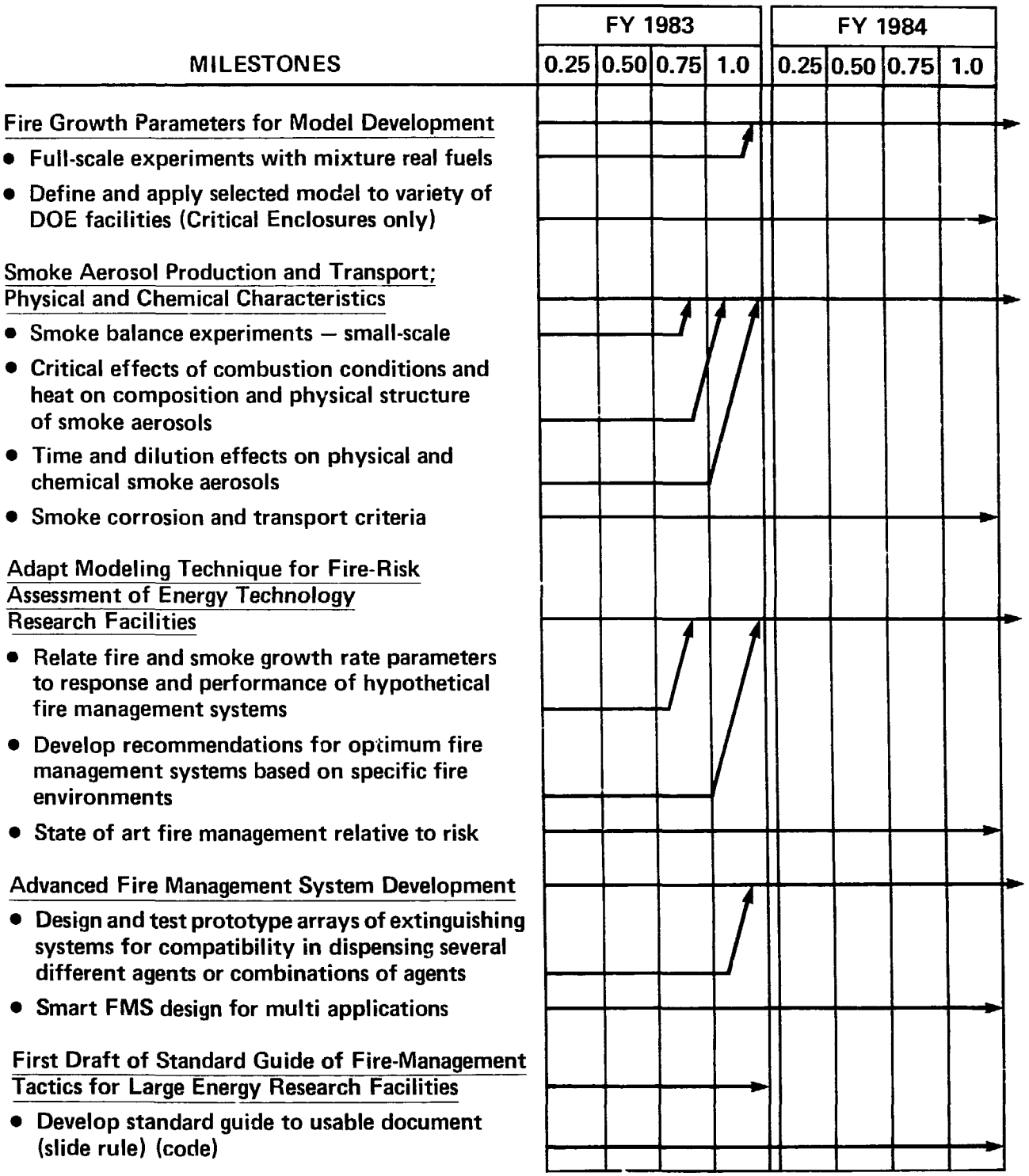

Figure 1. Descriptive chart of project milestones for LLNL fire-protection research for DOE facilities.

facilities that traditional countermeasures cannot negate.

In FY 82, we made significant progress in a variety of task areas. In general, we reduced data from our model-validation experiments to a form that could be applied to the Zukoski (or Cal Tech) model[4] so that our results could be accurately compared to data and results obtained from other fire models. Furthermore, we simplified the Cal Tech model to a closed-form integral, allowing faster and easier testing of the model. We were able to perform 27 model-validation experiments with a variety of closely defined fuels.

We performed a number of small-scale cable insulation experiments in the LLNL ease-of-ignition apparatus. The results from this test series has led us to a research plan that will enable us to predict a cable type's relative time to ignition without having to fire-test it. At the other end of the spectrum, we also completed six large-scale vertical cable burns. We are gaining more insight into the effect of packing densities and configurations from these results. We have instigated a protocol to define these effects.

In the area of chemical characteristics of smoke aerosol, we determined the corrosive and noncorrosive chemicals produced during the main degradation phase of a large number of commercial plastic insulations and their virgin counterparts. Also, we studied the effect of the heating rate in air at the onset of initial decomposition of the various insulations.

Finally, we applied the protocol for fire-loss assessment to a major magnetic-fusion experiment here at LLNL.

Large-Scale Cable Burns

As described in previous reports, the major proportion of available flammable materials in energy research facilities are jacket and insulations for electrical conductors in control, power, and diagnostic circuits.[2,3] Although a close similarity exists between nuclear power plants and energy research facilities, there is a major difference in cable specifications and the manner in which cable runs are distributed throughout the plant. Specifically, the majority of wiring in nuclear fission plants must meet the IEEE 383 standard for flammability[5]; the wiring is normally laid in cable trays according to a regulated protocol. In contrast, because energy research facilities are one-of-a-kind prototypes and are constantly changing their configurations, they must be flexible and much less rigorously structured, and this results in complicated and unconfined cable runs. Furthermore, the extremely high-power-carrying capacities required of these cables make specifications such as dielectric strength, flexibility, solvent resistance, etc. appear more important than fire resistance. Early in the project, we conducted literature searches and surveyed institutions performing cable fire research in the hope that others would be able to provide us with the fire data we needed. Unfortunately, as shown in Table 1, 99% of the work was specifically applied to the cable-tray problems of nuclear power plants. With the exception of generic material properties, the results from these studies could not be accurately extrapolated to energy facility problems.

Consequently, we initiated a cable-test program which began with small-scale experiments (ease-of-ignition, heat-release-rate calorimeter, TGA, etc.) that eventually provided input to our current series of large-scale vertical cable burns. We conducted large-scale experiments to obtain realistic fire data to account for as many variables as possible. These data will provide input to our fire-modeling efforts, and, hopefully, provide some correlation to small-scale tests. Ultimately, experimental results will aid in the specification of fire-safe cable materials for present and future DOE facilities.

Large-Scale Vertical Cable Experiments

We conducted large-scale fire experiments to define the effect of cable size, composition, number and packing density on the vertical flamespread rate, and, consequently, the mass-burning rate. However, many more parameters of interest can be measured on this scale, e.g., time of ignition; mass-loss rate; extent of flamespread; mass balance (quantity of smoke in proportion to mass-burning rate); combustion gas composition and rate of acid ion generation; oxygen consumption, and carbon monoxide, carbon dioxide, and hydrocarbon production; heat-release rate via oxygen depletion or carbon dioxide production.

These data can be compared to results from small-scale tests to assess their correspondence to

Table 1. Partial listing of organizations doing fire research on cables.

Sandia National Laboratories (SNL), Albuquerque [under contract to the Nuclear Regulatory Commission (NRC)] is evaluating cable-tray fires in nuclear power plants.

Sandia is looking specifically at –

1. Cable separation distances
2. Tray-to-tray fire spread
3. Rated and non-rated cables
4. Fire-resistant coatings and blanket protection
5. Active fire-suppression effectiveness of sprinklers, Halon 1301, and carbon dioxide
6. Fire modeling and network analysis

(Sandia also subcontracted work to University of California, Berkeley for cable-penetration experiments and to United Laboratories for vertical cable-tray fires.)

Factory Mutual Research Corporation (FMRC) [under contract to the Electric Power Research Institute (EPRI)] is evaluating cable-tray fires in nuclear power plants.

FMRC is looking specifically at –

1. Assessment of fire hazards to cable trays
2. Intermediate-scale fire tests of cable trays
3. Extinguishment and detection of cable-tray fires
4. Damage potential to cables in simulated fire environments
5. Small-, intermediate-, and large-scale test correlations by Tewarson of FMRC (We derived our HRR values from his small-scale tests. However, his threshold ignition values from small-scale tests of 20 kW/m^2 appears very low – the LLNL minimum ignition flux is at 50 kW/m^2.)

Bell Telephone of Canada and the *National Research Council of Canada* are doing general fire research on cables, particularly on telephone cable.

realistic conditions. Moreover, we can obtain specific fuel performance and enclosure fire parameters, e.g., the temperature profile through the fuel-array cross section and along the vertical surface, the temperature distribution throughout the test cell, and the enclosure ventilation changes resulting from the heat-release rate.

Figure 2 shows the experimental support structure for the vertical-cable runs. The bundle of electrical conductors is suspended from a steel cable threaded over two bicycle wheels (to decrease friction) and attached to a counterbalanced load cell. Adjacent to the specimen is a vertical, calibrated panel for visually observing the flame-spread and glass sampling ports for combustion-gas collection at mid-height and at the top of the specimen. Calorimeters and radiometers are located at the ignition source, near the specimen bottom, and at mid-height. Similarly, chromel-alumel thermocouples are located at strategic points on the apparatus and throughout the test cell. To monitor the melting insulation that might drip from a burning cable, a load cell is placed directly under the specimen centerline. Since these droplets are generally aflame, the load cell also supports a drip pan partially filled with water. This weighing of cable melt is necessary to estimate mass balance and fuel-consumption rates.

Ignition Source

To provide an ignition source of finite dimension producing specified heat-flux levels, we constructed a premixed natural gas and air burner with gravel as a diffusion medium. This burner, with a 30-cm o.d., produced a calibrated exposure flux of 5 W/cm^2 at an energy release rate of 20 kW. A heat flux of 5 W/cm^2 or greater was identified as a threshold ignition energy from heat-release-rate experiments conducted at SRI, International.[2]

Test Specimen

The test specimens for this experimental series were two-layer cable bundles formed into a perpendicular "Z" configuration as shown in Fig. 3. The vertical cable length was 1.8 m. To prevent undefined heat-loss effects on cable-burning

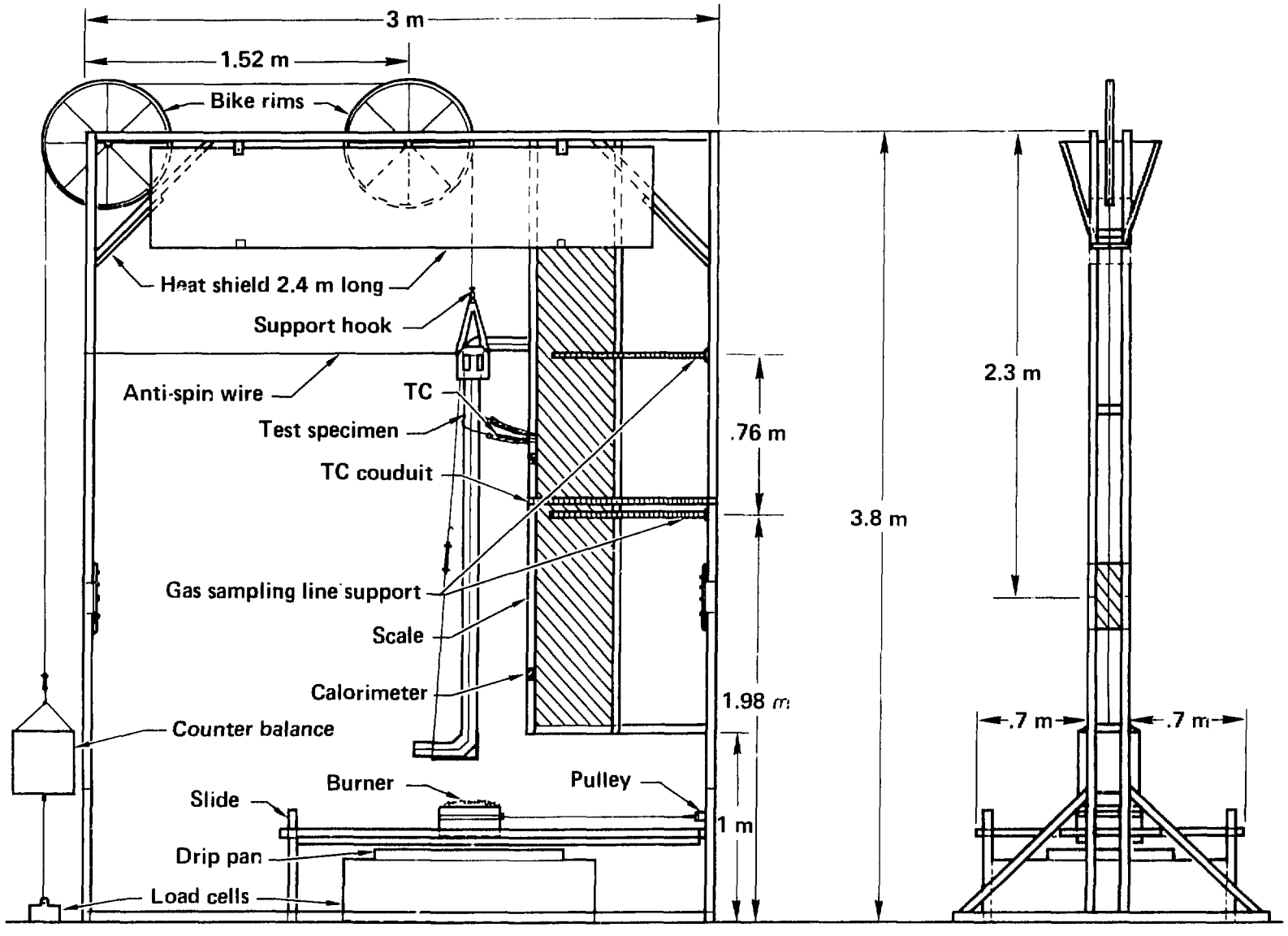

Figure 2. Experimental support structure for vertical cable burn (VCAB) experiments.

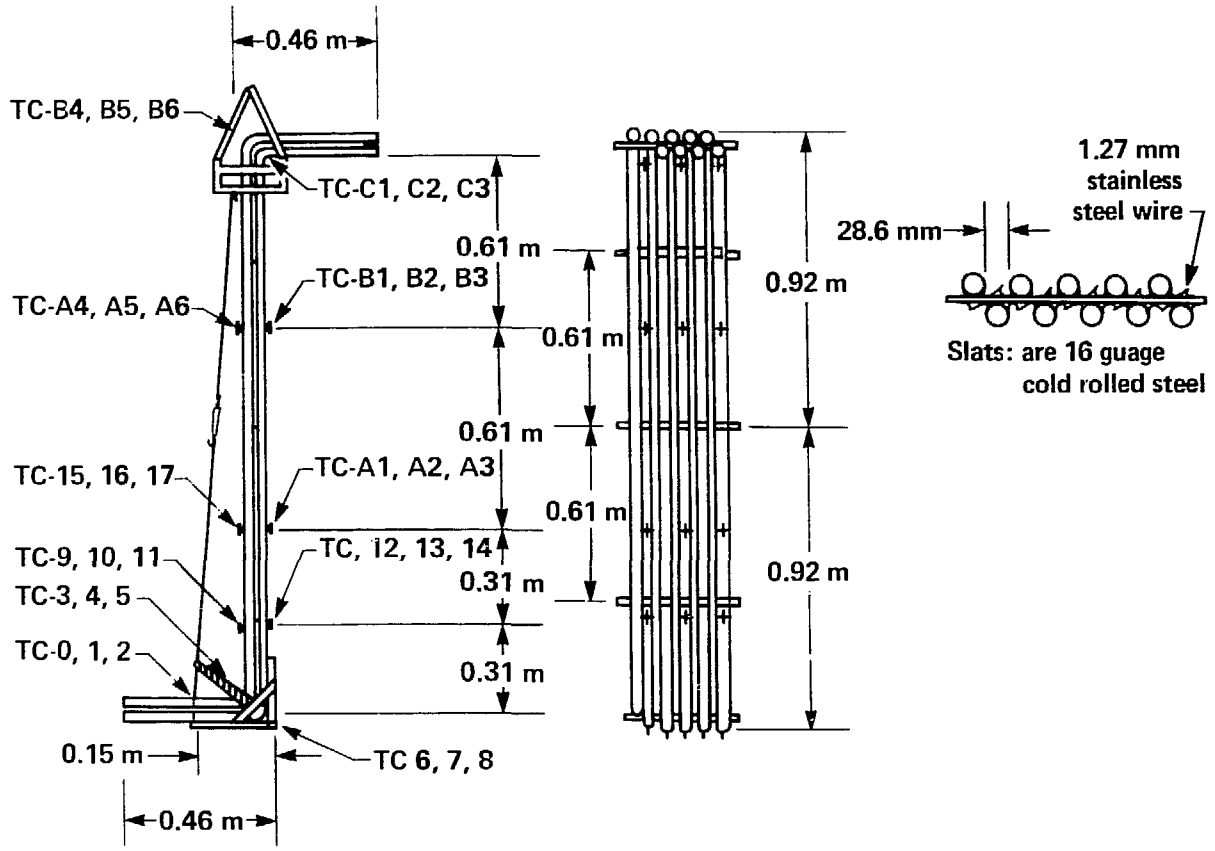

Figure 3. Thermocouple (TC) locations for vertical cable burns.

characteristics, we designed and fabricated special low-mass hardware to hold the cables. The vertical configuration was chosen to maximize the rate of flamespread and simulate a worst-case situation. To supplement our visual observations of fire growth, we attached thermocouples in a vertical array at approximately 0.4-m intervals on both faces of the specimens as well as between the two layers of cables.

We performed six experiments, designated VCAB-1 through VCAB-6, in the LLNL Fire Test Cell, which is a negative-pressure ventilation enclosure with a 4.7-m ceiling height and a total volume of 100 m^3. Table 2 lists the cable types we tested and Table 3 shows pertinent physical data for the six tests. Figure 4 is a photo of the test setup. Figures 5 and 6 document VCAB-5 during and after the experiment. The planned ventilation rate for the experimental series of 500 l/s was achieved in all tests except VCAB-1. Its ventilation rate is unknown due to an inadvertent closing of an exhaust damper.

Table 2 illustrates the variation in composition for the six cable experiments. An important variable is the percentage of conductor to jacket and insulation material. As in the small-scale ease-of-ignition tests, we must be able to identify (as well as possible) the individual effects of cable size, packing geometry, composition, and materials. Note both the Hypalon and Neoprene welding cables are about 80% stranded copper conductor. On the other hand, the PVC coaxial is 51% insulation and 49% conductor. The difference is the polyethylene insulation that accounts for 32% of the total weight. Once a comparison of these characteristics is made, we can begin to look at the results in Table 3 with a little more insight.

Experimental Notes

The first three experiments (VCAB-1 through -3) were "shake down" tests to evaluate the apparatus. From our observations and results, we established the following quasi-formal test protocol, which we will discuss point by point.

Table 2. Summary of the physical characteristics of cable types tested to date.

VCAB	Jacket mat'l (% wt.)	Insulation (% wt.)	Conductor (% wt.)	Cable o.d. (mm)	Total wt. (kg/m)	% Pack
1 & 2	Hypalon (16.2)	none	copper (83.8)	19.1	1.15	100
3	Neoprene (23.5)	none	copper (76.5)	19.1	1.29	100
4	PVC (18.9)	polyethylene (32.1)	copper (49.0)	25.5	1.12	100
5	PVC (18.9)	polyethylene (32.1)	copper (49.0)	25.5	1.12	50
6	PVC (18.9)	polyethylene (32.1)	copper (49.0)	25.5	1.12	25

Table 3. Summary of cable-fire results.

VCAB	Burner off (min:s)	Time to ignition (min:s)	Total flamespread (m)	Flamespread rate (m/s)	Avg. HRR[a] (kW)	Peak HRR (kW)	Time of HRR peak (min:s)	Test duration (min:s)
1	21:30	17:00	1.82	0.10	80.0	–	–	23:30
2	20:00	15:30	1.82+	0.36	79.9	350	27:05	31:30
3	35:45	23:15	1.82	0.10	25.9	50	33:20	49:15
4	25:25	23:25	0.91	0.09	12.8	15[b]		35:06
5	12:00	10:10	1.82	0.18	182.5	550	20:00	25:00
6	24:25	no	0.76	0.09	24.5	95	30:50	40:00

[a] HRR = Heat-release rate.

[b] VCAB-4 averaged 15 kW during experiment.

(1) In an attempt to evaluate the effects of decreasing the overall mass and increasing the cable spacing, we conducted tests on three separate cable bundles for each cable type, as shown in Fig. 7. The first specimen was normally a full cable run (100% pack) that averaged 20 cables in 2 layers, with a net vertical run of 1.8 m. The second specimen contained half this number (50% pack), which allowed for a 1-cable diameter space between each cable. The third specimen contained half of this number, or approximately 5 cables (25% pack), in a single layer.

(2) In addition to developing a packing protocol, we also modified the attachment of thermocouples on the cable bundle in tests VCAB-4 through -6 from surface mounting to imbedding the thermocouple 1.5–2.0 mm into the jacket insulation. Monitoring the actual jacket temperature is a more appropriate measurement, and it allows us to detect ignition at that point, which aids in both defining a threshold-ignition temperature and the rate and extent of flamespread as well. The flamespread to an imbedded thermocouple's location is confirmed when it registers a temperature between 75°C and 80°C. This technique for determining the flamespread rate has proven to be fairly consistent and is a more positive one than simple visual observation, which really does not accurately distinguish between actual flame attachment and flame extension "lapping." Figure 8 is a composite plot of the cable thermocouples located on the vertical run with their vertical locations noted where they cross the "75°C" line. The time at which a plot crosses the straight line drawn at approximately 75°C is the elapsed time to flame travel to this point. (Another important note is that the 20 kW ignition source is not removed for several minutes *after* visual cable ignition has been observed.)

(3) We attempted to calculate the heat-release rate of these experiments using both mass-loss rate and oxygen-depletion rate, but due to the high ventilation rate (500 l/s) and sparse cable burning, only two experiments depleted measurable quantities of oxygen. Consequently, the majority of heat-release-rate values for the various

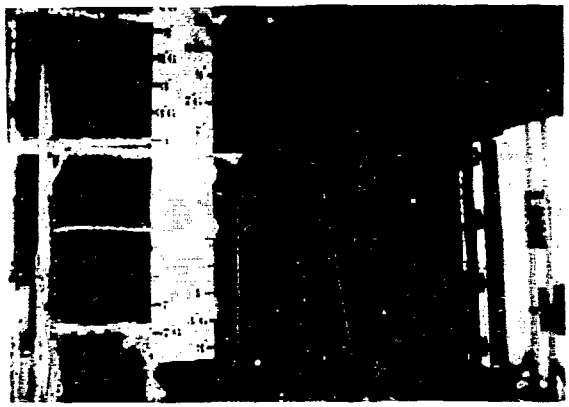

Figure 4. VCAB setup in LLNL Fire Test Cell.

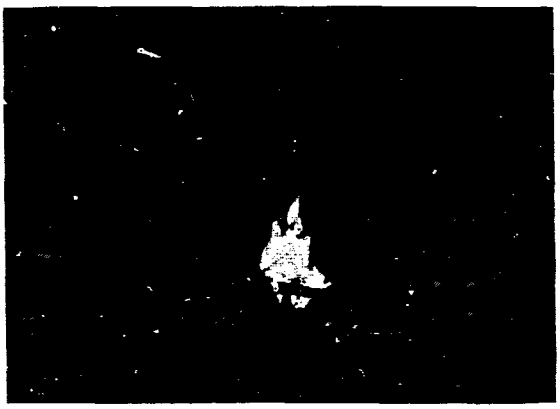

Figure 5. VCAB-5 during experiment.

experiments were derived from the mass-loss rate. Because many of the cable types are composed of several different polymeric materials, we had to use an average value for heat of combustion of the composite. For this reason, the oxygen depletion would be far more accurate and desirable.

Results

Experiments VCAB-1 and VCAB-2 (Hypalon jacket) were intended to be identical "shake down" tests. However, as mentioned previously, the ventilation rate in VCAB-1 was greatly reduced due to an inadvertant closing of the exhaust damper. Yet, studying the results listed in Table 3, this reduced airflow appeared to affect only the flamespread rate and the time-to-onset of mass loss. Referring to the latter, the rate of mass loss was essentially the same for both burns; however, VCAB-1 began losing weight 250 s later than VCAB-2. Similarly, VCAB-2 had a flamespread rate three times that of VCAB-1. All other parameters seem to be very close, indicating reproducibility.

A comparison of VCAB-1 and VCAB-2 to the Neoprene-jacketed welding cable test (VCAB-3) shows the effect different jacket materials have on cable fire performance. In this case, it is primarily a function of the material because all other variables, such as cable size, ratio of insulator to conductor, etc., were nearly identical. Table 3 shows

Figure 6. **VCAB-5 at end of test burn.**

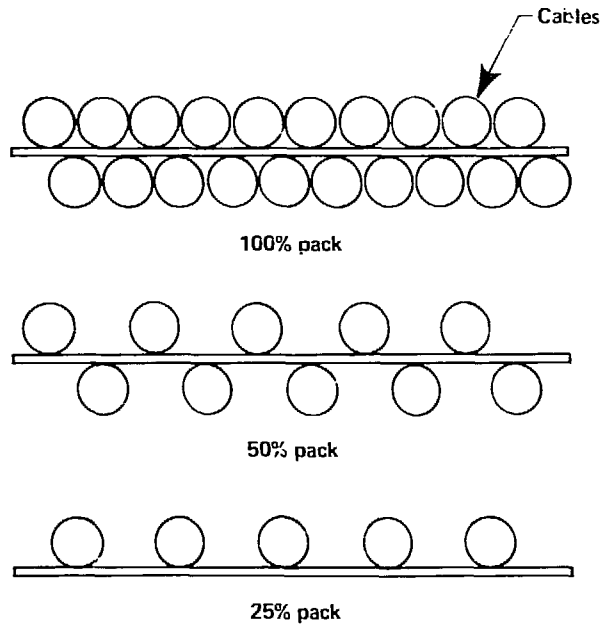

Figure 7. End view of test cable bundles showing different packing densities.

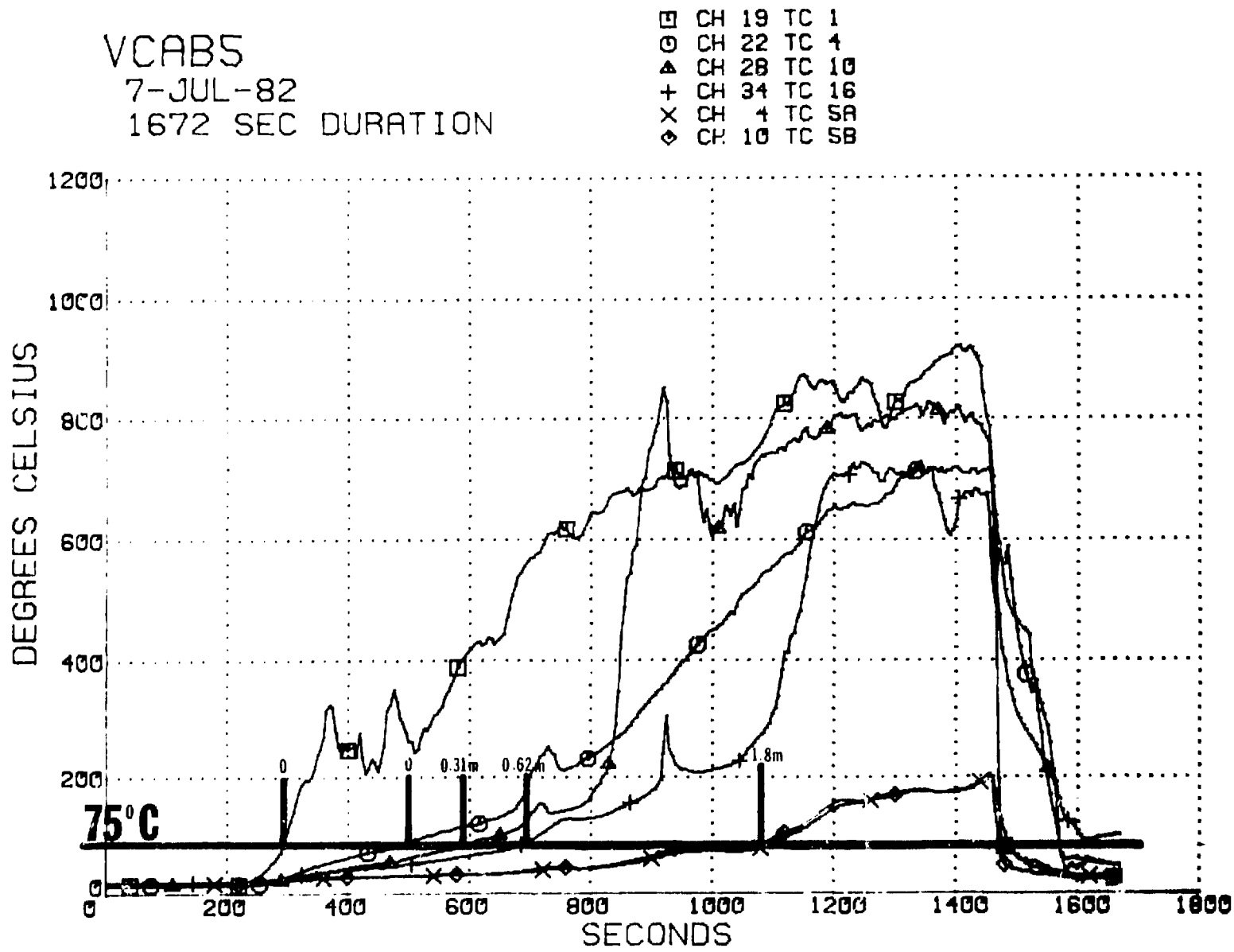

Figure 8. VCAB-5 composite plot.

that the time-to-ignition, as well as the elapsed time-to-burner removal, is noticeably greater for Neoprene. Furthermore, Neoprene exhibited one-third the flamespread rate of Hypalon. In terms of heat-release rate, Fig. 9 illustrates that Hypalon produces a much more severe fire. With the exception of VCAB-5, which will be discussed later, all other cable experiments produced heat-release rates of 50 kW or less as compared to a maximum of 200 kW for Hypalon. A preliminary conclusion from this limited data would be that the Neoprene cable required a higher ignition energy, and, once ignited, it produced a much slower rate of flamespread and heat release.

As shown in Table 3, VCAB-4 through -6 of the PVC-jacketed power cable with polyethylene insulation inaugurated the packing protocol described earlier for each cable type. Our results indicate that the 50%-packed vertical run produced the worst fire. The burner was shut off in approximately half the time as VCAB-4 and -6, which means that ignition occurred relatively quickly. Similarly, the rate of flamespread is twice that of the others and the heat-release rate is an order of magnitude greater. Comparing the PVC 100% pack test to the Neoprene (VCAB-3) and Hypalon (VCAB-2), we see that the PVC 100% pack is lowest in total flamespread, heat-release rate, and flamespread rate. However, comparing the 100% pack Neoprene and Hypalon to the 50% pack PVC, the 50% PVC is the highest in all of the above categories, which gives some credence to varying the number and spacing of cables in the vertical array. We will continue to use our protocol in future experiments, as well as evaluate the effect of varying the ignition source strength, airflow, cable composition (i.e., multiconductor vs solid copper, etc.), and cable diameter.

Finally, Figs. 10(a) and 10(b) compare the difference in heat-release rates between VCAB-2 and VCAB-5 using mass-loss rate vs oxygen depletion. In both cases, the curves show greater and greater dispersion as the intensity of the fires increase with time. This pronounced spread in the latter stages reflects the averaging of calorific values of heterogeneous materials and the uncertainty of actual polymer formulations, which makes the oxygen-depletion technique more accurate and desirable.

Observations from Vertical Cable Burn Experiments

Under the conditions of this experimental series, we can make the following preliminary observations:

- When exposed to the 20 kW ignition source, the majority of cable types were very difficult to ignite.
- Once ignited, the flamespread rate was very slow.
- Similarly, heat-release rates remained low and were slow to peak.
- Fire performance* was due primarily to the power-cable diameter (1.25 cm to 2.54 cm) and large percentage of conductor, and the packing density [100% = too dense, 50% = optimal (most severe fire), and 25% = too sparse].

* Based on only one test series.

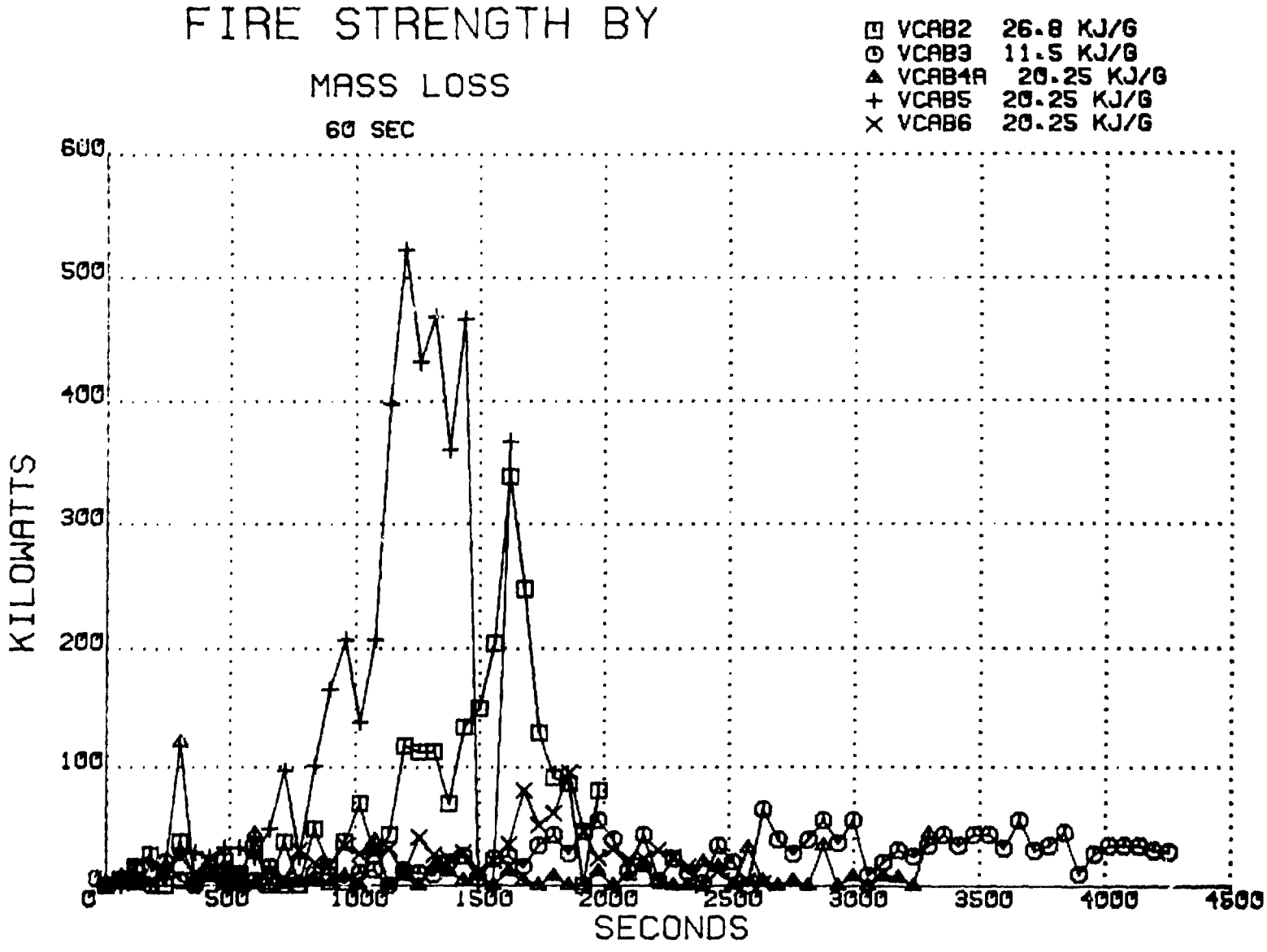

Figure 9. Heat-release rate graph of all VCABs.

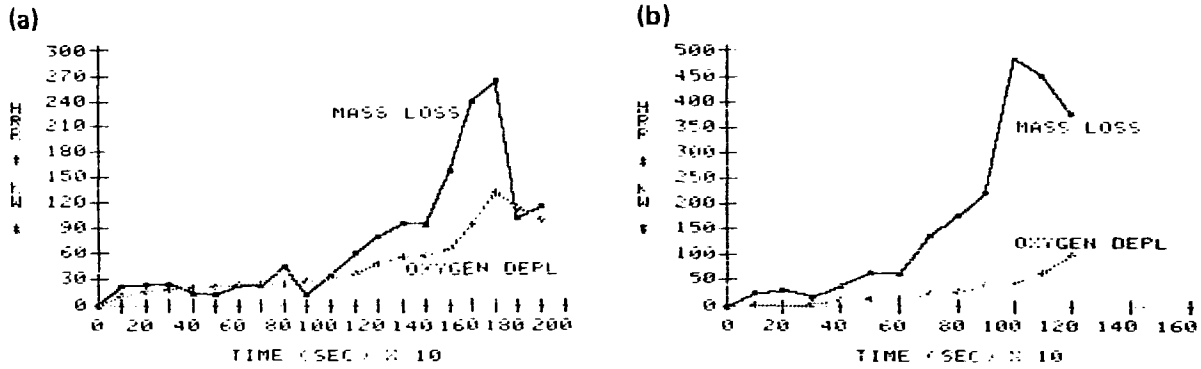

Figure 10. Comparison of heat-release rates of (a) VCAB-2 (Hypalon) and (b) VCAB-5 (PVC) using mass loss vs oxygen depletion.

Small-Scale Cable Tests in the LLNL Ease-of-Ignition Apparatus

In FY 82, we were able to reactivate our ease-of-ignition apparatus to perform experiments on approximately 22 cable samples which were identified in FY 81 as representative types from LLNL stock. As mentioned in the FY 80 report, we are using the FY 80 performance standard as a research tool to obtain relative ignition rankings for electrical cable insulations. This ranking, in turn, provides a screening tool for large-scale cable fire tests.

Summary of Test Method

Figures 11 through 13 show the test apparatus and related instrumentation. Due to other experimental efforts, we were only able to include the thermopile, water-temperature thermocouple, and photodiode for this series (as opposed to the variety of monitors used in the previous series). Two parallel vertical specimens, 140 mm wide and 152 mm high, face each other at a distance of 53 mm apart. The facing surfaces of both specimens are exposed to a methane diffusion flame supplied from a multiported burner located below the lower edge of the specimens. The reason for having two specimens facing each other was to simulate the reinforcement that would occur in a worst-case fire situation.

The time to ignition is indicated both by the time at which a flame attachment on a specimen surface is observed and by the time when the specimens begin to contribute a significant quantity of fuel, as indicated by a rise in the voltage of a thermopile, which consists of a bank of thermocouples located 6.4 mm above the top edge of each specimen and 6.4 mm out from the plane of their surfaces.

Significance

This method, as a standard, is intended to evaluate the relative ignitability of materials that form part of the exposed wall and ceiling surfaces of a room, including the vertical surfaces of furniture, by determining the times to ignition when test materials are exposed to an extended-area flame source simulating the flame from a burning chair, waste basket, etc. The materials must be tested in the thicknesses at which they are intended to be used, unless it can be demonstrated that the time to ignition is independent of the thickness range being tested. However, we are using this concept with a different emphasis: because the above ignition scenario is a severe one, we are using this standard exposure to determine relative ease of ignition of a broad spectrum of cable types and materials. Results from this method will help prevent unnecessary and costly large-scale fire testing.

Test Specimens

Eight rectangular cable specimens of each type of cable 140 mm wide and 152 mm high were tested in a specially designed specimen holder. Two specimens were required for each test, and four replicate tests were conducted. The specimen

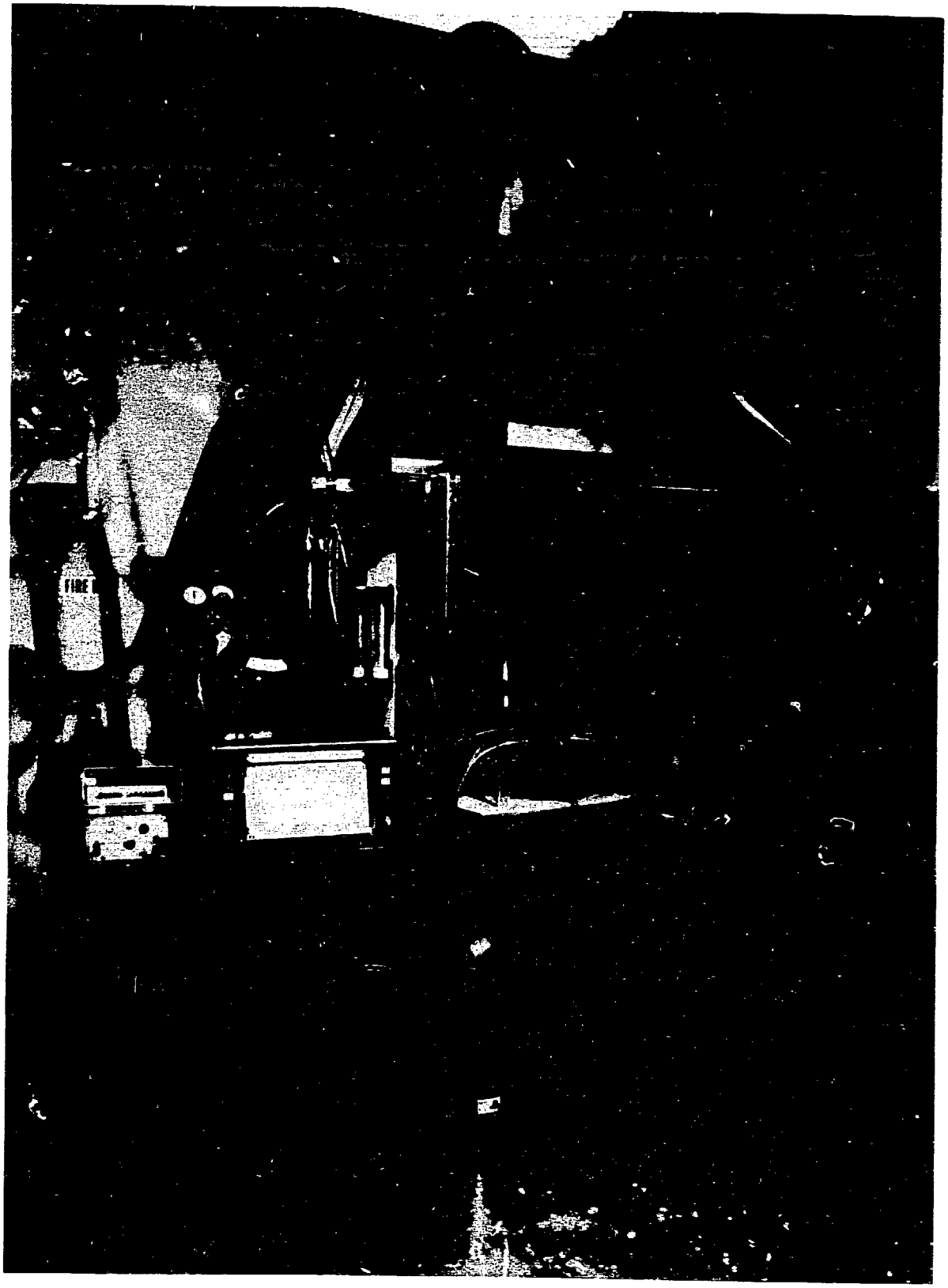

Figure 11. Ease-of-ignition test apparatus.

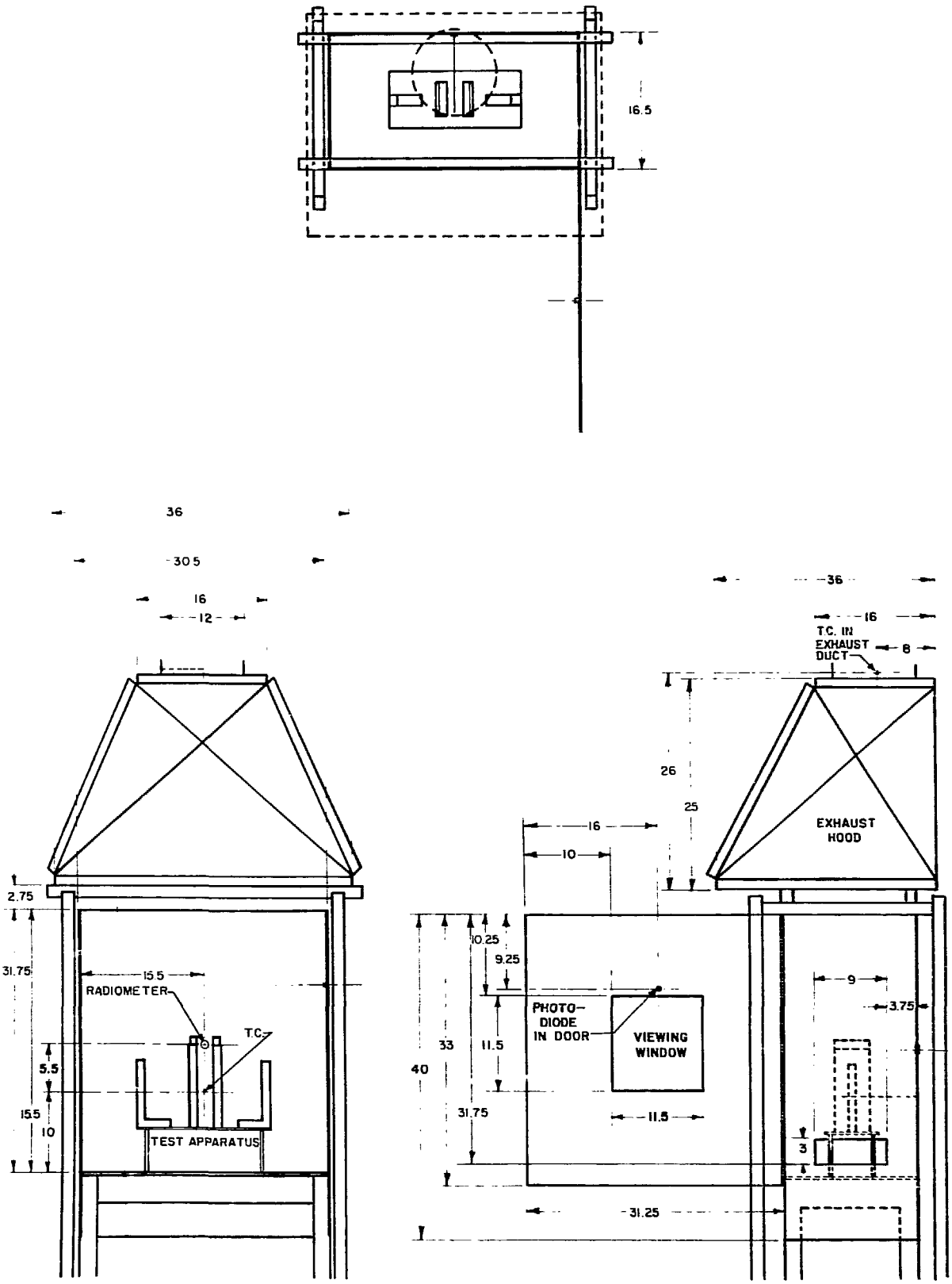

Figure 12. Schematic of ease-of-ignition apparatus.

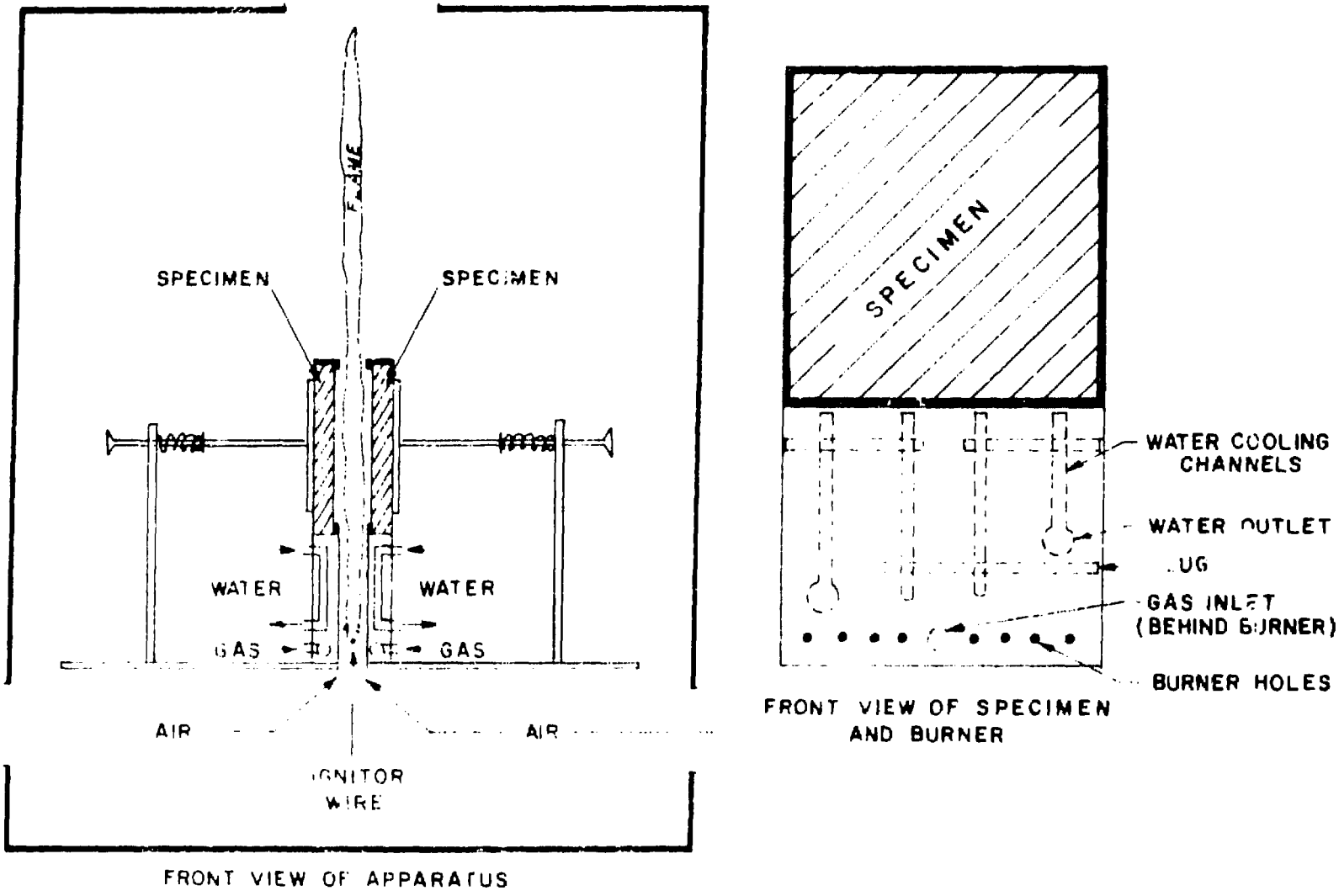

Figure 13. Sketch of ease-of-ignition apparatus showing inlet and outlet ducts.

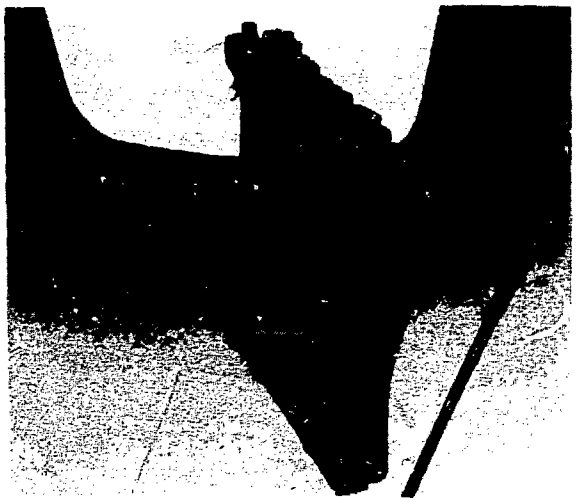

Figure 14. Specially designed cable specimen holder. There were two specimens for each test and we conducted four tests.

holders gripped cable samples at their ends (Fig. 14), and this provided sufficient tension to prevent deformation of the individual cables due to heating, which ensured reasonable reproducibility among all samples. Two inert specimens of the same dimensions were prepared from 12.7-mm-thick calcium silicate board stock. These blank specimens were used for determining the temperature baseline and for preheating.

Test Apparatus Specifications

The specifications listed below were the baseline parameters for conducting our standard ease-of-ignition tests.

Gas Flow

The gas-flow rate through each of the independently controlled burners was set to approximately 100 cm^3/s (12.5 SCFH) of technical-grade methane producing a heat flux of 3.2 W/cm^2 ± 0.2 W/cm^2 from a total gas flow of 200 cm^3/s ± 10 cm^3/s (25 SCFH ± 1.3 SCFH) that resulted in an energy release of about 7 kJ/s.

Test Procedure

At the beginning of each test day, cooling water was turned on to a predetermined flow rate and the hood draft was turned on. Two pieces of miranite were mounted in the test flame, the data acquisition system was started, the electrical spark igniter was turned on, and the solenoid gas valves were opened. The box was preheated for 60 s, which provided the baseline thermopile output for the day's testing. After this period, the burners were shut off, the miranite boards were replaced by actual samples, and formal testing begun.

The time to flame attachment (visual) was noted with a time marker on a strip-chart recorder. Generally, just before the time that flame attachment was noted, the thermopile voltage increased, indicating the onset of fuel contribution. The time to fuel contribution was picked from the recorder trace as the time at which the trace began to rise above the baseline, as determined by a straight-line projection of the rising part of the thermopile trace back to the baseline. Small increases in thermopile voltage of less than 10% of the baseline were ignored.

The test was terminated three seconds or more after (1) the trace either exceeded the baseline by 30% or a maximum temperature had been reached, and (2) a flame attachment had occurred. Otherwise, it was continued for a total duration of five minutes. We conducted four tests of each cable type.

Table 4 lists physical descriptions of the six cable types tested thus far. There is a variety of sizes and material combinations. Figures 15 and 16 are exemplar plots of thermopile and photodiode outputs. Table 5 lists the mean times to fuel

Table 4. Physical characteristics of cables tested during FY 82.

Cable	o.d. (mm)	Circumference (mm)	Jacket thickness (mm)	Time to ignition (s)	Dielectric jacket materials
95	7.6	23.9	11.7	11.7	polyethylene, PVC, multiconductor
12	3.7	11.2	1.6	67.3	rubber
3	5.6	17.5	0.79	75.0	PVC, nylon
007	22.9	71.9	3.9	83.2	rubber or Neoprene
104	10.3	32.3	0.79	126.4	polyethylene, PVC
RG 11 A/U	10.3	32.3	[illegible]	150.2	polyethylene, PVC

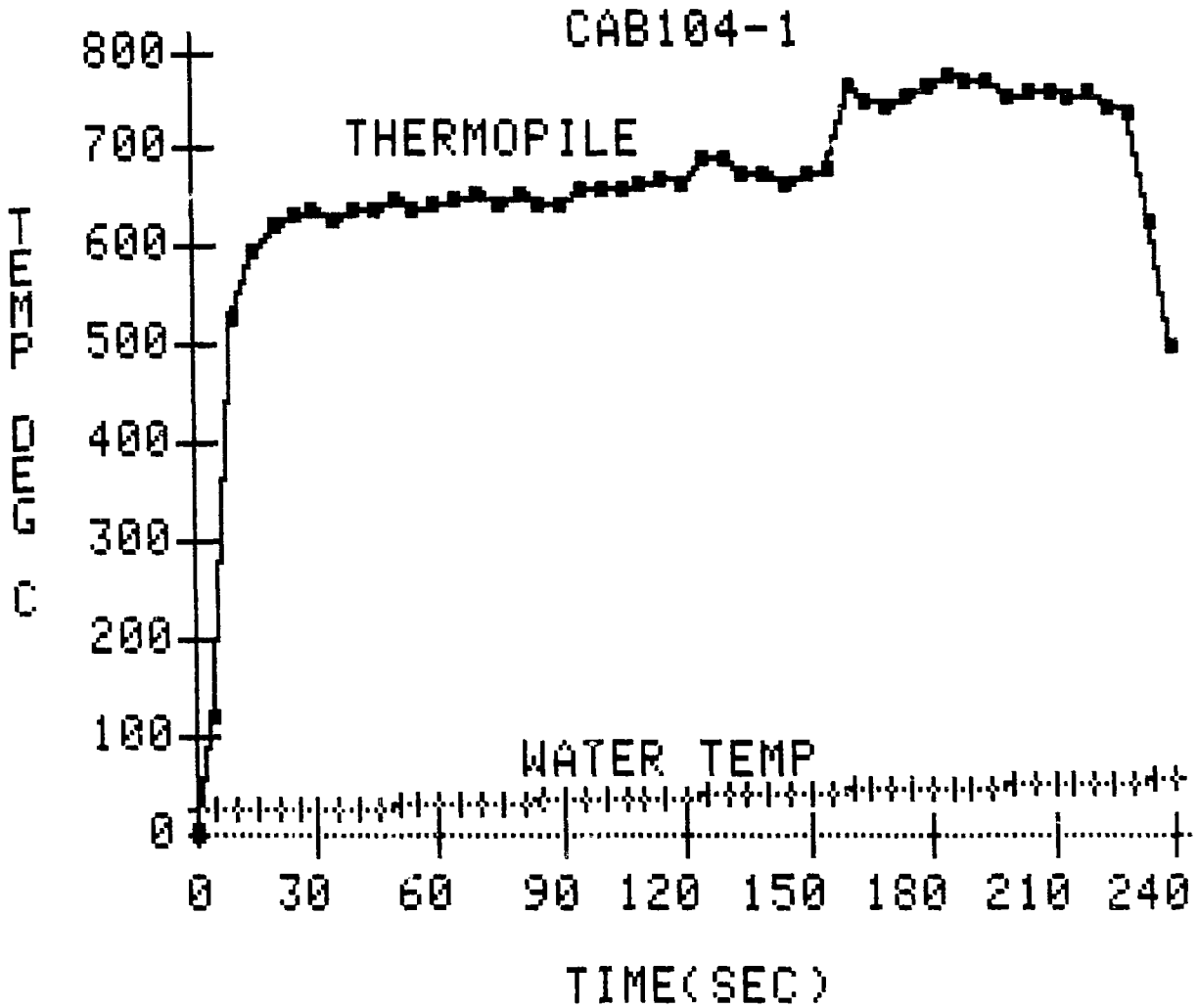

Figure 15. Exemplar plots of Cable-104 test (thermopile).

contribution and the coefficient of variation for each group of four replications. In addition, each of the cable types is ranked in ascending order of time to ignition.

Results

Several facts become apparent upon analysis of the data. The most obvious fact is the wide spread in ignition times as indicated by the coefficient of variation. Because we performed only four replications of each cable type, one anomalous run had a significant effect on the standard deviation for the time to ignition of a given cable type. Considering the many variables in both the experimental apparatus and the test specimens (change in configuration due to deformation of individual cables), this variation is not surprising.

More importantly, more cable types must be tested to evaluate the individual effects of cable size, geometry, composition, and materials on ignitability. It can be seen from the ranking of the data in Table 5 that both size and jacket material have significant influences. Figures 17(a) and (b) illustrate the variety of cable types and sizes tested thus far. Furthermore, for this scale experiment, the outer jacket thickness should account for the ease or resistance to ignition. Referring to Table 5, we see that although cable 95 has an o.d. of 7.6 mm, it has the shortest time to ignition at 11.7 s. This may be because it is a multiconductor cable with a polyethylene outer jacketing. On the other hand, cable 007, which has more than twice

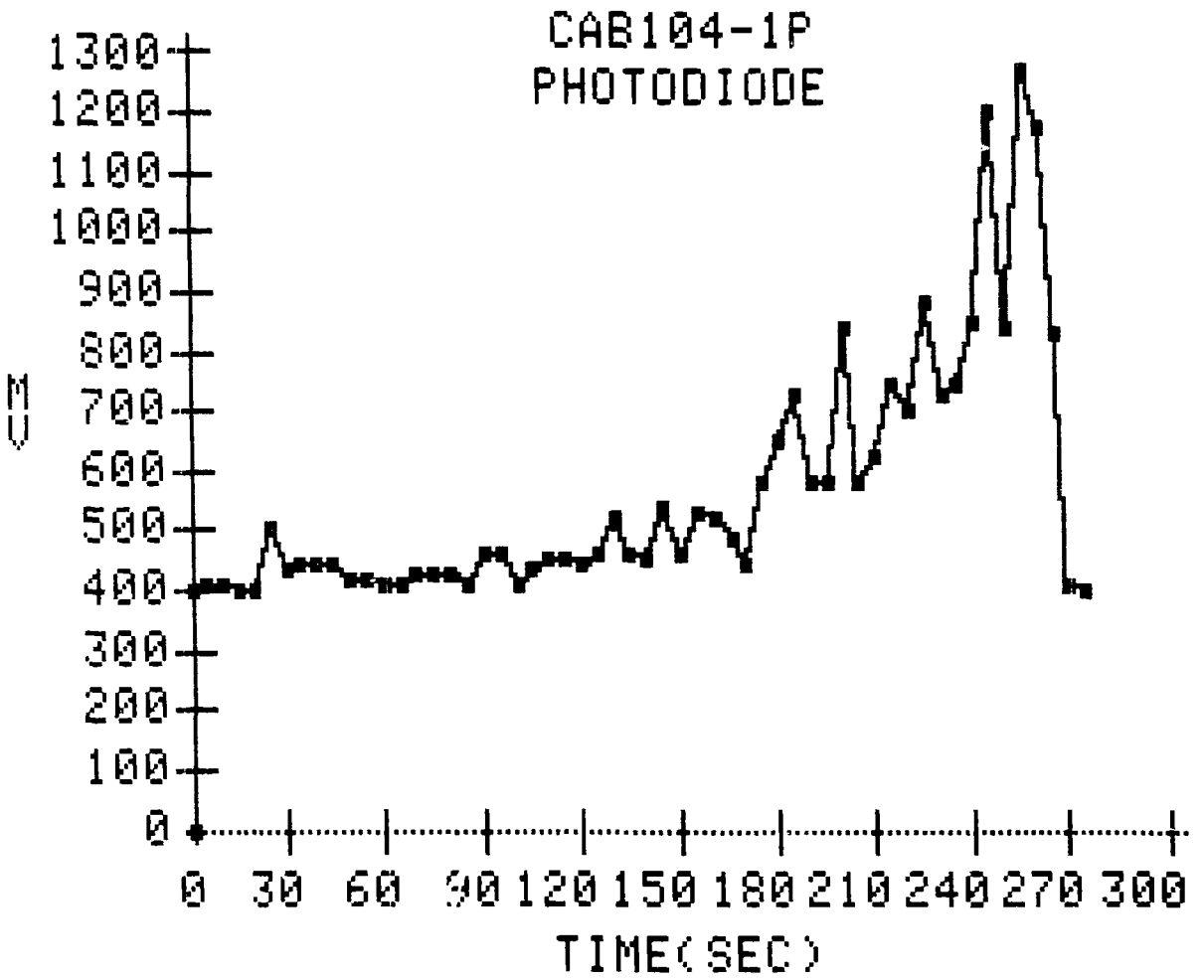

Figure 16. Exemplar plots of Cable-104 test (photodiode).

Table 5. Ease-of-ignition experiment results (series 1). The cables are listed in order of increasing times to ignition (example: Cable 95 is the easiest to ignite and RG 11 is the most difficult to ignite).

Cable type	Mean time to fuel contribution (sec)	Coefficient of variation (%)
Cable 95 (polyethylene)	11.7	31.2
Cable 12 (rubber)	67.3	10.7
Cable 3 (PVC)	75.0	43
Cable 007 (rubber or Neoprene)	83.2	7
Cable 104 (PVC)	126.4	42
RG 11 A/U (PVC)	150.2	16.9

the diameter of the next largest cable, falls to a median position in the ranking.

In an attempt to evaluate some of these size and geometric effects, we used several quasi-normalization techniques; these results are presented in Table 6. By comparing the rankings obtained through these manipulations to the actual experimental times to ignition, we should be able to theorize which physical or chemical cable properties cause better or worse fire performance. In other words, when the time to ignition is modified by any of the size parameters, the cable order by increasing difficulty of ignition changes depending upon which relationship is used. For example, cable 12 has the second shortest experimental time to ignition, and is ranked best and second best by three of the four techniques; it also is difficult to ignite relative to its size. In order to determine the change in performance due to the jacket material or the conductor configuration (i.e., multiconductor, stranded, solid, etc.), other cable types of different jacket materials but of the same

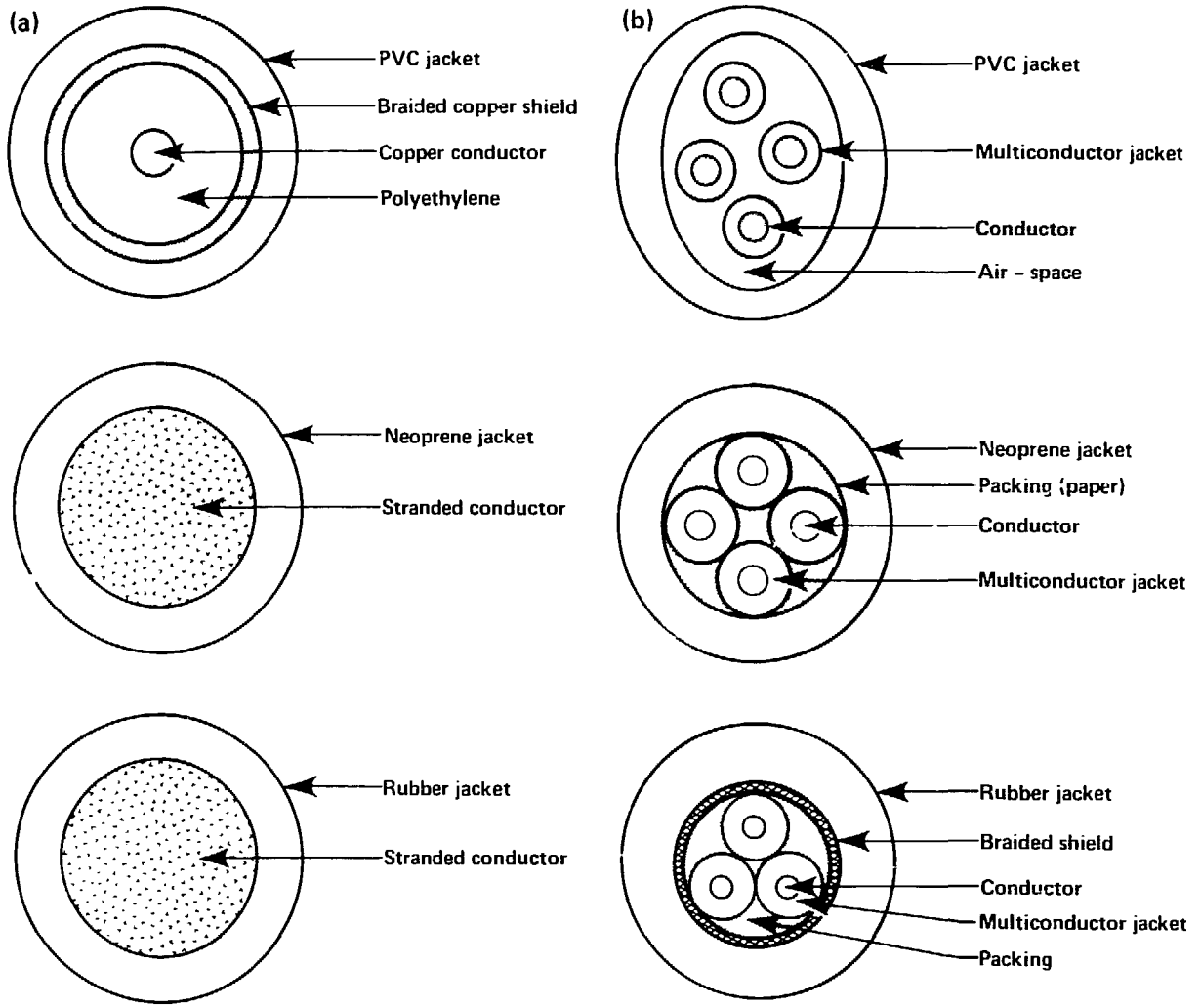

Figure 17. Cross sections of (a) single conductor cables and (b) multiconductor cables.

size could be identified and tested. We will follow this through in FY 83, and we will attempt to use these results to predict a cable type's relative ease of ignition without having to test it. We will also look at ways to modify the apparatus, thus improving its reproducibility.

Table 6. Time-to-ignition (TTI) rates of various cables. Numbers in parentheses denote ranking of the cables according to the times to ignition of each one, with 1 = shortest time to ignition and 6 = longest time to ignition.

Cable	Time to ignition (s)	TTI/o.d. (s)	TTI/circum/jacket (s)	TTI/jacket/o.d. (s)
95	11.7 (1)	39 (1)	0.385 (1)	113.6 (1)
007	83.2 (4)	92 (2)	4.59 (4)	153.7 (2)
104	126.4 (5)	312 (3)	3.09 (2)	531.9 (4)
3	75.0 (3)	341 (4)	3.37 (3)	480.9 (3)
RG 11 A/U	150.2 (6)	371 (5)	5.56 (5)	1641.6 (6)
12	67.3 (2)	467 (6)	9.64 (6)	1294.8 (5)

Fire Modeling

As part of our ongoing program to create a versatile model for enclosure fires in order to assist us in fire-risk assessment, we conducted another series of idealized enclosure fires in the LLNL fire test cell. Goals of these tests included:

- Evaluating and ratifying fire models for enclosures served by HVAC systems where air pumps provide negative pressure in the enclosure;
- Determining enclosure and ventilation properties that control fire output parameters;
- Determining the heat transfer from forced-ventilation enclosure fires to enclosure gases, enclosure surfaces, exit ventilation systems and exit gases;
- Determining the ceiling-layer descent velocity and level for such fires;
- Determining the density of combustion aerosols in the vertical plume and ceiling jet;
- Relating fire-plume heights to heat-release rate and fire dimensions;
- Measuring radiative heat to and from the fire source or second fuel source; and
- Determining fire characteristics that affect the inlet ventilation and aeration of the fire in a forced-ventilation enclosure.

Tests conducted during FY 81 (the first set of ideal model test fires) were useful as preliminary data sources for model validation, and they provided us with practical experience. Extensive data analysis revealed the following problems encountered during this series:

- Ventilation analysis indicated that too much air escapes from the inlet directly to the outlet.
- There were problems with rake stability. There were only 10 thermocouples and the thermocouple plane varied from the design positions from test to test.
- Water vapor was not removed before entrance into gas analyzers.
- Methane tests used a float rotometer which was not methane-calibrated nor was its temperature and pressure measured during tests.
- There were no pre-fire or post-fire baseline data.
- The fire duration was short and no tests to quasi-equilibrium were conducted.

During the planning for FY 82 experiments, these problems were rectified, and, in addition, we implemented the following improvements and modifications during FY 82:

(1) We conducted more varied tests (31 in all with wider fuel geometries and types). We also conducted some pool fires.

(2) We improved the input ventilation to promote low-air release and mixed conditions before reaching the exit duct. We added 2 rakes with 15 thermocouples each and a rigid support with provisions for thermal expansion. We added water traps in the gas-sample lines. We added a critical orifice and a turbine flowmeter for gas-fuel metering, both of which are temperature-compensated and pressure-recorded.

(3) We sampled high and low gases in the cell as well as the gases in the duct. We made more thermal measurements (heat transfer) and wall-temperature measurements.

Table 7 lists the experiments we conducted during FY 82. We include information on the type of fire, and the heat-release rate and forced-ventilation rate of the design.

The type of fire depended upon the fuel phase and method of fuel control. In the tests using "burner," pure methane, metered by a critical orifice and turbine meter, was conveyed to a 0.28-m diameter rock-filled pan. Gas entering the pan bottom distributed uniformly through the rock bed to form a jet above rock bed surface.

Fire types that we designated "spray" had liquid fuel flow from a pressurized reservoir through a previously calibrated rotometer to an opposed jet nozzle located in the center of a 0.91-m diameter steel pan. Liquid from the nozzle was sprayed on a plane normal to the orifice axis in a radial distribution. We ignited it remotely by an energized electric arc; the atomized spray was quickly evaporated and burned before it contacted pan surfaces. The resulting fire had every appearance of a natural pool fire. Figure 18(a) shows the opposed jet nozzle, (b) the jet in the 0.91-m pan, (c) the jet nozzle spray pattern, and (d) a spray-type fire.

Pool fires were contained in the 0.91-m pan. We defined the heights of fuel so that the pan edges did not influence the burning rate.[6]

We ran several tests either as preliminary "shake down" experiments, or as insurance tests. We conducted these experiments in the fire-test cell described in previous reports.[3] Because the modeling of these data was to be performed by several external agencies, detailed schematics of the test-cell geometry and instrumentation were prepared and distributed to interested individuals.[7] Figure 19 shows sectional-cell and exit-duct dimensions for the case where test-cell extraction is from the high (3.6 m) exit air opening. Figure 20, an exploded view of the test cell, shows the placement of air temperature and heat transfer-sensors.

Table 7. FY 82 fire test experiments.

Test	Type	Fuel and formula		Q (kW)	V (l/s)
1	Burner	Methane	CH_4	125	250
2	Burner	Methane	CH_4	50	500
3	Burner	Methane	CH_4	50	100
4	Burner	Methane	CH_4	200	100
5	Burner	Methane	CH_4	400	500
6	Burner	Methane	CH_4	400	100
7	Burner	Methane	CH_4	125	250
8	Spray	Isopropanol	C_3H_8O	400	500
9	Spray	Isopropanol	C_3H_8O	800	500
10	Spray	Isopropanol	C_3H_8O	100	100
11	Spray	Isopropanol	C_3H_8O	100	500
12	Spray	Isopropanol	C_3H_8O	800	100
13	Spray	Isopropanol	C_3H_8O	400	500
14	Spray	Isooctane	C_8H_{18}	400	500
15	Spray	Isooctane	C_8H_{18}	800	500
16	Spray	Isooctane	C_8H_{18}	800	100
17	Pool	Isopropanol	C_3H_8O	0.91 m	500
18	Pool	Isopropanol	C_3H_8O	0.91 m	100
19	Pool	Isooctane	C_8H_{18}	0.91 m	500
20	Pool	Polystyrene	$(C_8H_8)_n$	0.91 m	500
23[a]	Spray	Isooctane	C_8H_{18}	400	100
24	Spray	Isooctane	C_8H_{18}	200	100
25	Spray	Isopropanol	C_3H_8O	200	100
26	Spray	Isopropanol	C_3H_8O	400	100
27	Spray	Isopropanol	C_3H_8O	400	250

[a] Tests 21 and 22 were cancelled.

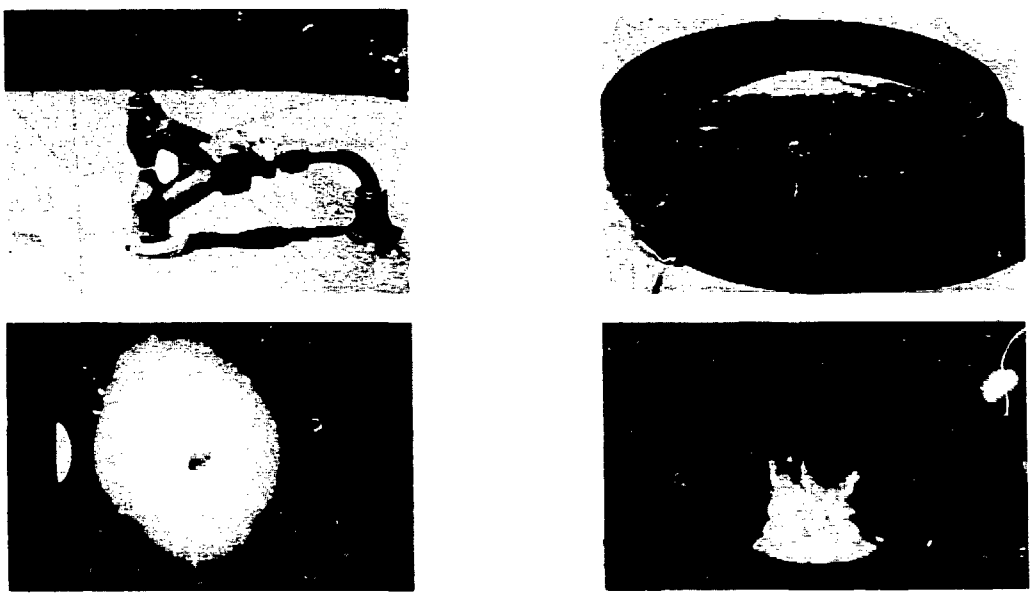

Figure 18. Detail of typical spray-type fire test. Photos show the (a) opposed jet nozzle, (b) jet in the 0.91 m pan, (c) nozzle jet-spray pattern, and (d) a spray-type fire.

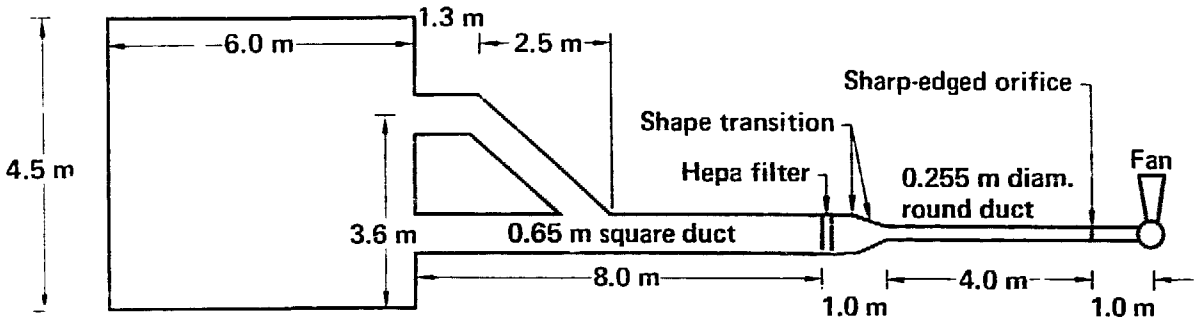

Figure 19. Test cell and exit duct dimensions (vertical section).

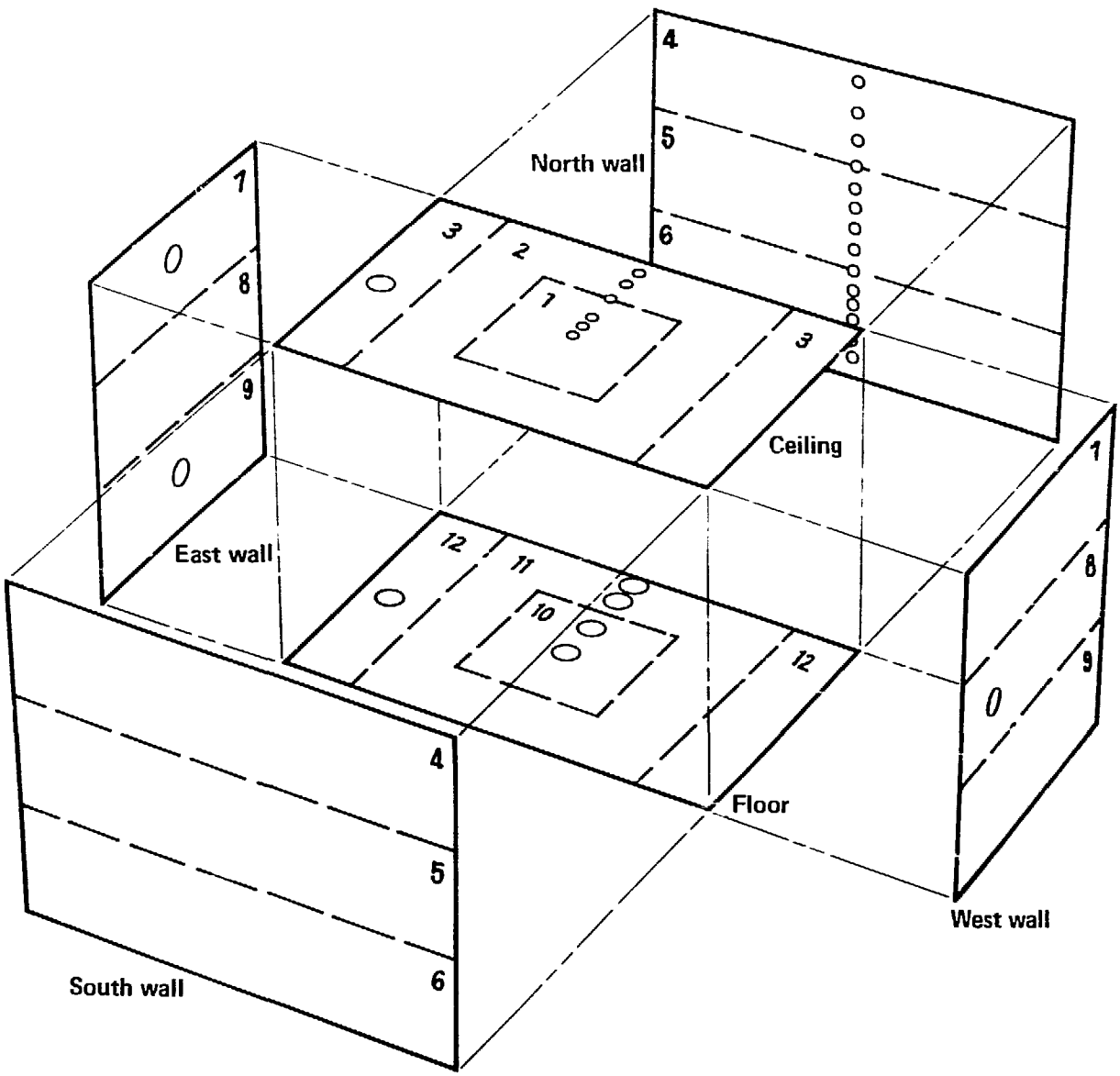

Figure 20. Blow-up representation of cell showing thermocouple locations and marked surface zones.

FY 81 measurements indicated that most of the combustion energy is absorbed in enclosure surfaces (up to 80%). To ascertain the distribution of surface energy deposition, we installed thermocouples on test cell surfaces in the array shown in Fig. 20. We designed this array under the assumption that thermal energy deposition is symmetrical in the test cell.

Figure 21 is a fire portrait illustrating some of the important data from a 400 kW isopropanol spray fire, ventilated at 250 l/s. The curves and scales are as follows: CO_2, CO, and total hydrocarbon production on 0–12% scale, O_2 production on 0–30% scale, exit-air flow, south-wall temperature, and entrance-to-duct temperature on 0–600 scale, and inlet airflow on −600 to +600 scale.

A typical characteristic of our forced-ventilation enclosure tests is the reverse flow out of the inlet duct just after ignition. This reversal is caused by the fire rapidly expanding the room air and correlates directly with the rate of air temperature rise in the room. For large fires ($\dot{Q} > 200$ kW) with a low ventilation rate, this effect is pronounced and causes flow reversal in the inlet duct, as indicated in Fig. 21.

Because enclosure surfaces are good insulators, the time to thermal equilibrium in the cell is extremely long. Both air- and surface-temperature measurements indicated a rapid temperature rise during initial heatup of the cell, after which the rising temperature rates were greatly reduced and appeared to be approaching equilibrium. Note that air temperature is larger than wall temperature, but this difference is small, which indicates that substantial thermal energy is given up to the walls.

Measurements of oxygen depletion and generation of combustion products show complementary patterns of special production, reaching maximum levels which then decrease slightly prior to termination of the test. This behavior may have resulted from internal-balance mechanisms where over-shoot in combustion equilibrium was rectified by transport processes.

Figure 22 shows two fire portraits that contrast thermal, combustion, and flow parameters between fires of high and low fire strengths at the same 500 l/s ventilation rate (Tests 9A at 800 kW and 11A at 100 kW).* The effects of inadequate ventilation are replete in Test 9A: large production of unburned hydrocarbon, high CO production, and gas temperature peak and decrease. While in Test 11A, the same functions attain quasi-equilibrium condition.

Figure 23 compares the effect of fuel type on thermal, chemical, and ventilation flow results for 400-kW fires ventilated at 500 l/s. Tests 5, 13 and 14 used methane (CH_4), isopropanol (C_3H_8O), and isooctane (C_8H_{18}) as fuel. Even though the design thermal output and ventilation rate were the same, all measured parameters appeared different for each fuel. Close inspection showed that the maximum values of temperature rise, and CO_2 formation for the two liquid fuels are essentially the same. Oxygen depletion is different in all cases and both the total hydrocarbon and CO appear only for CH_4 and C_8H_{18}. At this time, we cannot fully explain the difference between these data. One possible explanation relates to the methane fire where the combination of a high-fuel flow and a small burner diameter produced a turbulent momentum jet, not the buoyant plumes produced with the spray fires.

The four pool-fire tests we conducted during this series are shown in Fig. 24. Tests 17 and 18 show C_3H_8O-pool fires at ventilation rates of 500 l/s and 100 l/s, respectively. Test 19 shows the C_8H_{18} fire at a 500 l/s ventilation rate and Test 20 shows output from a polystyrene-bead pool fire at a 500 l/s ventilation rate. All the pool fires, except for Test 17, show extreme ventilation-control characteristics. Since these pools burn naturally, fuel consumption is directly dependent upon fire-plume efficiency. Thus, output characteristics will reflect this efficiency. The obvious contrast between Test 17 and the other pool fires, regardless of the kind of fuel, is a good example of the different feedback response of well and poorly ventilated, naturally burning fires.

Figure 25 (combine rake data), which shows thermocouple output from rake* thermocouples for Test 8, is a map of the temperatures recorded by alternate thermocouples. Air-temperature measurements appeared to have established their distribution in about 300 s. This observation is confirmed by noting the evolution of temperature profiles, shown in Fig. 26, at selected times early in the test. These data indicate that the profile is indeed well-formed by 300 s into the test. Figure 27 shows the temperature profile drawn by both east and west rakes after 1200 s of continuous burn. The profile shapes are very similar to

* Scale ranges are the same for all fire portraits included in this section of the report as in Fig. 21.

* Rake thermocouples located at east and west side of burn pan. Vertical array at one foot vertical increments.

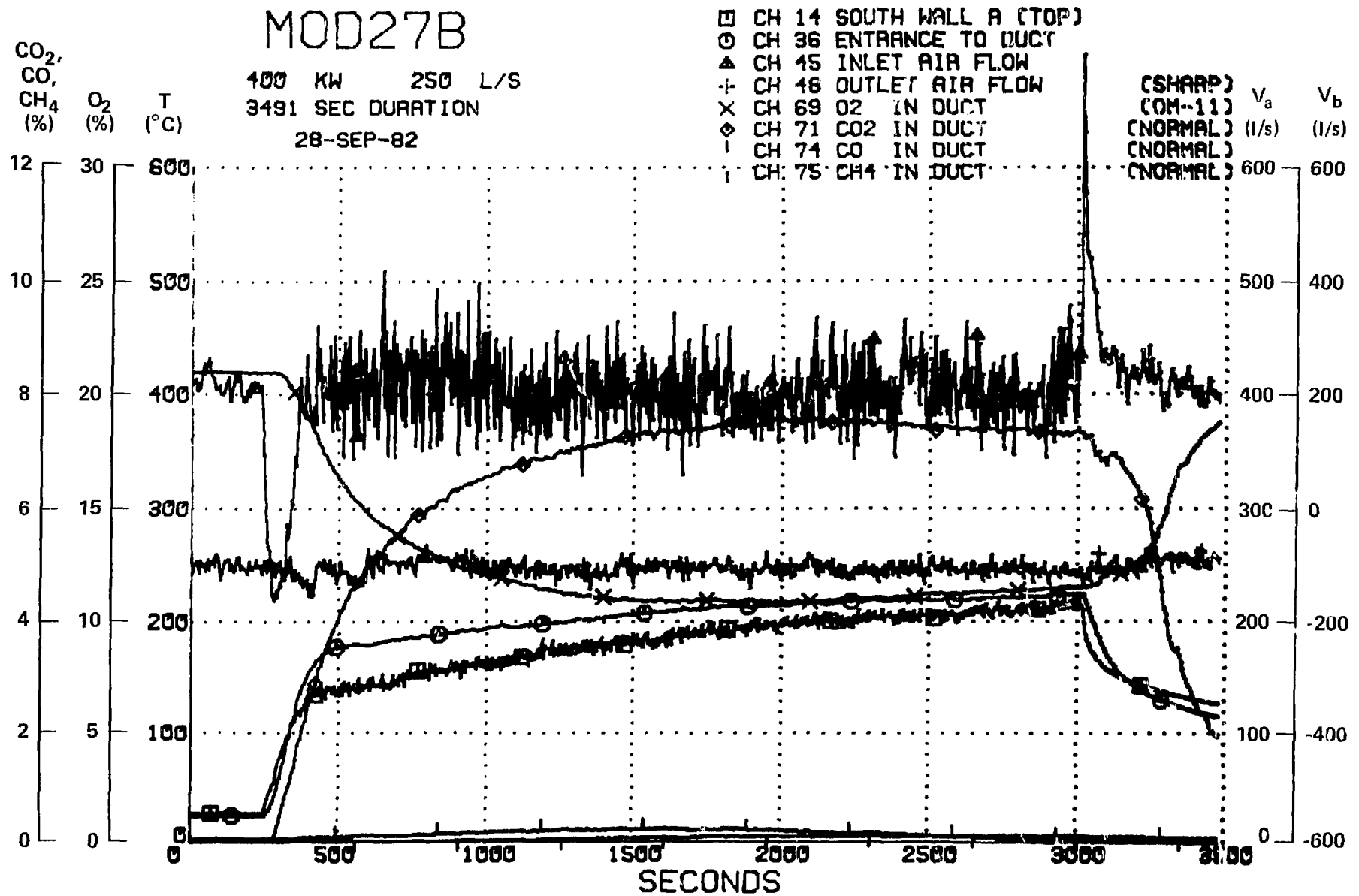

Figure 21. Modeling tests (Mod 27B) of a 400 kW fire that lasted over 58 minutes. The scale range is explained in the text (V_a = outlet air flow and V_b = inlet air flow, both in l/s).

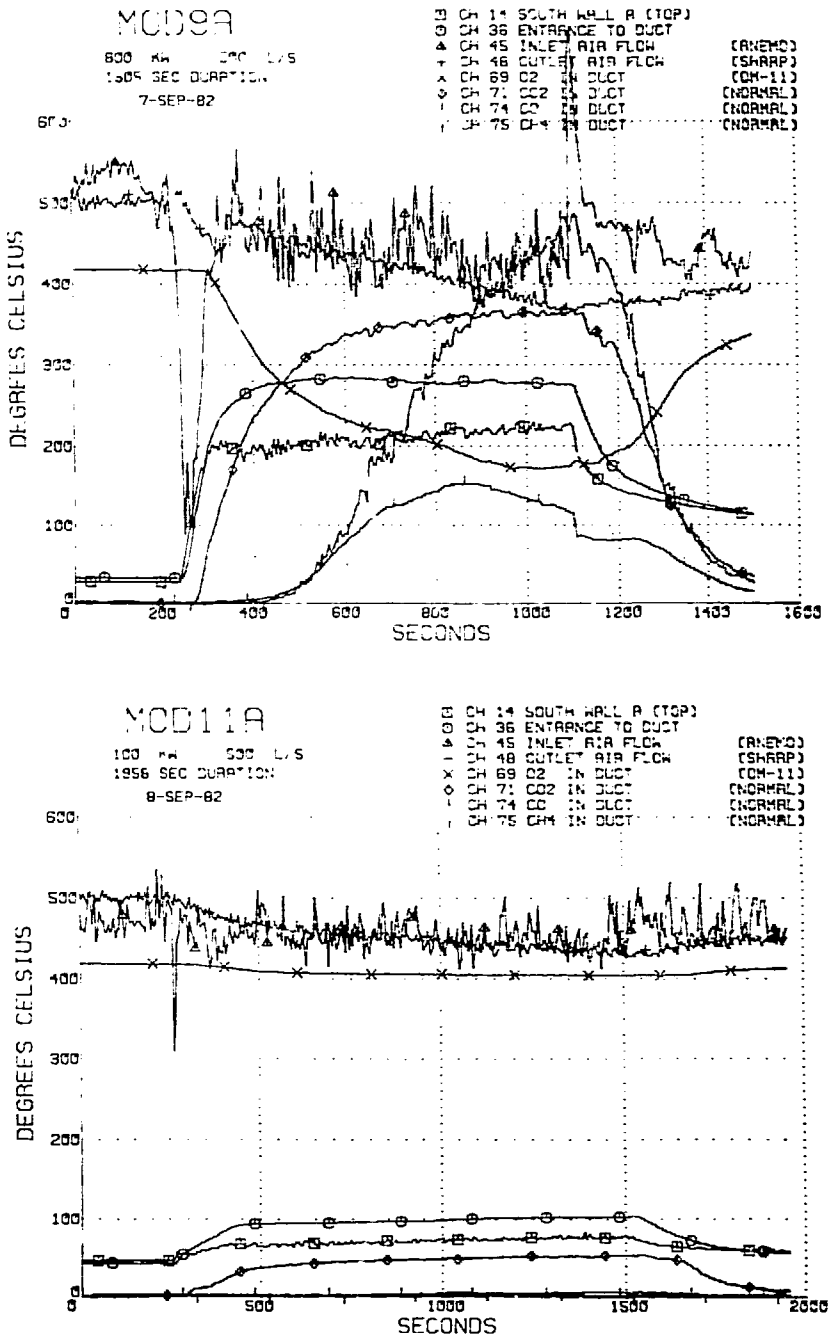

Figure 22. Mod 9A and Mod 11A.

that at 300 s, except that most individual temperature readings are about 50°C higher, as we would expect. The shape of temperature profiles as shown in Figs. 26 and 27 is dependent upon the flow dynamics of the fire plume and entrance- and exit-airflow patterns.

Most fire models predict that a fire will produce stratified flow conditions in a room that can be represented by a hot and cold layer of air separated by an interface. We choose to apply Steckler's conservation technique[6] to our temperature profiles in order to represent them in the two-layer condition used by some models. Results from this procedure are shown in Fig. 28 for both east and west rakes and the average calculated profile of both rakes.

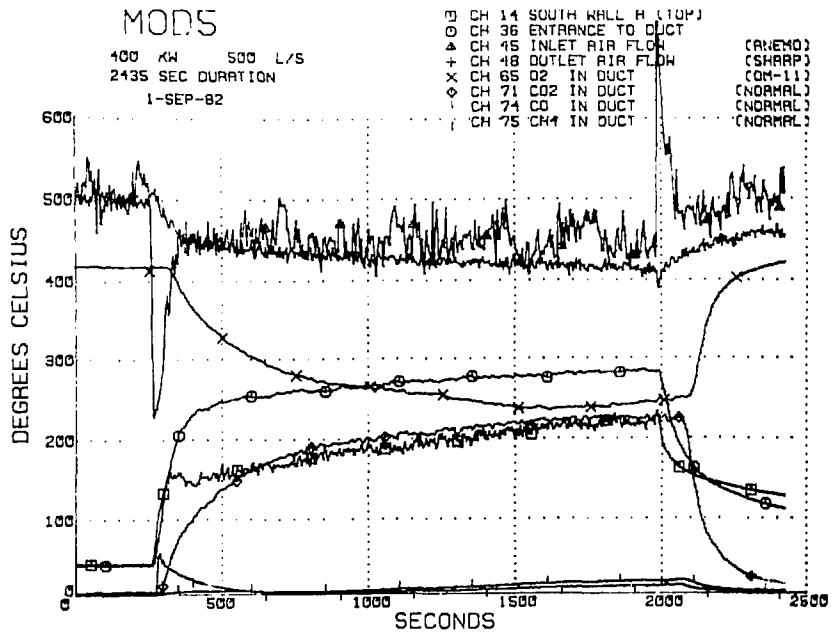

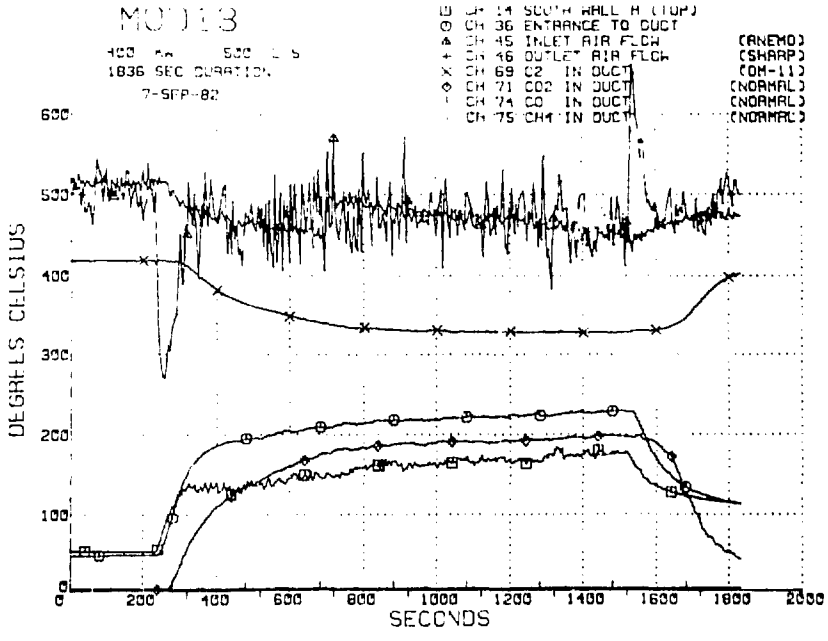

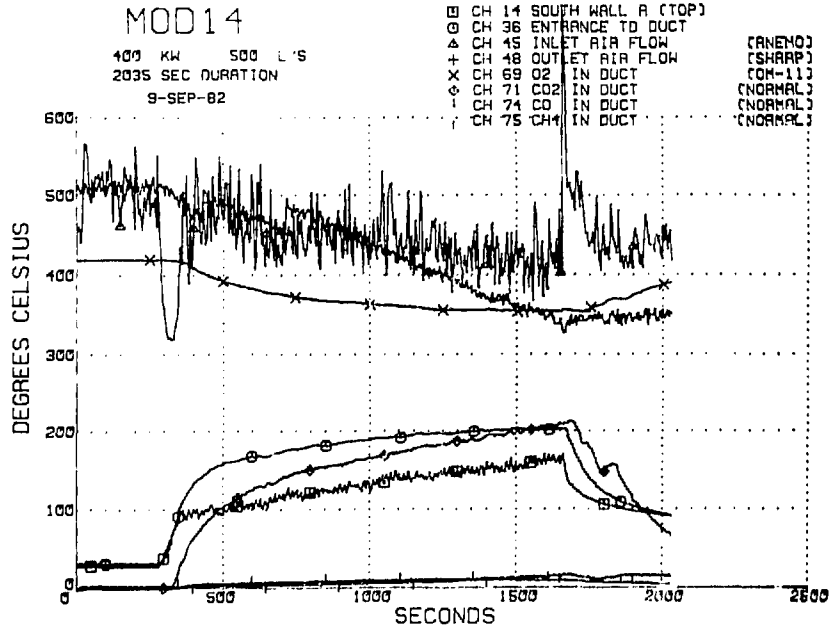

Figure 23. Mod 5 (methane), Mod 13 (isopropanol), and Mod 14 (isooctane).

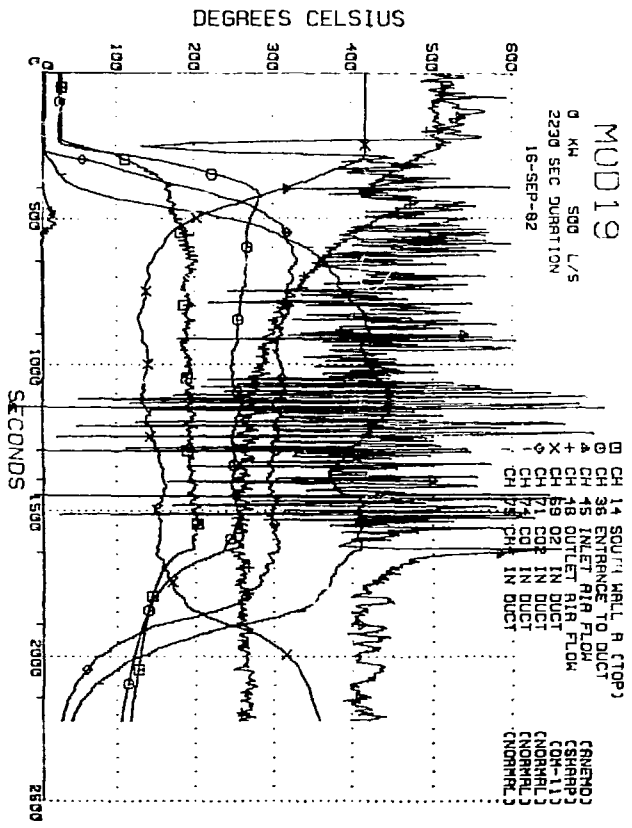

Figure 24. Mod 17, Mod 18, Mod 19, and Mod 20.

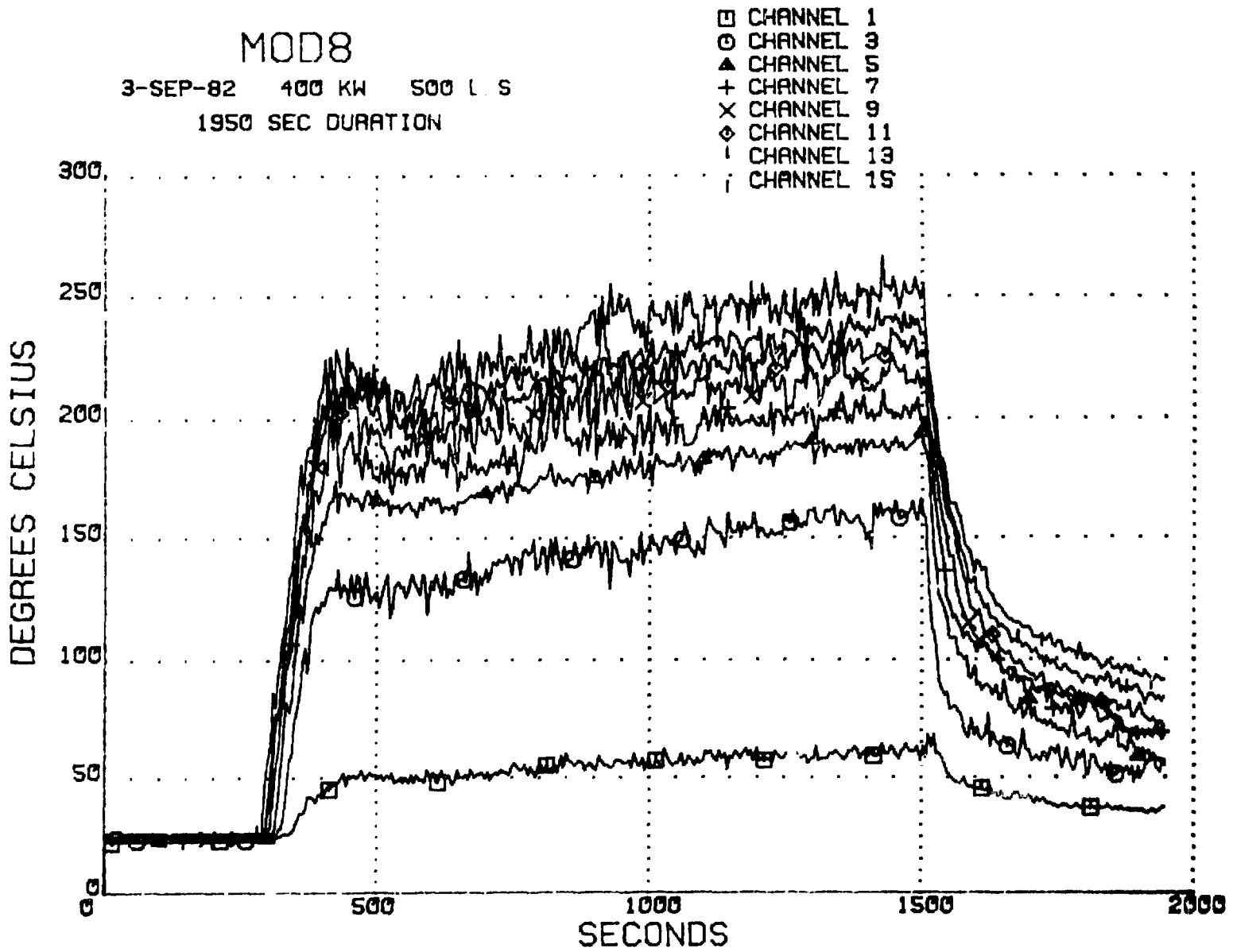

Figure 25. Mod 8 rake thermocouples (400 kW, 500 l/s).

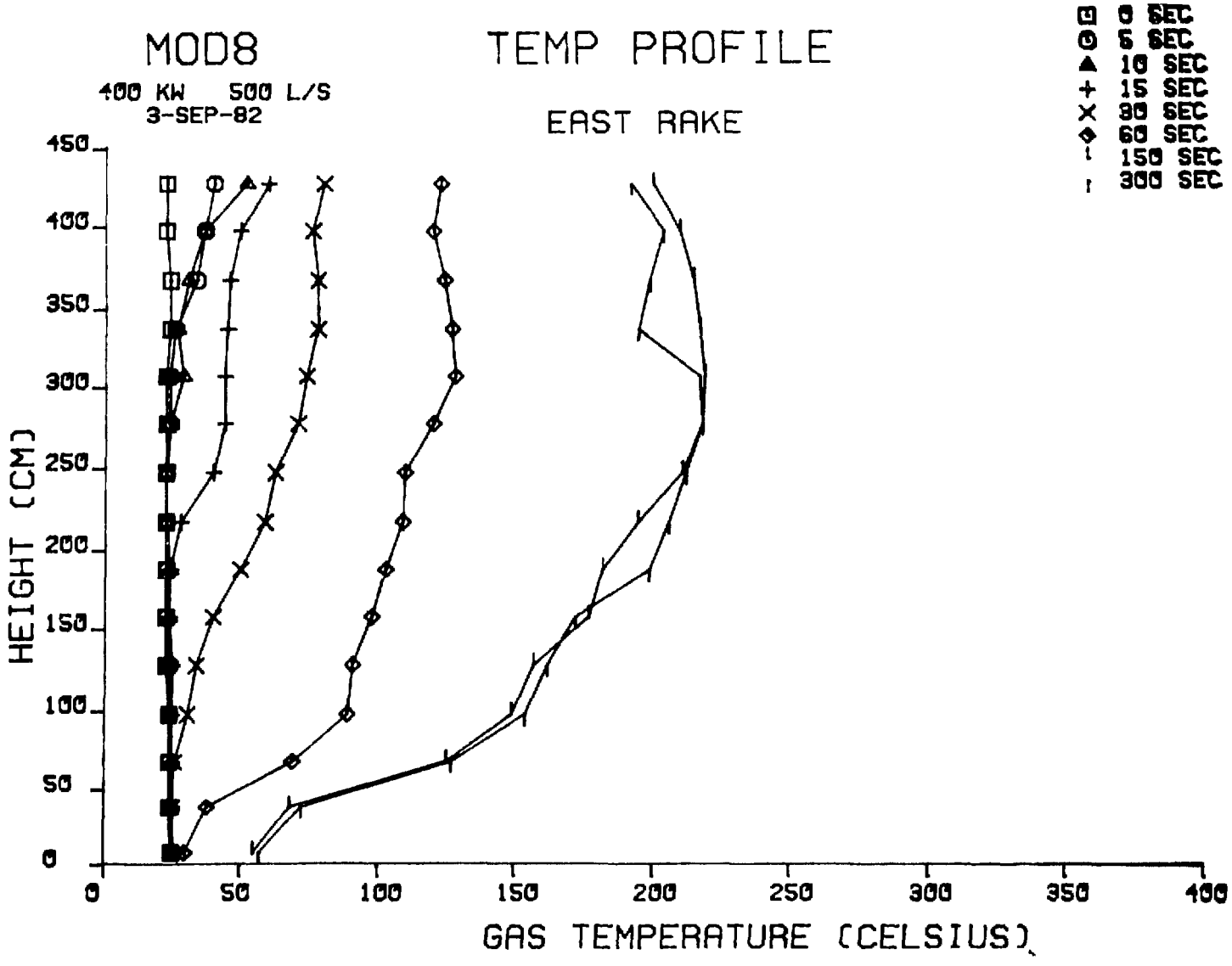

Figure 26. Mod 8 temperature profile (east rake).

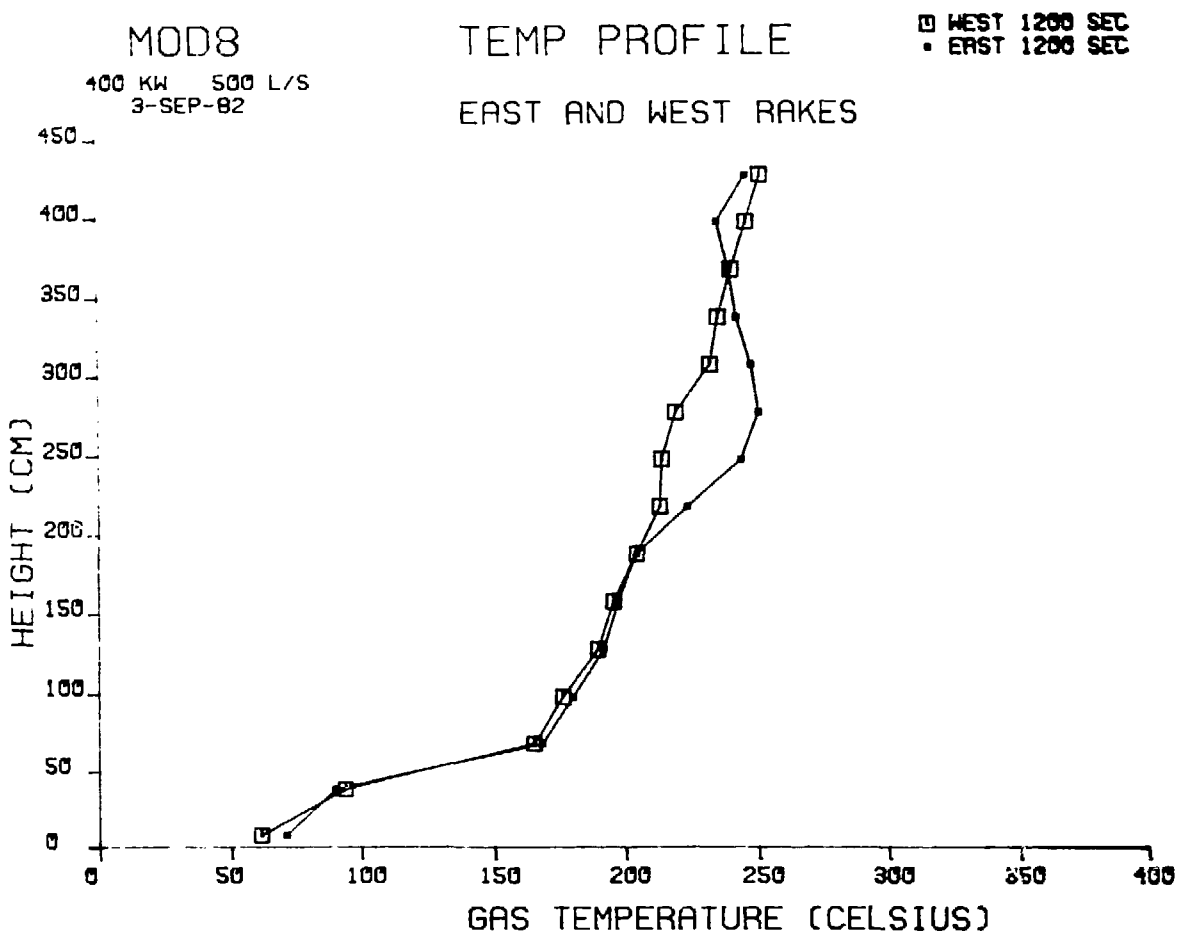

Figure 27. Mod 8 temperature profile with east and west rakes combined.

For model validation, it is necessary to ensure that measured parameters are as precise as possible. Therefore we took extreme care during data analysis to develop accurate information for other researchers. Perhaps the most important function is the equilibrium fire strength. Fire strength is defined initially by the direct measurement of fuel consumption and indirectly by measurement of CO and CO_2 production. Fire strength can also be defined independently by plume-height measurements of the fire.[4] Table 8 compares fire-strength values calculated using these procedures. In general, we note there is a reasonable correlation between fire-strength values and adequately ventilated fires. In the cases where fires are poorly ventilated, wide discrepancies are apparent between fire strength calculations. Figure 29 is a graph of the empirical relationship between flame heights and fire strength developed by California Institute of Technology researchers and the flame-height data produced during our measurements. Note that we used this correlation to calculate fire strength from our measured flame-height data.

Appendix A contains the balancing equations we used to validate the accuracy of our data after all volumetric functions were converted to mass units. This procedure marks data inconsistencies, measurement faults, and equipment or calibration errors. We will now discuss the comparisons using these equations.

Figure 30(a) shows mass balance for Test 27B. Since the "mass net" hovers around zero, we are confident there were no leaks throughout the ventilation circuit and test cell. Figure 30(b) compares fire strength as computed by the product of fuel-flow rate and heat of combustion, and fire strength computed from CO and CO_2 production. The fact that these two fire strengths do not match indicates inefficient burning. Since the discrepancy is not large, we can assume that the fire was

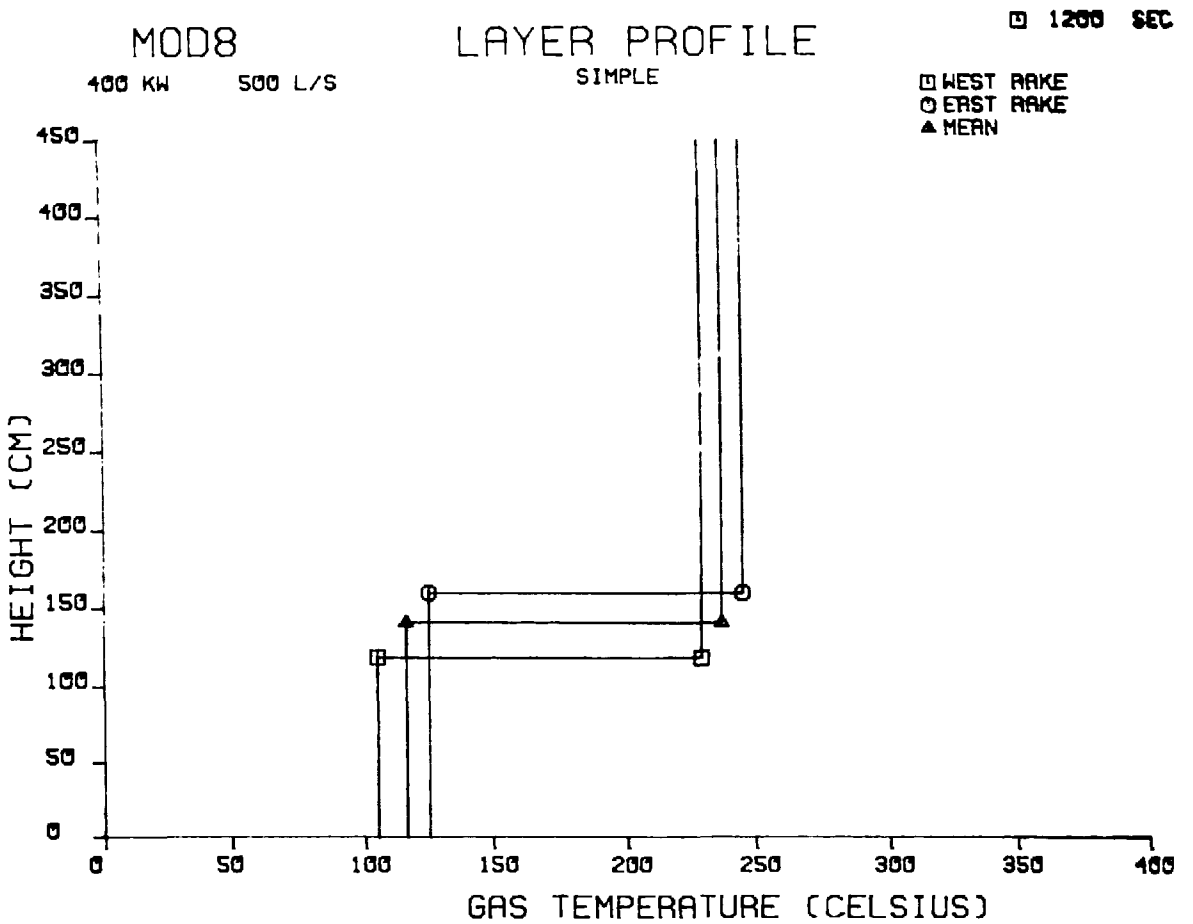

Figure 28. Mod 8 layer profile.

only slightly ventilation-controlled. Figure 30(c) accounts for gas energy into and out of the enclosure. Also, by subtracting the net energy to the gas from the fire strength determined by CO and CO_2 production, we can calculate directly the total energy to enclosure surfaces which is indicated as θ wall in (c). Figure 30(d) shows the generation and removal of atomic species in the enclosure during the test. The reason we did not attain species balance was again due to inadequate ventilation of the fire.

Figure 31 contains the same balancing data for a fully ventilated fire. Here, Fig. 31(a) shows the only inconsistency of these data. Mass-balance calculations indicate more gas leaving than entering the test cell. Apparently, the anemometers were not calibrated or the test cell leaked. Figures 31(b) through (d), however, show excellent balance, indicating fully ventilated conditions for the fire. The imbalance of the mass-flow of air is not important for these parameters since they depend only on conditions in the outlet duct.

Table 9 lists the results of the FY 82 test series. We found Tests 2, 3, 11, 20, 21 and 22 insufficient for our modeling purposes and eliminated them. Data contained in this table are semi-equilibrium values. These data will be used to preliminarily rate models and to establish criteria for FY 83 tests.

Table 8. Comparison of fire strength calculations.

Test		Fuel type	Air flow (l/s)	Physical fire strength (kW)	Measurement procedure	CO, CO_2 fire strength (kW)	Flame height fire strength (kW)
MOD	1	Methane	250	135	By critical	159	197
	2	Methane	500	55	orifices and	90	74
	3	Methane	100	60	turbine flow-	76	65
	4	Methane	100	230	meters	222	280-500
	5	Methane	500	455		592	450
	6	Methane	100	460		214	≃800
	6A	Methane	100	470		245	≃800
	7	Methane	250	135		175	182
	8	Isooctane-Propanol	500	400	By flow rates	420	310
	9	Isooctane-Propanol	500	800	and physical	891	≃500
	9A	Isooctane-Propanol	500	800	calibration	712	≃500
	10	Isooctane-Propanol	100	100		81	121
	11	Isooctane-Propanol	500	100		135	121
	11A	Isooctane-Propanol	500	100		120	121
	12	Isooctane-Propanol	100	800		234	≃500
	13	Isooctane-Propanol	500	400		437	342
	14	Isooctane-Propanol	500	400		389	310
	14A	Isooctane-Propanol	500	400		335	310
	15	Isooctane-Propanol	500	800		422	≃380
	16	Isooctane-Propanol	100	800		142	≃390
	17	Propanol	500	600	By weight loss	127	≃500
	18	Isooctane	100	500-350		168	342
	19	Isooctane	500	1100-500		567	342
	20	Polystyrene	500	500-400		52	60
	23	Isooctane	100	400	By flow rates	188	195
	24	Isooctane	100	200	and physical calibration	155	195
	25	Propanol	100	200		198	250
	26	Propanol	100	400		280	≃300
	27	Propanol	250	400		339	≃400
	27A	Propanol	250	400		323	≃400
	28	Propanol	250	400		366	342

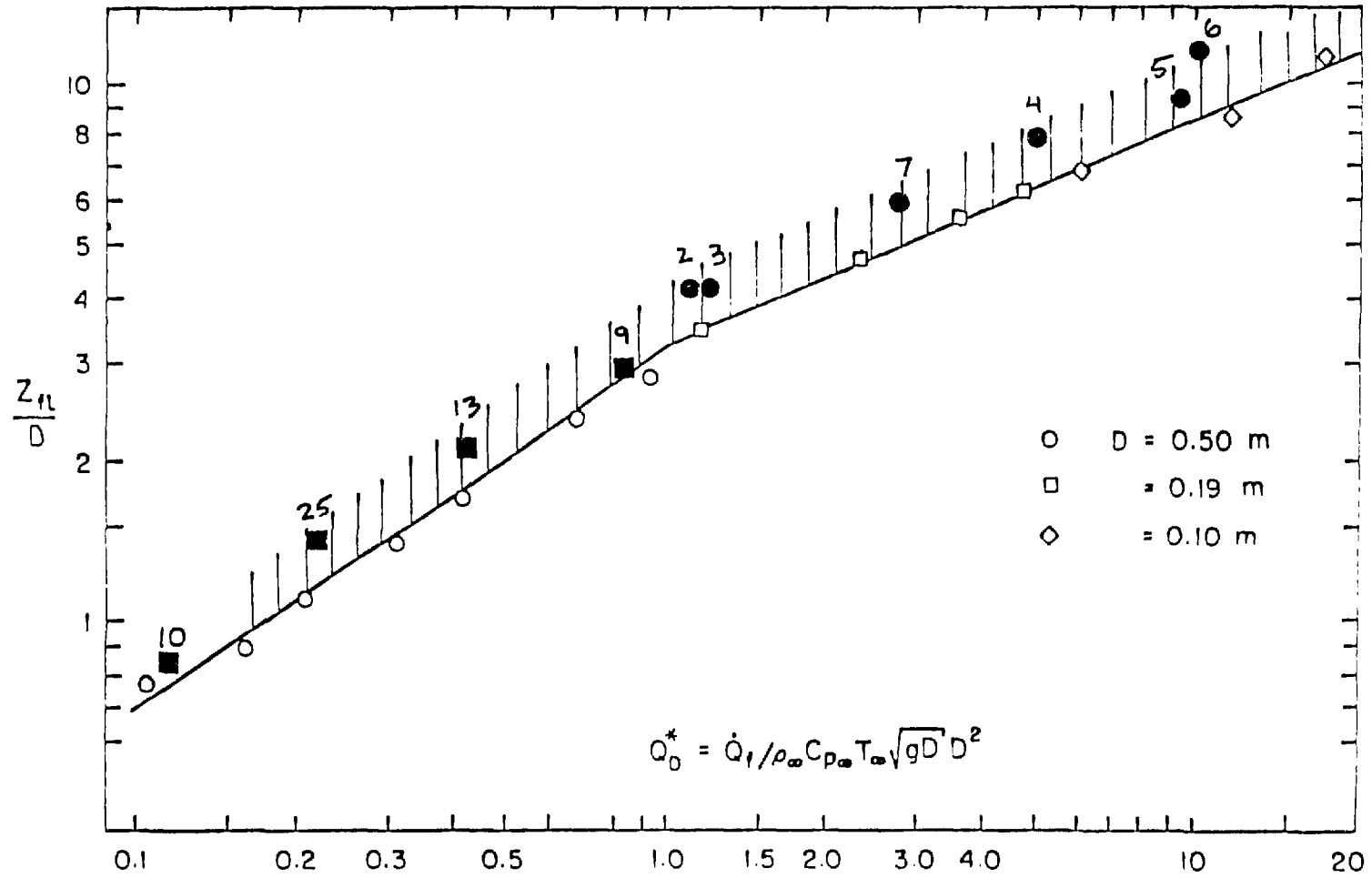

Figure 29. Comparison of FY 82 LLNL model test data with Zukoski's calculations.

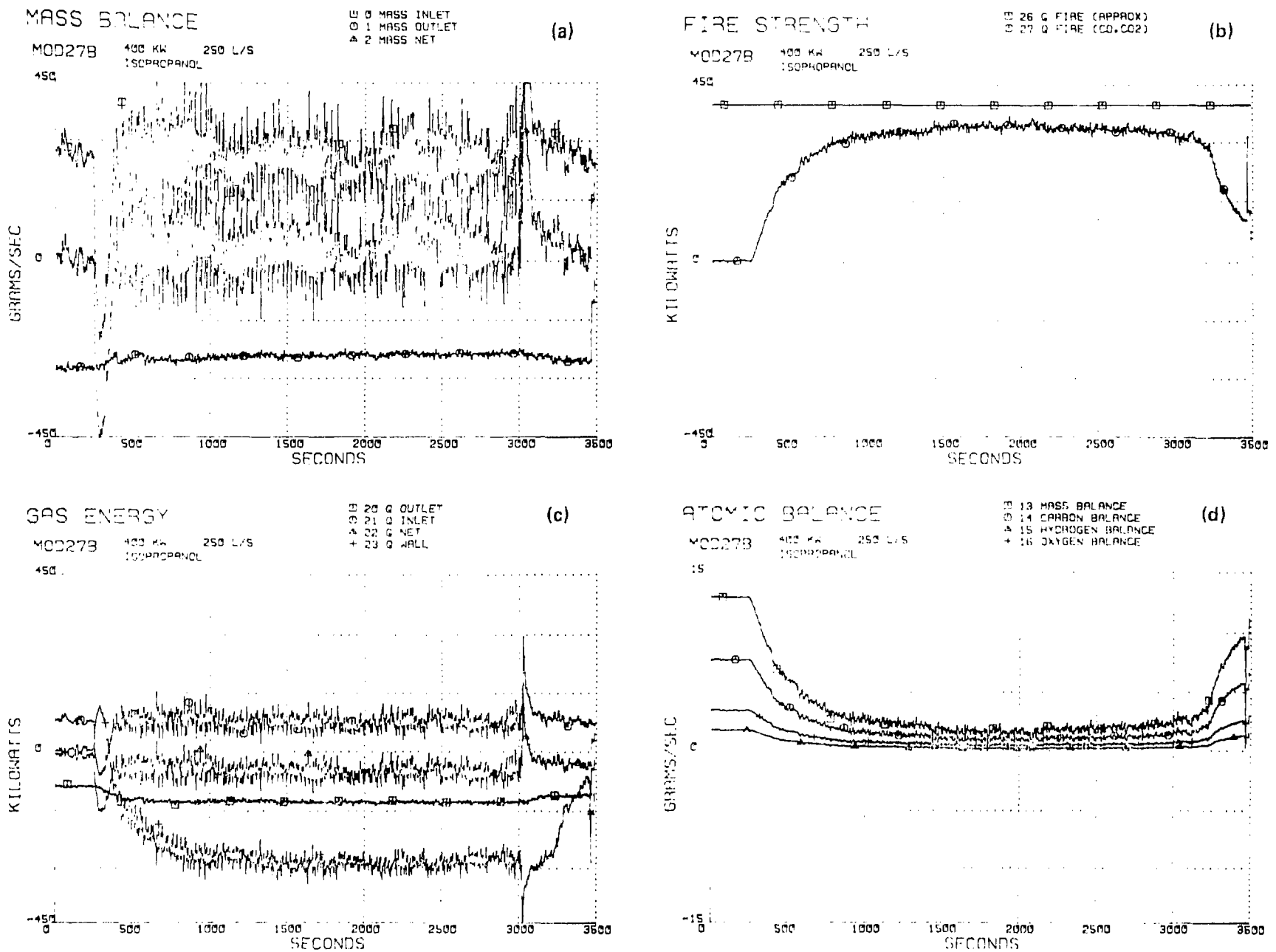

Figure 30. Four views of Mod 27B profile (a) mass balance, (b) fire strength, (c) gas energy, and (d) atomic species balance.

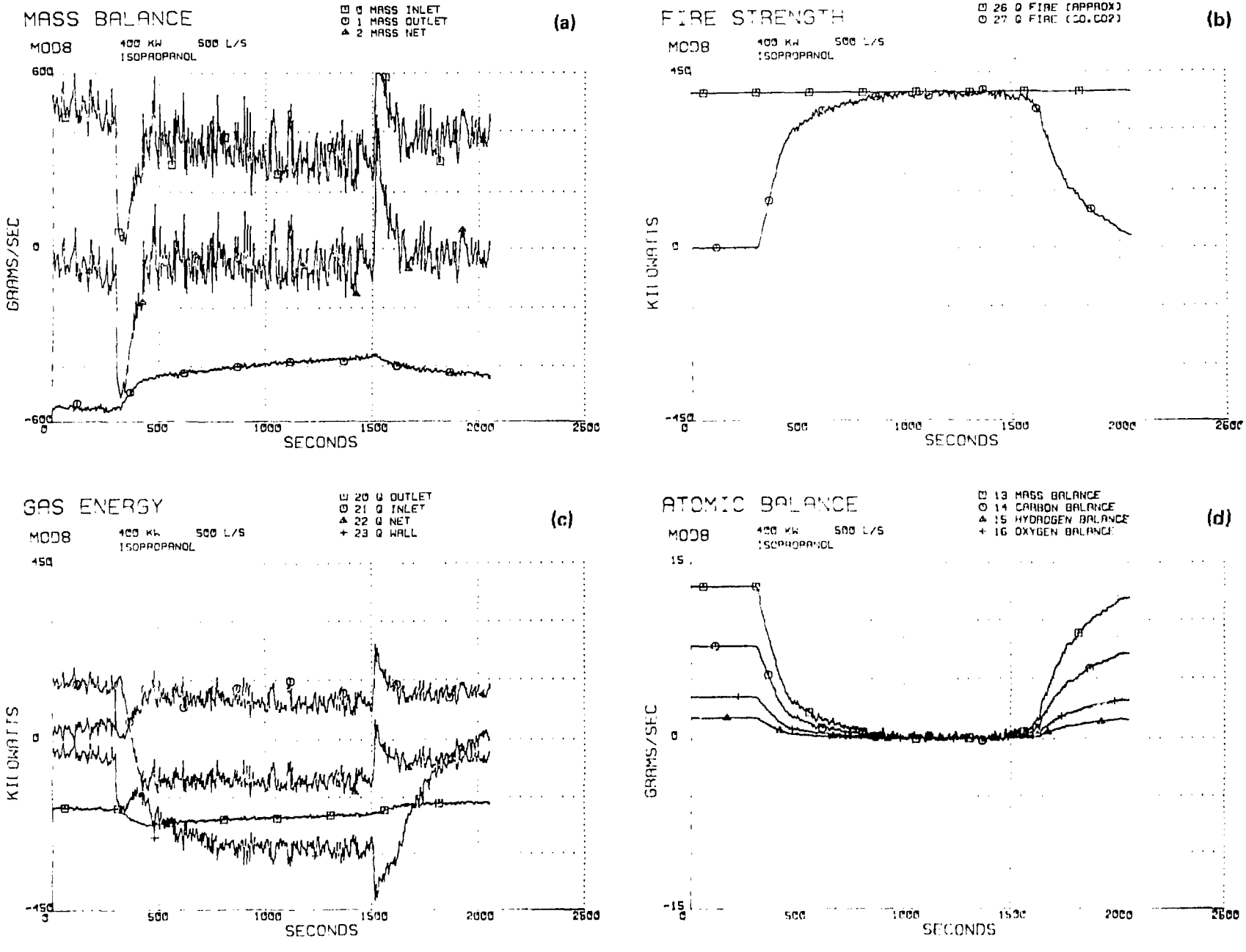

Figure 31. Four views of Mod 8 (a) mass balance, (b) fire strength, (c) gas energy, and (d) atomic species balance.

Table 9. FY 82 results for fire modeling.

MOD No.	Q (kW)	Fuel flow (l/s)	Fuel formula	Inlet reversal bottom value	Observed flame height (m)	Steckler layer height (m)	Exit and air temp. (°C)	Top wall temp. (°C)	% Heat loss to walls	O_2 consumed (g/s)	CO_2 (g/s)	CO (g/s)	CH_4 (g/s)
10	100	100	C_3H_8O	-180[a]	0.8	1.27	100	80	87	2.4	5.8	–	–
4	230	100	CH_4	-200	2.2[b]	1.36[c]	170	150	95	13.8	10.7	1.3	0.3
24	200	110	C_8H_{18}	-80	1.1[d]	1.05	150	145[e]	83	10.3	10.5	0.3	0.07
25	200	90	C_3H_8O	-260	1.3	1.24	160	160[e]	86	14.2	12.5	1.7	0.03
6	400	100	CH_4	-440	3.0[b]	1.39[c]	200	160	100[f]	12.4[g]	9.9	1.5	0.58
6A	400	100	CH_4	-430	3.0[b]	1.39[c]	190	170	100[f]	13.7[g]	10.8	2.2	0.61
23	400	130	C_8H_{18}	-300[a]	1.1	1.12	180	150	83	15.9	13.1	–	0.66
26	400	100	C_3H_8O	-300	1.6	1.11	180	180[e]	–	17.8	14.7	5.3	0.37
5	455	500	CH_4	-150	2.5[b]	1.44[b]	280	210	83	36.0	32.6	–	0.04
8	400	500	C_3H_8O	+20	1.6	1.24	200	160	83	29.0	30.3	–	–
13	400	500	C_3H_8O	-60	1.6	1.12	230	180	79	20.9	31.5	–	–
14	400	500	C_8H_{18}	+40	1.5	1.04	200	150	79	12.4[g]	27.1[g]	–[g]	0.04
14A	400	500	C_8H_{18}	-60	1.5	0.90	200	150	68	13.9[g]	23.4[g]	–[g]	0.04
9	800	500	C_3H_8O	-170	2.3	1.10	280	225	88	55.2	50.5	13.2	2.0
9A	800	500	C_3H_8O	-200	2.3	1.47	280	220	87	44.8	46.9	4.3	1.9
15	800	500	C_8H_{18}	-360	1.7 +	1.11	255	200	82	17.0[g]	29.4[g]	–[g]	1.7
1	135	250	CH_4	-100	1.6	1.45[c]	130	90	84	8.7	8.7	–	–
7	135	250	CH_4	-100	1.6	1.24	140	105	82	9.3[h]	9.6	–	–
27	400	250	C_3H_8O	-180	1.7 +	1.10	220	220[e]	95	23.6	21.4	2.9	0.02
27A	400	250	C_3H_8O	-400[a]	1.7 +	1.02	210	200[e]	91	20.7	23.3	–	0.14
27B	400	250	C_3H_8O	-160	1.6	1.05	205	185[e]	89	24.9	26.4	–	0.11
17	600	500	C_3H_8O	-180	2.0	1.08	250	195	63	5.6[g]	6.8[g]	2.2[g]	–
18	400	100	C_3H_8O	-460	1.6	1.12	160	150	83	9.3[g]	7.6[g]	4.3[g]	–
19	1100	500	C_8H_{18}	-330	2.0 +	1.09	255	200	–	36.3	29.0	9.9	–
12	800	100	C_3H_8O	600	2.5	–	–	–	–	–	–	–	–
16	800	100	C_8H_{18}	700	1.7 +	–	–	–	–	–[g]	–[g]	–[g]	–

[a] *Besides a gradual flow reversal, there was an extreme spike.*

[b] Note that the flame was in the hot layer.

[c] Test was terminated before it reached quasi-equilibrium.

[d] This fire did not fill the pan.

[e] The polystyrene fire changed the heat transfer of the walls. We can note the difference in the temperatures of the test runs after the the polystyrene.

[f] This fire should have been a 200 kW fire, but it was a 100 kW fire for the first two minutes.

[g] A leak in the sample diluted all of these measurements.

[h] *MOD 7 ran 800 seconds longer than MOD 1.*

Fire Chemistry: Thermal Degradation of Cable and Wire Insulations

Introduction

Last year's study on thermal degradation of PVC and rubber cable insulations showed that the decomposition of the insulations is influenced by the additives that are incorporated into the plastic formulations. Some of the additives, such as alkyl phthalates or adipates, enhance the degradation rate of the pure polymer and/or themselves thermally degrade into flammable species that feed the flames. We also learned that the formation rate of corrosive products, mainly HCl, is enhanced by higher rates of heating. However, higher heating rates do not increase the total HCl production. The amount of HCl released into the environment is governed by acid acceptors (e.g., ZnO, MgO, Sb_2O_3 and $CaCO_3$) incorporated into the plastic formulations. Flame retardants like Sb_2O_3, alumina trihydrate, and triaryl phosphates increase the extent of charring and decrease the degradation rate, especially in the dehydrochlorination region.[3]

This year we subjected the PVC and previously studied rubber insulations to heating rates of 80 and 160°C/min to see what effect these may have on the degradation rate of the plastic formulations, and we also extended our detailed studies to other wire and cable insulations, including additional rubber insulations, polyethylene, polypropylene, nylon, polyurethane and mylar. Samples were subjected to differential scanning calorimetric analysis (DSCA) and to thermogravimetric analysis (TGA) at several heating rates to determine the effect of heating on the temperature responsible for the onset of initial weight loss, the generation rate of corrosive products, and the amount of residual ash. In addition, we subjected the gaseous and liquid pyrolyzates to gas-chromatographic and mass-spectrometric analysis.

Experimental Procedure

In the first set of experiments, we heated virgin polymers and various cable and wire insulations in air in our thermogravimetric analyzer at rates of 10, 20, 40, 80 and 160°C/min from ambient temperature to 900°C. As reported previously, we monitored the samples' weights and the generation of acidic components as a function of temperature. As before, the acidic components and other thermal degradation products were directed to a container filled with 200 ml of distilled water buffered to a pH of 6.8–7.0. The aqueous solution was gently stirred with a magnetic stirrer to achieve uniform mixing and the change in pH was measured with a pencil-size pH reference electrode and recorded on a multichannel recorder.

DSC analysis was performed on a DuPont-900 differential scanning calorimeter using a standard cell. Our samples weighed between 5 and 10 mg and all were heated in air at 20°C/min.

In the second set of experiments, we sought to identify the major degradation products formed during the initial and most active phases of pyrolysis. Such knowledge is particularly useful when choosing or designing early-warning smoke alarm systems, or identifying formulations that contain highly flammable additives or contain additives which in themselves are not flammable but form highly flammable species at high temperatures that contribute to flamespread.

Degradation products were either generated in the thermogravimetric analyzer or in a tube pyrolyzer. All samples were pyrolyzed in air and the degradation products were collected in a liquid-nitrogen-cooled trap. We chose the pyrolysis temperature used in the tube pyrolyzer on the basis of our TGA results; the pyrolysis temperature was set at temperatures responsible for the initial as well as the main degradation phase. After collection, a plastic bag was wrapped tightly over the top of the liquid-nitrogen-cooled trap and then the trap was brought to room temperature. This technique separated the gaseous components from the liquid pyrolyzates and allowed for simultaneous gas chromatographic analysis of both the gaseous and liquid mixtures. Aliquots of 4.0 cc of the gaseous mixtures were injected into a 10 ft × 1/4 in. glass column packed with 0.19% picric acid on 80/100 Carbopack C. The column was held at 40°C for 2 minutes, then programmed to 55°C at 15°C/min and held at this temperature for 10 minutes. To separate out the heavier gaseous components, the column was next raised to 70°C at a rate of 15°C/min and allowed to remain there until the end of each run. We used nitrogen as our carrier gas at a flow rate of 30 ml/min and the injection port and a flame ionization detector were both set at 100°C. The compounds comprising the gaseous mixture were identified by comparing the

retention times with the retention times of standard compounds.

The glass trap was next washed with methylene chloride and the solvent containing the liquid pyrolyzate was concentrated down to 0.5 ml. A 3-μliter aliquot was then injected into a 25-m Carbowax-20M fused-silica capillary column, a 25-m SE-30 fused-silica capillary column, and a SE-54 fused-silica capillary column. The use of the polar and non-polar general purpose columns, as well as the SE-54, which is designed for separation of the polycyclic components, gave us a better idea of the pyrolyzate mixture. As mentioned in previous reports, the column oven was programmed to heat from 70°C to 220°C at a rate of 10°C/min. Helium flow rate was maintained at 6 ml/min, and the injection port, mass-spec transfer line, and jet separator were set at 250°C. The components that comprised the separated peaks were identified with the help of our computerized spectral library system.

Experimental Results

PVC

The PVC insulations used in our experiments were designed for high-power cables, multistrand general-purpose cables, and general appliance cables.

Detailed description of the thermograms of the various PVC cables appeared in last year's report.[3] This year's data on the effect of higher heating rates on the degradation mode of the various Neoprene insulations we tested is summarized in Table 10. We see that higher heating rates do not drastically alter the temperature responsible for the onset of weight loss in either the main degradation phase or the subsequent phase or phases of degradation. The small variations in temperature leading to the onset of weight loss in the second and third phases seem to be within experimental error and cannot be attributed primarily to heating rates. As expected, higher heating rates increase degradation rates with the most pronounced effect being in the main phase of pyrolysis that is responsible for the production of HCl. Although faster heating rates tend to meld the different degradation phases, and it appears that the length of the main phase increases with the faster heating rates, the total amount of HCl formed during pyrolysis remains constant at all heating rates (Fig. 32).

Weight-loss rates varied among the different PVC formulations, and, in general, seemed to be lower than those of virgin PVC. The total weight loss in each region was also governed by the additives present and varied from one formulation to another. The different additives also influenced the amount of char formed at the end of pyrolysis. For example, at a heating rate of 40°C/min, PVC-3 left a char residue of 11%, PVC-95 left a 23% char, and PVC-104 left a char residue of 5%. In contrast, virgin polymer did not leave any residue. The principal char-forming additives used in PVC formulations associated with fire retardance are Sb_2O_3, alumina trihydrate, calcinated clay, and phosphate esters. Depending upon the manufacturer, commonly used PVC formulations contain anywhere between one and three of the above mentioned additives in a single formulation.[3]

Last year's gas-chromatographic, mass-spectrometric analyses of the liquid pyrolyzates showed that the largest variety of products are formed in the dehydrochlorination region, or the main decomposition phase, and the components collected in subsequent phases consist mainly of polynuclear hydrocarbons. Since these results did not include analysis of the gaseous pyrolyzates, and since we felt there may have been some loss of the liquid pyrolyzate through condensation on the walls of the TGA furnace tube, this year's work included analyses of the gaseous products as well as repeat analyses of the liquid products generated in the tube pyrolyzer. The tube pyrolyzer allowed us to use larger samples as well as diminish some of the liquid-pyrolyzate loss through condensation prior to liquid nitrogen trapping.

Gas-chromatographic analysis results of the gaseous products of virgin PVC and a representative PVC insulation are shown in Figs. 33(a) and (b). The chromatograms show that both virgin PVC and the PVC-104 give off methane, ethylene, acetylene, ethane, propane, propylene, propyne, isobutane, n-butane and 1-butane, isobutylene and ethylacetylene. In addition, PVC-104 shows 1,3-butadene, pentane, 4-methyl-pentene-1, and cis-hexene-2. All except 1,3-butadiene elute between 16 and 45 minutes after injection (not shown in these chromatograms) and appear in PVC-3 and PVC-78. We attribute these formations to the degradation of some of the additives used in the formulations. Results of the analysis of the liquid pyrolyzate are summarized in Appendix B (Figs. B1–B4). The chromatograms show that although the dehydrochlorination region leads

Table 10. The effect of heating rate on the thermal degradation of PVC.

Sample	Heating rate (°C/min)	Main phase[a]-1st phase		2nd phase		3rd phase		Wt loss in main phase (%)	Char at end of pyrolysis (%)
		Onset of wt loss (°C)	Degradation rate (%/min)	Onset of wt loss (°C)	Degradation rate (%/min)	Onset of wt loss (°C)	Degradation rate (%/min)		
PVC-3	10	290	9.0	432	1.7	515	21.2	41.5	16[a]
	20	280	16.0	425	3.5	510	22.0	46	15
	40	260	37.0	390	6.0	480	23.0	51	11
	80	290	80.0	420	20.0	430	26.0	56	8
	160	308	59/30 s[b]	418	22.0	520	45.0	59	8
PVC-104	10	270	9.0	441	6.5	530	4.0	9	14
	20	255	11.0	410	12.5	510	6.0	9	14
	40	270	28.0	400	4.0	515	21.0	18	5
	80	270	40.0	380	35.0	500	25.0	20.5	5
	160	280	25/12 s[b]	365	33/30 s[b]	510	30.0	25.5	5
PVC-95	10	262	12	402	2.5			31	23
	20	270	22	405	3.0			30	23
	40	280	40	406	5.0			34	23
	80	280	80	420	12.0			51	10
	160	260	51/18 s[b]	410	18.0			53	13
Virgin PVC	10	257	18	403	3.0			29	0[a]
	20	265	30	411	10.0			41	0
	40	260	56	405	14.5			47	0
	80	285	70	420	11.0			52	0
	160	270	60/30 s[b]	380	45.0			60	0

[a] pH change in main phase that occurred in PVC-3 and virgin PVC at 10 and 20 °C/min was 7.10 and 4.42 and 7.14 and 3.7%, respectively.

[b] Degradation rate occurred in less than 1 minute (example: 25% in 12 seconds).

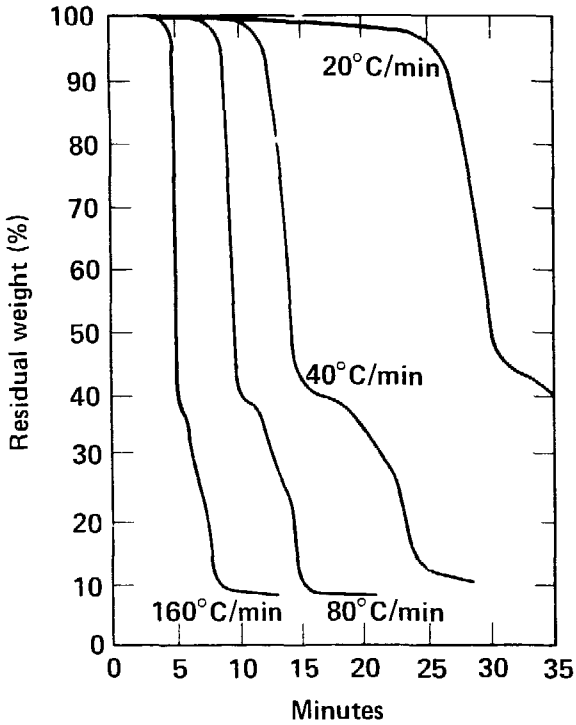

Figure 32. Effect of heating rate on thermal degradation of PVC.

mainly to the production of HCl, other compounds, predominantly of an aromatic nature, are also formed. Some of the compounds are degradation products of plasticizers, e.g., phthalic anhydride, from dioctylphthalate in PVC-3 and PVC-78, and lauric acid from dibutylene dilaurate and stearic acid from calcium stearate present in PVC-104.

Rubber Insulations

We used rubber insulations designed for high-power, high-current cables, welding cables, single-conductor high-voltage cables, and multiconductor power cables. The insulations consisted of Neoprene, or polychloroprene, chlorinated and sulfonated polyethylene, and other synthetic rubbers. The insulations designated as Neoprene-007, Neoprene-84, Neoprene-435 and Rubber-134 were studied extensively last year.[3] This year, we extended our detailed studies to five other rubber insulations and we performed additional thermogravimetric analyses and gas-chromatographic analyses on the gaseous pyrolyzates of the previously studied formulations.

The effects of heating rates as high as *80°C/min* and *160°C/min* on the degradation of Neoprene-007, -84, -435, virgin polychloroprene, and rubbers are shown in Table 11. As we previously described, the higher heating rates do not lower the temperature responsible for initial degradation of the various insulations. Higher heating rates increase the degradation rates of all the insulations and therefore lead to faster production of HCl. Of the insulations studied, Neoprene-435 degrades the fastest and Neoprene-84 degrades the slowest and leaves the most char. The very high heating rates appear to meld the phases of pyrolysis, and, as a result, it seems that the main phase of pyrolysis has become extended in the process. However, the total amount of HCl formed remained constant at the higher heating rates.

Figure 34 contrasts the thermograms of four rubber formulations heated in air of 20°C/min. The greatest difference appears in rubber-12 which is an insulation used for high-voltage cable. Degradation begins at 285°C; however, the main degradation phase does not start until 415°C and this leads to a char residue of 54.5%. Rubber-1138 and -138 require 385°C and 388°C, respectively, to start their main phases, but they leave a char residue of 11% and 25%. All three formulations show very low H_3O^+ production. As mentioned in our previous reports, the low amount of HCl and its detection at higher temperatures might be due to the presence of H_3O^+ acceptors such as Sb_2O_3, MgO, or ZnO, that react with the HCl evolved at lower temperatures. Rubber-1132 produces copious amounts of HCl, leaves a low amount of char, and shows that its main degradation phase starts at a relatively low temperature.

The effect of higher heating rates, as shown in Table 11, is most pronounced on the decomposition rates in the main phase of pyrolysis which, in the case of rubber-12, occurs in the second phase of pyrolysis. In this series of formulations, the fastest degradation rates appear in rubber-1132, which is also a high HCl producer, and the lowest degradation rates appear in rubber-1138, which is a very low acid producer. Higher heating rates tend to blend all the phases together and the weight loss in the main phase, consequently, appears to be larger. Figure 35 further illustrates the effect of additives on the degradation scheme of the insulations. Thus, rubber-12 shows an exotherm at 280°C that is probably due to decomposition of the metal oxide, an exotherm (which begins at 360°C) that can be attributed to loss of water from $CaCO_3$, and a series of exotherms that begin at 405°C and are attributed to decomposition of this insulation as well as the plasticizers. Rubber-1138 shows an endotherm at 100°C that is

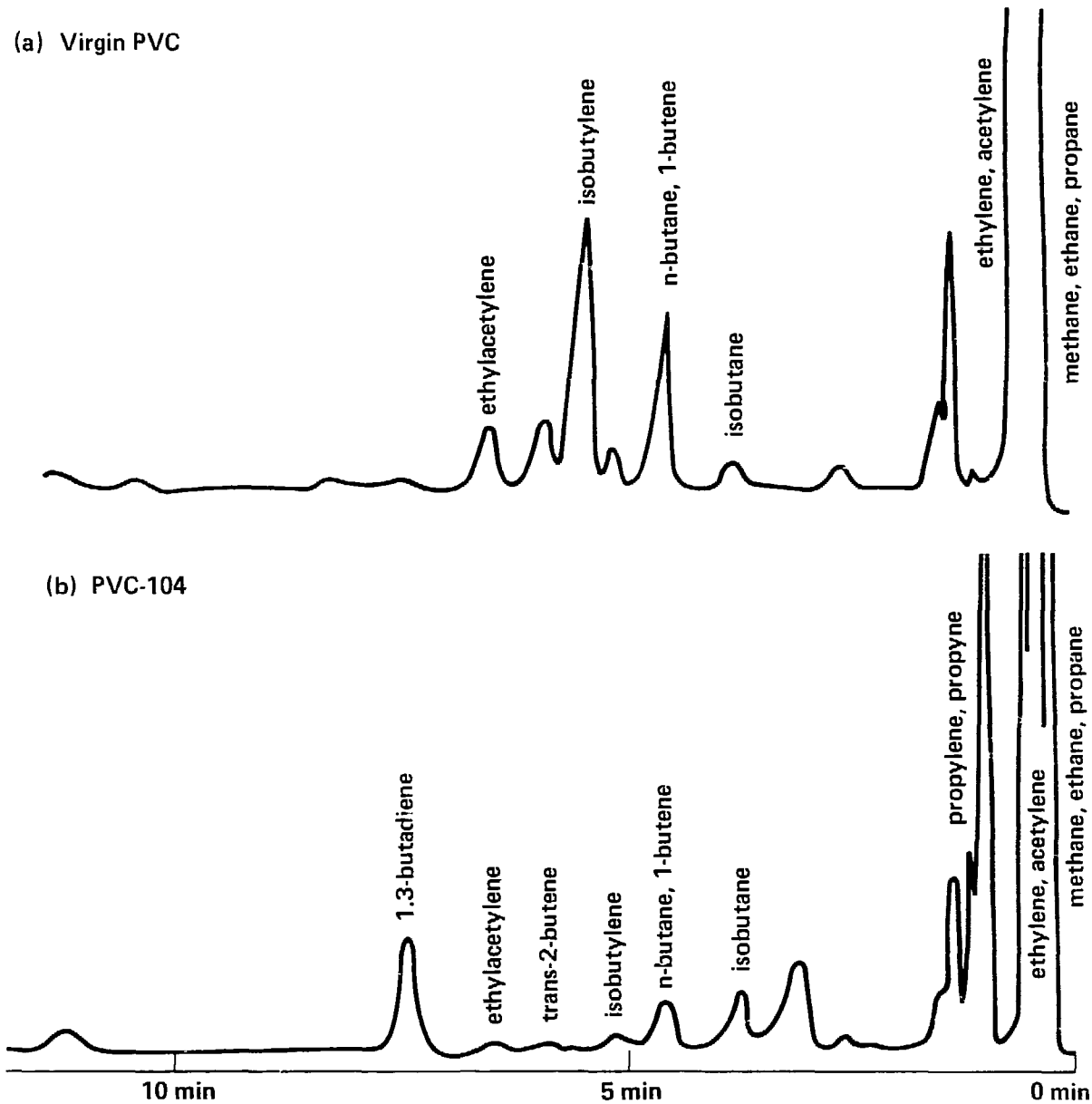

Figure 33. Comparison of gaseous degradation products of virgin PVC with those of PVC-104.

due to water and a series of exotherms beginning with one at 375°C, which again could be due to loss of water from $CaCO_3$, and several exotherms starting at 410°C that we attribute to dehydrochlorination of this insulation and degradation of the plasticizer. Rubber-138 shows an endotherm at 80°C that is moisture loss, an indication of an exotherm at 375°C, again due to water loss from $CaCO_3$, and an exotherm at 425°C that occurs in the dehydrochlorination region of the formulation. Rubber-1132, which is a high acid producer, has three exotherms: one at 287°C, another starting at 318°C which we attribute to the degradation of the insulation and the plasticizer, and the third one at 425°C which we attribute to the oxidation of the highly crossed-linked region.

Results of the gas-chromatographic analysis of the gaseous products of virgin Neoprene and rubber-12 (which is a low acid producer) show the following hydrocarbons: methane, ethylene, acetylene, ethane, propane, propylene, propyne, isobutane, n-butane, 1-butene, isobutylene,

Table 11. The effects of heating rates on the thermal degradation of various rubber insulations.

Sample	Heating rate (°C/min)	Main phase-1st phase: Onset of wt loss (°C)	Main phase-1st phase: Degradation rate (%/min)	2nd phase: Onset of wt loss (°C)	2nd phase: Degradation rate (%/min)	3rd phase: Onset of wt loss (°C)	3rd phase: Degradation rate (%/min)	Wt loss in main phase (%)	Char at end of pyrolysis (%)
Neoprene-007	10	290	7.0	495	11.0	578	2.0	5	25[a]
	20	300	13.0	512	12.5	608	10.0	11	24.5
	40	305	21/6 s[b]	403	11.0	575	8.0	22	22.0
	80	305	27/6 s[b]	485	29.0	630	17.5	18	20.0
	160	290	24/3 s[b]	425	25.0	622	22.0	25	21.0
Neoprene-84	10	235	3.0	355	1.5	498	12.0	4	48[c]
	20	238	5.0	325	3.5	505	14.0	4	44
	40	240	8.0	340	5.0	520	15.5	7	46
	80	260	38.0	360	20.0	560	19.0	9	44
	160	260	11/6 s[b]	380	36.0	588	15.0	10	44
Neoprene-435	10	283	11.5	368	1.5	480	13.5	7	7.5[d]
	20	308	27.0	387	2.0	522	14.0	15	6.0
	40	310		390	3.9	445	17.0	27.5	7.0
	80	310		blends with 3rd phase		440	28.5	30.0	12.0
	160	300		blends with 3rd phase		420	33.5	36.0	17.0
Rubber-134	10	248	7.5	420	1.7			38	8[e]
	20	240	14.5	410	2.4			31	26
	40	230	37.8	400	6.5			39	11.5
	80	260	68	405	10			51	11
	160	290	55/30 s[b]	380	21.5			56	12.5
Virgin polychloroprene	10	323	8.0	410	4.0	480	15.0	16	2.0[f]
	20	325	16.0	425	7.0	500	16.0	20	1.0
	40	309	47.1	400	12.0	485	25.0	25	1.0
	80	315	56.0	430	17.0	540	22.0	35	0
	160	310	39.5/10 s[b]	415	20.0	530	30.0	–[g]	
Rubber-1138	10	380	7.0	470	10.0	510	30.0	20	10[h]
	20	385	12.0	490	21.0			23	11
	40	370	21	510	20.0			33	8.3
	80	368	36	530	24			27	17.7
	160	325	33	530	30			38	18

Table 11. (Continued)

Sample	Heating rate (°C/min)	Main phase-1st phase: Onset of wt loss (°C)	Main phase-1st phase: Degradation rate (%/min)	2nd phase: Onset of wt loss (°C)	2nd phase: Degradation rate (%/min)	3rd phase: Onset of wt loss (°C)	3rd phase: Degradation rate (%/min)	Wt loss in main phase (%)	Char at end of pyrolysis (%)
Rubber-1132	10	255	12	390	1.5[i]			22	15.3[j]
	20	250	19	395	3.3			28	13.8
	40	245	38	392	7.0			35	15
	80	270	76	405	13.5			40	13
	160	280	21/18 s[b]	390	21.0			44	20
Rubber-138	10	390	7	490	25			21	22[k]
	20	388	10	493	25			19	25
	40	380	27	505	20			30	20
	80	380	48	520	24			38	9
	160	340	74	510	24			50	9
Rubber-12[l]	10	260	1	417	32			14	54.5[m]
	20	285	3	415	25			22	54.5
	40	280	5	395	37			21	54.5
	80			395	46			24	57.3
	160			370	25/36 s[n]			27	57.3

[a] pH change in main phase for Neoprene-007 that occurred at 10 and 20°C/min was 7.18 and 3.96, respectively.

[b] Degradation rate took less than 1 minute (example: 21% in 6 seconds).

[c] pH change in main phase for Neoprene-84 that occurred at 10 and 20°C/min was 7.14 and 5.10, respectively.

[d] pH change in main phase for Neoprene-435 that occurred at 10 and 20°C/min was 7.1 and 3.39, respectively.

[e] pH change in main phase for rubber-134 that occurred at 10 and 20°C/min was 7.07 and 4.48, respectively.

[f] pH change in main phase for virgin polychloroprene that occurred at 10 and 20°C/min was 7.28 and 3.85, respectively.

[g] pH change at 45.

[h] Low acid.

[i] There was no third phase for rubber-1132, -138, or -12.

[j] High acid.

[k] pH change in main phase that occurred at 10 and 20°C/min was 7.23 and 6.58, respectively.

[l] Second phase became the main phase.

[m] pH change in main phase that occurred at 10 and 20°C/min was 7.19 and 7.00, respectively.

[n] Degradation rate occurred in less than 1 minute (example: 25% in 36 seconds).

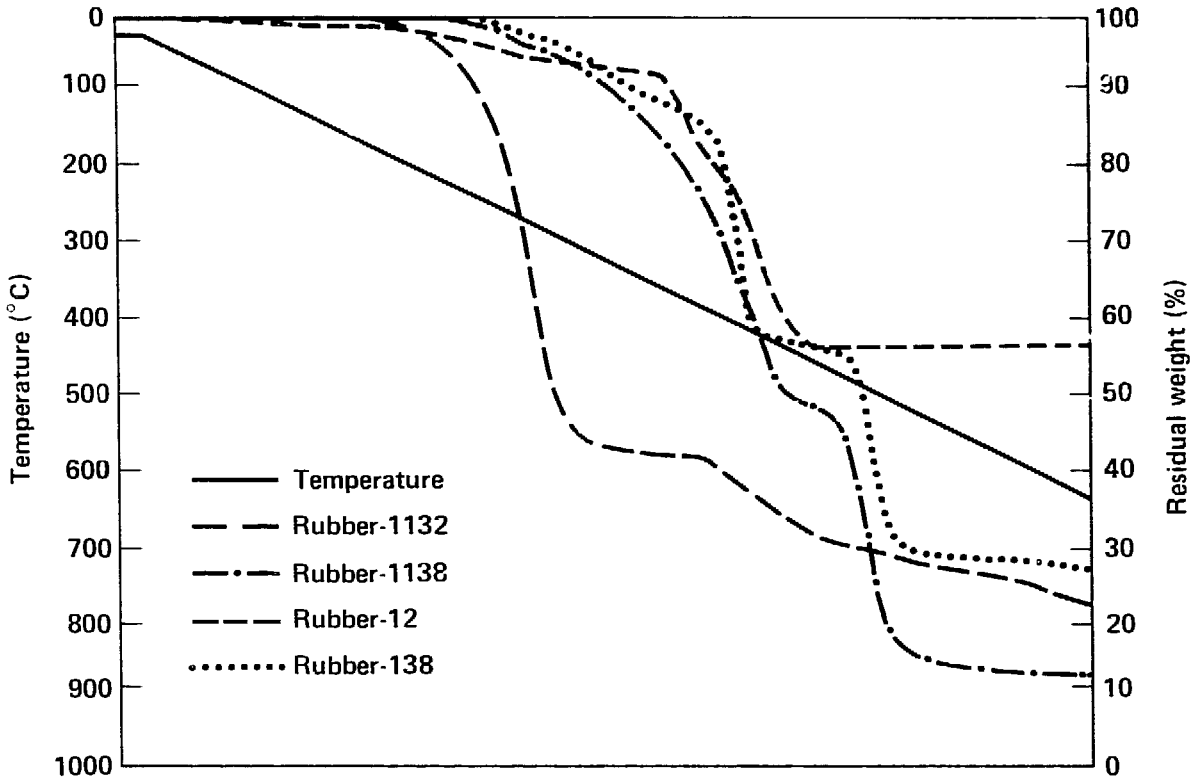

Figure 34. Thermograms of rubber insulations heated in air at 20°C/min.

cis-2-butene, trans-2 butene, ethylacetylene, 1,3-butadiene and 4-methyl-pentene-1. The two insulations also formed 4-methyl-pentene-2 and cis-hexene-2. The virgin neoprene produced approximately four times as much of the light hydrocarbons as did the insulations. Results of the gas-chromatographic, mass-spectrometric analysis of the liquid pyrolyzates from Neoprene-007, -84, -435 and Rubber-134 on a Carbowax-20M fused-silica capillary column have been presented previously.[3] Additional analysis results of virgin Neoprene, Neoprene-007 and Neoprene-435 pyrolyzates were obtained from the SE-54 fused-silica column and are presented in Appendix B (Figs. B5–B7). Our chromatograms showed additional aromatic and polycyclic compounds previously undetected on the Carbowax-20M column. These are substituted benzenes and naphthalenes as well as other cyclic compounds. As expected, the insulations show such products as substituted phthalates and adipates which are degradation products of the plasticizers used in the formulations.

The results of the gas-chromatographic, mass-spectrometric analysis of the liquid-pyrolyzate cable formulations rubber-12, -138, and -1138 are shown in Appendix B (Figs. B8–B10). The pyrolyzates of rubber-12 and -138 show high molecular-weight hydrocarbons as well as some aromatic compounds. In addition, rubber-138 shows palmitic acid and dioctylphthalate, which are degradation products of the plasticizers. The degradation products of rubber-1138 were generated in our large-scale test cell. They were collected on glass wool at one of the exits in the ductway, extracted in the Soxhlet extractor with 50 ml dichloroethylene, concentrated to 3 ml and injected in an SE-30 fused-silica capillary column. The liquid pyrolyzate contained high molecular-weight aliphatic hydrocarbons, breakdown products of phthalates and adipates which are used as plasticizers, as well as alkyl phosphates and silicates which are breakdown products of the flame retardants incorporated in these formulations.

Polyethylene

The polyethylene insulations used in our experiments were designed for small signal wires. The TGAs of the polyethylene insulations show several stages of pyrolysis that suggests the polyethylene used in these formulations is a low-density, highly branched polymer (Fig. 36). The

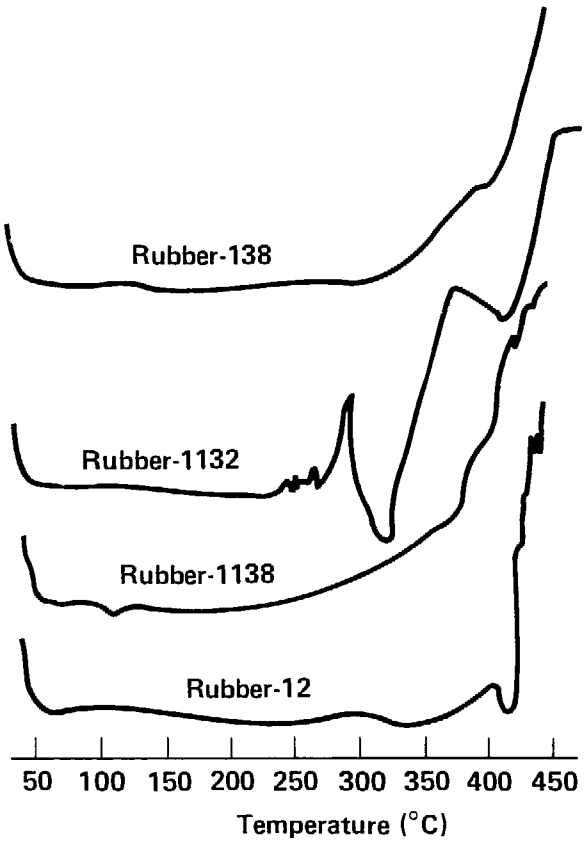

Figure 35. DSCs of rubber insulation heated in air at 20°C/min.

first stages of pyrolysis between 230°C and 325°C are due to the destruction of the branching points.[9] Higher temperatures between 325–365°C lead to chain scission and molecular enlargement, both of which occur simultaneously. Chain scission occurs via inter- and intramolecular hydrogen abstractions, and it is responsible for the formation of low molecular-weight compounds as well as other pyrolyzates.[9,10] Molecular-enlargement reactions, due to the combination of alkyl radicals, cause an increase in the long-chain, branched material. The last stage of pyrolysis in the range of 350° to 470°C is due to degradation of the polymer's char-like residue.

In comparing the degradation mode of the polyethylene-77 and -95 to that of virgin polyethylene, we see the degradation rate of the insulation in the initial stage of pyrolysis is slightly lower than that of the virgin polyethylene. However, the degradation rate of the polyethylene insulation in the active pyrolysis region is slightly higher than that of the virgin polyethylene. The oxidation of the polyethylene insulations' char-like residue begins at a slightly higher temperature than that of the virgin polymer. We attribute these differences to the additives incorporated into the insulation.

The effects of heating rates on the degradation of polyethylene-77, -95, and virgin polyethylene are summarized in Table 12. As expected, higher heating rates increase the degradation rates of all three formulations. Higher heating rates also increase the overall weight loss in the active pyrolysis region and therefore delay the onset of the third major phase of pyrolysis. Heating rates higher than 40°C/min meld the three major phases of pyrolysis into essentially one major phase that leaves no residue at the end of pyrolysis. We also found that heating rates of 40°C/min and higher decrease the temperature responsible for initial degradation as well as the active pyrolysis region of polyethylene-95. However, the same heating rates increase the temperature leading to initial degradation of polyethylene-77, and their effect is inconsistent on both the initial and the active pyrolysis region of virgin polyethylene.

DSCA results of polyethylene-95 in air showed an endotherm at 100°C, which we attributed to melting, and an exotherm at 224°C, which was due to oxidation, as evidenced by a slight weight gain in that region in our thermogravimetric experiments (Fig. 37). Another exotherm at 327°C appeared in the active pyrolysis region and corresponded to thermal decomposition. Polyethylene-77 showed an endotherm at 106°C, an oxidation exotherm at 258°C, and an exotherm at 315°C, which is the beginning of the active pyrolysis region. Virgin polyethylene also showed an endotherm at 100°C, an exotherm at 246°C, and a thermal degradation exotherm at 350°C. The slightly lower exotherms exhibited by polyethylene-95 is attributed to the additives.

The results of the analysis of the gaseous pyrolyzates of polyethylene-95 showed large amounts of methane, ethylene, acetylene, ethane, propane, propylene, propyne, n-butane and butene. In addition, the mixture showed some isobutylene, 1,3-butadiene, cis-2-butene, pentane, 4-methyl-pentene-1, and cis-hexene-2.

In contrast, virgin polyethylene showed copious amounts of all of the above identified C_1–C_6 hydrocarbons as well as some as yet unidentified hydrocarbon-type compounds. The constituents of the liquid pyrolyzates, shown in Appendix B (Figs. B11–B13), are long-chain saturated and unsaturated hydrocarbons and high molecular-weight aldehydes, alcohols, and esters.

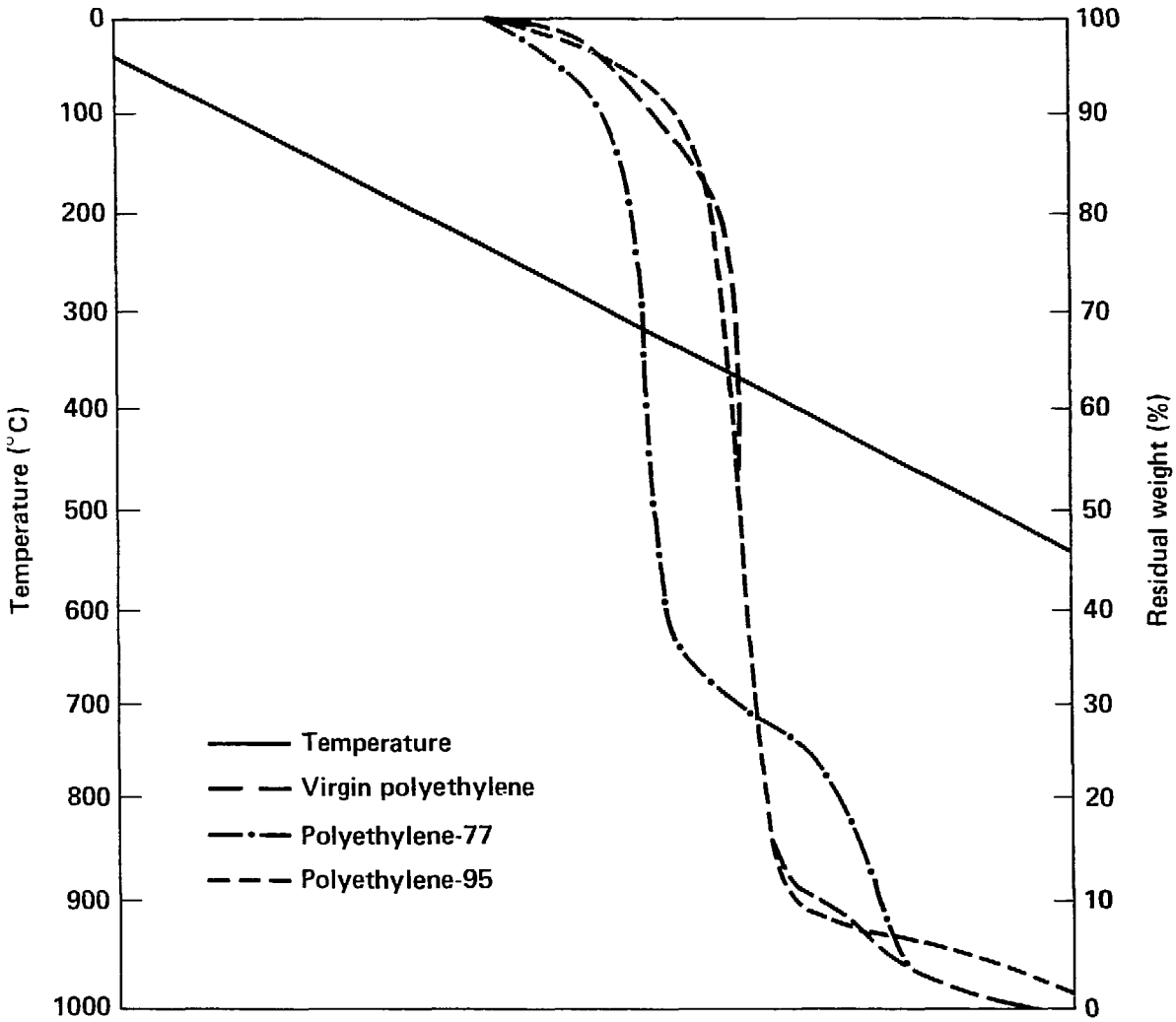

Figure 36. Thermograms of polyethylene heated in air at 20°C/min.

Polyethylene-95 also showed di-n-butylphthalate among its degradation products, which is due to the degradation of the plasticizer.

Polypropylene

We used polypropylene insulation designed for fiber optics' use.

Thermal decomposition of polypropylene involved both chain-scission and chain-transfer reactions as does polyethylene. In this polymer, every other carbon atom is tertiary, and thus both tertiary C-H bonds and all C-C bonds are readily susceptible to attack. TGA results of both the polypropylene-90 and the virgin polypropylene showed essentially one main phase of pyrolysis that, at a heating rate of 10°C/min, began at 250°C for both the insulation and the virgin polymer (Table 13). The main degradation phase was preceded by an induction period and followed by a short weight-loss region that was due to ignition of the carbonaceous residue. The oxidation of the carbonaceous residue began at lower temperatures when the samples were heated at a rate of 10 and 20°C/min, and, at the end of pyrolysis in the case of polypropylene-90, resulted in a char content of 3.5% and 7%, respectively. Virgin polypropylene leaves no char at the same heating rates. The degradation of the char of both the insulation and virgin polypropylene at heating rates of 40°C/min and above began at higher temperatures and left no char at the end of pyrolysis. The temperature leading to initial degradation of virgin polypropylene remained unaffected by higher heating rates. Polypropylene-90 had to be heated

Table 12. The effect of heating rate on the thermal degradation of polyethylene.

Sample	Heating rate (°C/min)	Main phase-1st phase Onset of wt loss (°C)	Main phase-1st phase Degradation rate (%/min)	2nd phase Onset of wt loss (°C)	2nd phase Degradation rate (%/min)	3rd phase Onset of wt loss (°C)	3rd phase Degradation rate (%/min)	Wt loss in main phase (%)
Polyethylene-95	10	250	0.75	325	21	350	rate of	35[a]
	20	250	1.5	350	45	380	degree	63
	40	230	4.0	330	65	380	impossible	60
	80	235	5.5	330	85	450	to	86
	160	230	14	320	98	450	determine	89
Polyethylene-77	10	235	1.5	335	10.5	350	rate of	11[b]
	20	245	3.0	315	52	358	degree	35
	40	250	7	320	86	phase	impossible	70
	80	260	13.5	335	80	disappears	to	80
	160	285	phase disappears	phase disappears	phase disappears		determine	95
Virgin polyethylene	10	250	1.5	325	15	360	rate of	50[c]
	20	270	1.8	345	46	370	degree	58
	40	245	4.0	348	70	375	impossible	62
	80	290	8.5	340	76	430	to	82
	160	250	17	310	98	430	determine	93

[a] At 10°C/min., there was less than 0.5% char for polyethylene-95. By 20°C/min., there was no char at all.

[b] pH change that occurred in main phase at 10 and 20°C/min was 7.10 and 6.77, respectively.

[c] pH change that occurred in main phase at 10 and 20°C/min was 7.15 and 6.73, respectively.

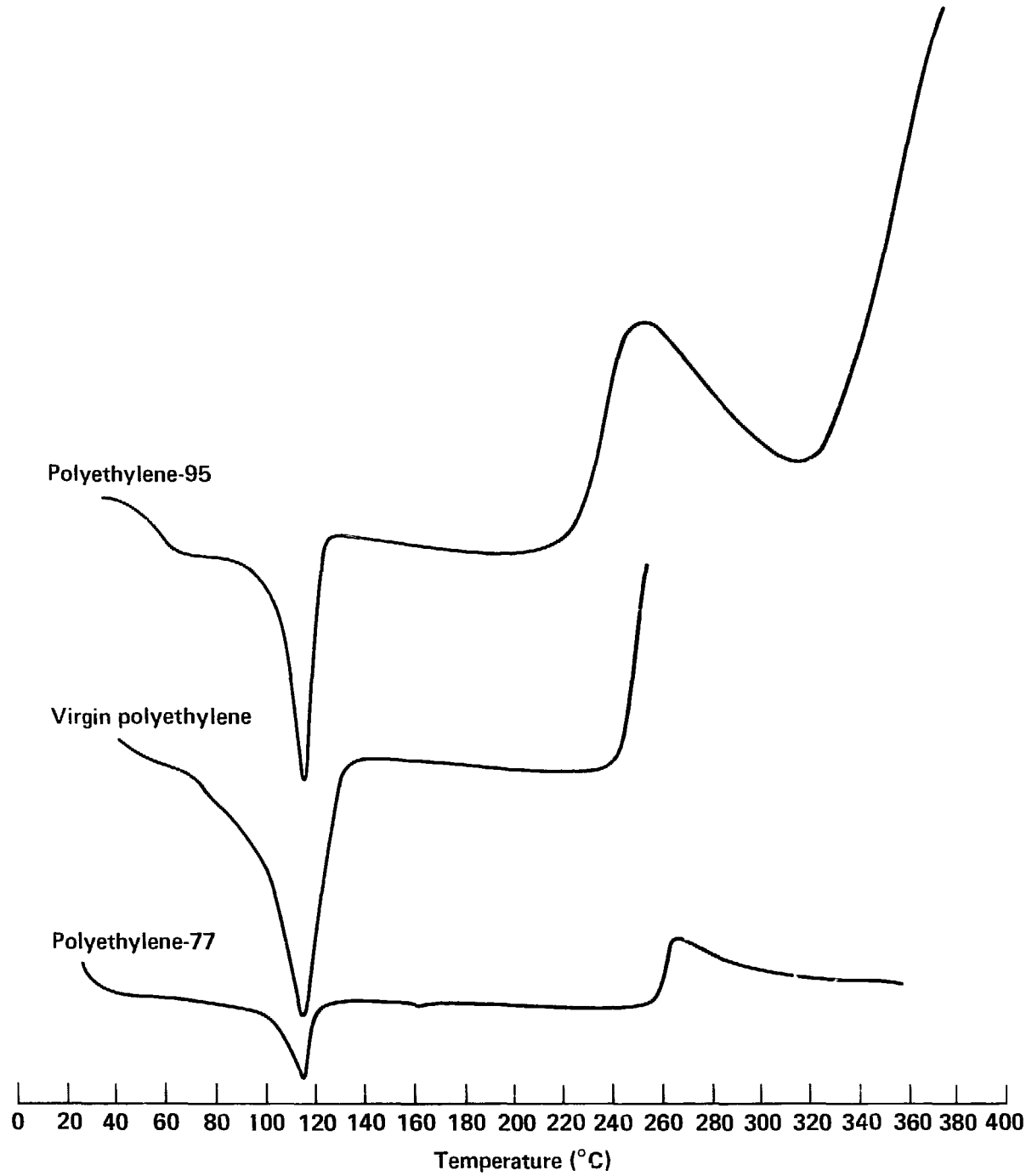

Figure 37. DSCA of virgin polyethylene, polyethylene-77, and polyethylene-95 heated in air at 20°C/min.

to 382°C when heated at a rate of 80°C/min, and to 370°C when heated at 160°C/min, to cause initial degradation. The rates of degradation in the main phase of pyrolysis of both the insulation and the virgin polypropylene increased with higher heating rates. Polypropylene-90 degraded faster at higher heating rates than did the virgin polypropylene at identical heating rates (Fig. 38).

DSCA at 20°C/min in air showed an endotherm at 144°C for both the polypropylene-90 and virgin polypropylene which we attributed to melting. Polypropylene-90 showed an exotherm at

Table 13. The effects of heating rate on the thermal degradation of polypropylene.

Sample	Heating rate (°C/min)	Main phase-1st phase: Onset of wt loss (°C)	Main phase-1st phase: Degradation rate (%/min)	2nd phase: Onset of wt loss (°C)	2nd phase: Degradation rate (%/min)	Wt loss in main phase (%)	Char at end of pyrolysis (%)
Polypropylene-90							
	10	250	14	300	impossible	60	3.5[a]
	20	250	24	320	to determine	69	7.0
	40	240	59	325	rate as phase	82	0
	80	382	50/30 s[b]	450	consists of	70	0
	160	370	75/18 s[b]	450	several sub-phases	77	0
Virgin polypropylene							
	10	250	18	295	impossible	60	0
	20	250	33	309	to determine	81	0
	40	250	55	330	rate as phase	79	0
	80	250	80	350	consists of	93	0
	160	250	95/30 s[b]	phase disappears	several sub-phases	96	0

[a] pH change that occurred at 10 and 20°C/min was 7.17 and 6.95, respectively.

[b] Degradation rate took less than 1 minute (example: 50% in 30 seconds).

250°C, which was the beginning of thermal degradation, two small exotherms at 295°C and 302°C which we attributed to degradation of the additives, and an exotherm at 350°C which was due to oxidation of the carbonaceous residue. Virgin polypropylene showed a slight oxidation exotherm at 216°C, evidenced by the weight gain shown by the TGA; another exotherm at 250°C corresponded to the initial degradation, and there was another exotherm at 340°C which again was due to the oxidation of the carbonaceous residue (Fig. 39).

In addition to the C_1-C_6 hydrocarbons, which are the major degradation components, the liquid pyrolyzate portion of polypropylene-90 and virgin polypropylene consisted predominantly of saturated and unsaturated ketones, tetrahydrofuran derivative and aldehydes. Results of the chromatograms are shown in Appendix B (Figs. B14 and B15).

Polyurethane

We used polyurethane insulation designed for use in fiber optics.

Our TGA results on polyurethane insulation indicated a two-step weight loss pattern (Fig. 40). The major weight-loss phase is preceded by an induction phase which, at a heating rate of 20°C/min, started at 260°C and ended at 271°C. The first phase, which began at 271°C, is due to the loss of lower molecular-weight polyols and aliphatic fragments that formed on polymer degradation. The char remaining after the first phase was derived primarily from thermally stable polyisocyanates. The second phase that started at 332°C involved thermo-oxidative degradation of the char. The char content at completion of pyrolysis was 1.0%.

The effect of heating rate on the degradation rate of this insulation is summarized in Table 14. We see that the effect of high heating rates is consistent for the first phase of pyrolysis. The temperature responsible for the onset of the second phase of pyrolysis remains essentially constant up to 80°C/min. At this heating rate, and at 160°C/min, the temperature responsible for the second phase is considerably higher than that seen at the lower heating rates. The degradation rate is considerably higher in the first phase of pyrolysis than in the second phase. The degradation rates in both phases increased with the increasing heating rates. The char content remained the same at all heating rates.

DSCA measurements showed two small endotherms at 80°C and 105°C which we assigned to the glass transition temperatures of the hard and soft segments of the polyurethane formulation (Fig. 41). A wide endotherm at 170°C was due

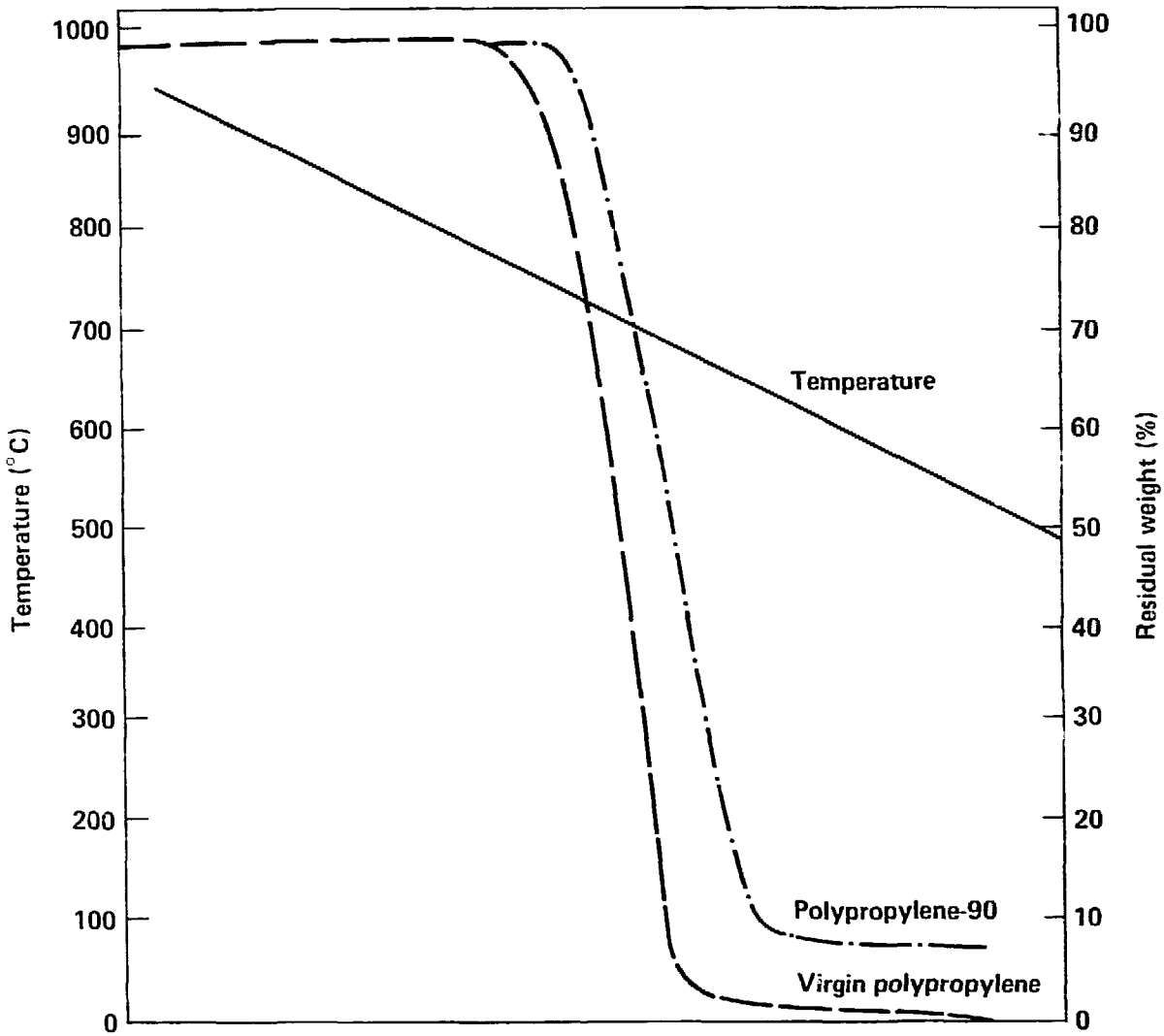

Figure 38. Thermograms of virgin polypropylene and polypropylene-90 heated in air at 20°C/min.

to the melting of the insulation. An endotherm at 260°C, which appeared just before the main decomposition phase, was probably due to activation of the weak links and eventual scission of the bonds. An exotherm which started at 292°C is attributed to oxidation and/or recombination of radicals. We assigned the exotherm at 335°C, which corresponds to the second phase of pyrolysis, to the oxidation of the char.

The Carbowax-20M results on the liquid pyrolyzate indicated the presence of alcohols, ketones, hydrocarbons, 1,4 butanediol, dodecan-6,7-dione, and aniline. Constituents of the gaseous pyrolyzates contained large quantities of ethylene, ethane, acetylene, propane, propylene, propyne, isobutylene, trans-2-butene, and ethylacetylene. There was some 1,3-butadiene, pentane, and 4-methyl-pentene-1. In addition, other researchers have reported formation of hydrogen cyanide, carbon monoxide, and nitrogen oxide.[11] The amounts of hydrogen cyanide and carbon monoxide formed during pyrolysis have been reported to increase between 300 and 700°C.

Nylon

Here, we used insulation designed for use in hook-up wires.

TGA curves showed an initial phase of low weight loss ending with a total weight loss of 5% at 350°C (Fig. 42). We attribute this weight loss mainly to absorbed water. Our DSCA study showed two events in this phase: an endotherm at

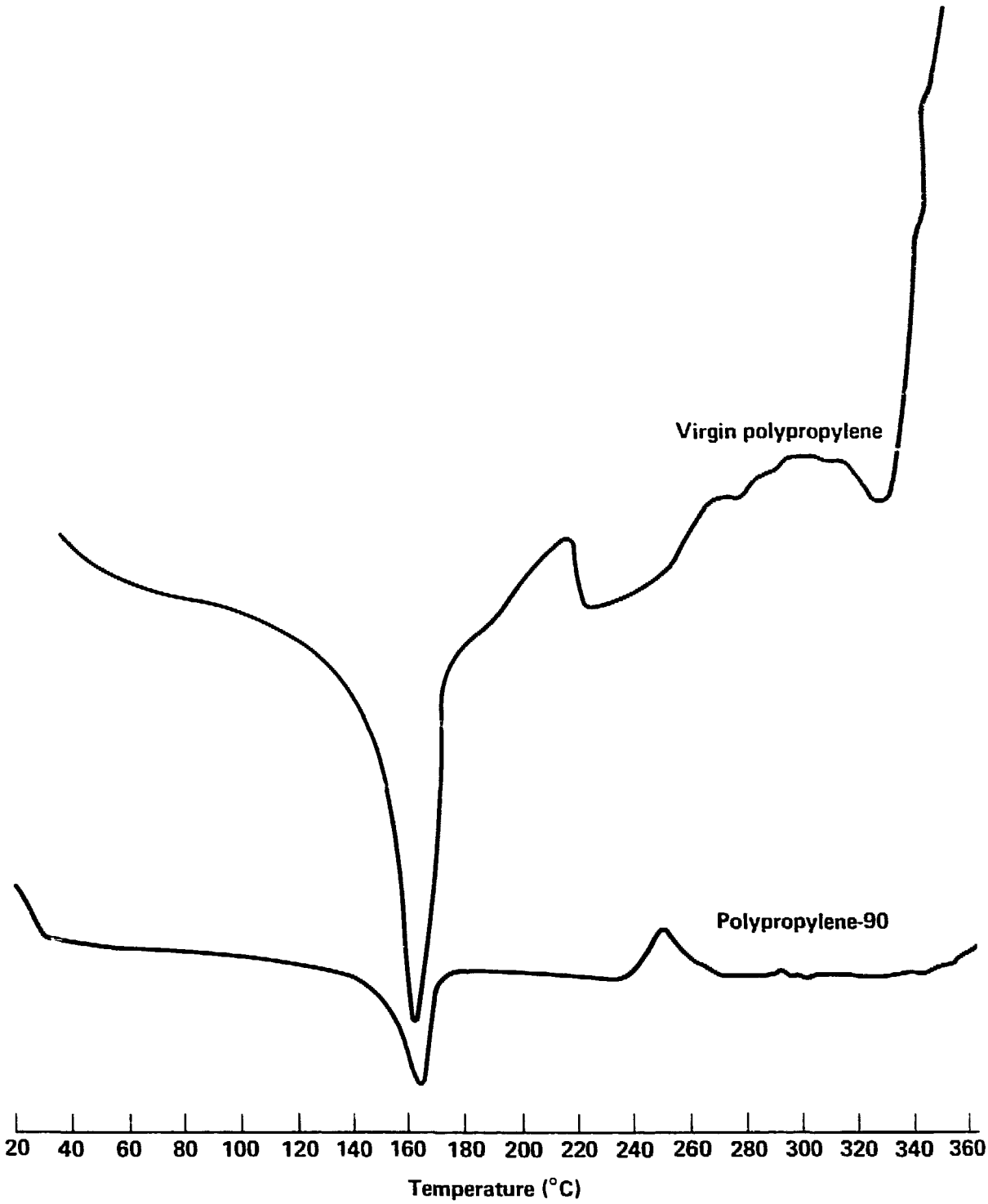

Figure 39. DSCA of virgin polypropylene and polypropylene-90 heated in air at 20°C/min.

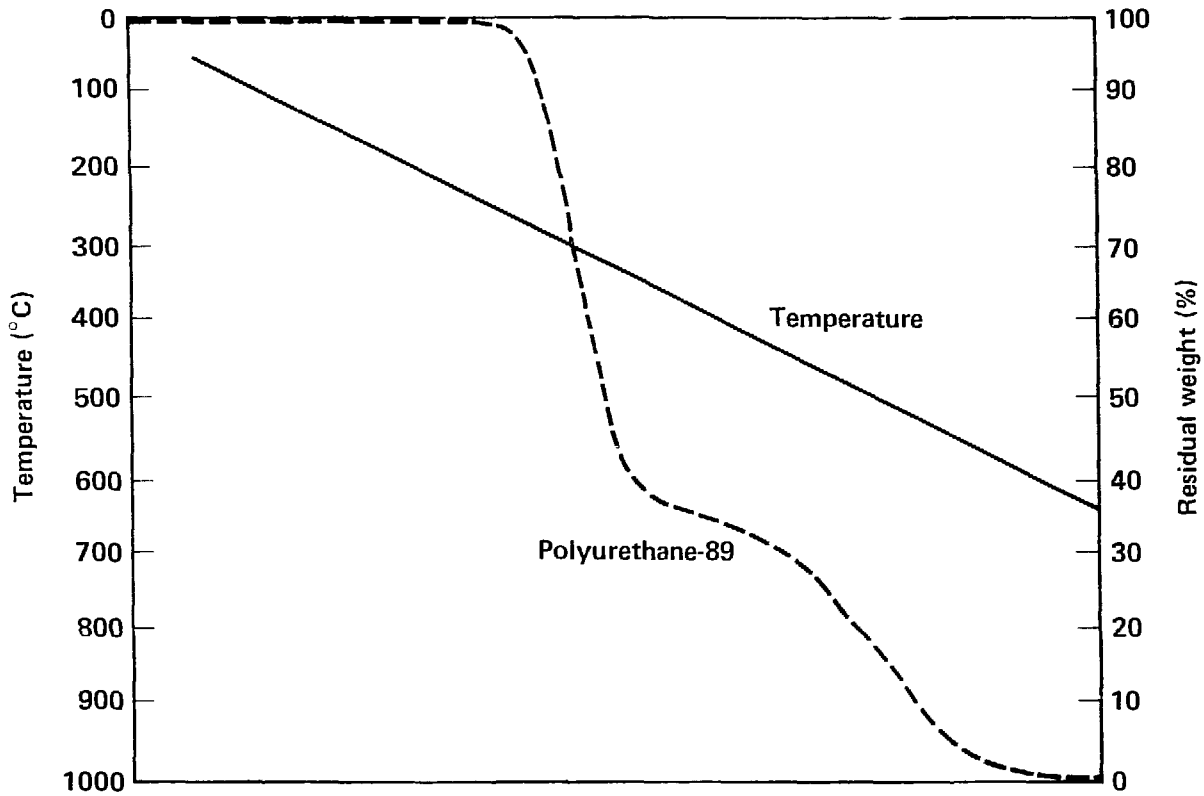

Figure 40. Thermogram of polyurethane-89 heated in air at 20°C/min.

217°C, which we attribute to melting, and a slight exotherm at 337°C, which we attribute to oxidation (Fig. 43). Some researchers believe that the insignificant weight loss at this phase of pyrolysis is due to random C-N bond breaking to form oligomers without the subsequent formation of volatiles.[12] At a temperature of about 380°C, we noticed rapid weight loss accompanied by a series of exotherms due to degradation of the polymer itself as well as the various additives.

Higher heating rates, shown in Table 14, increased the temperature responsible for the onset of the first phase of weight loss but did not have a similar effect on the second or the main decomposition phase. As observed with other insulations, higher heating rates led to increased rates of degradation and decreased amounts of char. Thus, the char content decreases slowly up to the heating rate of 40°C/min and becomes completely oxidized at a heating rate of 80°C/min. The gaseous pyrolyzates of this formulation are currently being analyzed. The liquid pyrolyzate generated in our thermogravimetric analyzer during the main phase of pyrolysis and analyzed via gas-chromatographic, mass-spectrometric analysis on the Carbowax-20M fused-silica capillary column show caprolactam and its various degradation products, including 1-hexene, 1-methylimidazole, 2,3-dimethylpyramid- 4-one and methyl-succinic acid [Appendix B (Fig. B16)].

Mylar

This material was designed for use in insulation of small signal wire.

TGA results of mylar-139 and virgin mylar in air showed three regions of weight loss (Fig. 44). There is a very gradual weight loss region, a main degradation phase, and a char-oxidation region. For samples heated in air at 20°C/min from ambient to 700°C, the first phase of pyrolysis begins at 220°C, the second phase at 390°C, and the last phase at 500°C, leaving no char at the end of

Table 14. The effects of heating rates on the thermal degradation of polyurethane, nylon-3, mylar-139, and virgin polyethylene terephthalate.

Sample	Heating rate (°C/min)	Main phase-1st phase: Onset of wt loss (°C)	Main phase-1st phase: Degradation rate (%/min)	2nd phase: Onset of wt loss (°C)	2nd phase: Degradation rate (%/min)	Wt loss in main phase (%)	Char at end of pyrolysis (%)
Polyurethane-89							
	10	260	10.0	328	0.5	32	1.0[a]
	20	271	23.0	332	1.7	49	1.0
	40	264	44.0	330	1.8	53	1.8
	80	270	80.0	350	4.0	63	1.0
	160	250	76.5	390	10.0	70	1.0
Nylon-3							
	10	120	0.1	392	14	56	13.0[b]
	20	120	0.3	425	24	46	12.5
	40	135	0.3	400	46	61	9.0
	80	150	0.5	400	68/30 s[c]	85	0
	160	160	0.5	420	87/30 s[c]	86	0
Mylar-139							
	10	381	14.0	463	3.5	30	0[d]
	20	391	32.0	500	6.0	45	0
	40	395	52.0	525	8.5	58	0
	80	385	88.0	515	7.5	71	0
Virgin polyethylene terephthalate							
	10	390	20	492	2.5	46	0[e]
	20	365	17	486	6.0	67	2
	40	365	40	515	8.5	73	0
	80	410	81/30 s[c]	560	10.0	73	0
	160	510	69/24 s[c]	–	–	71	0

[a] pH change in main phase that occurred at 10 and 20°C/min was 7.21 and 6.63, respectively.

[b] pH change in main phase that occurred at 10 and 20°C/min was 7.19 and 6.80, respectively.

[c] Degradation rate took place in less than 1 minute (example: 68% in 30 seconds).

[d] pH change in main phase that occurred at 10 and 20°C/min was 7.20 and 6.97, respectively.

[e] pH change in main phase that occurred at 10 and 20°C/min was 7.27 and 6.68, respectively.

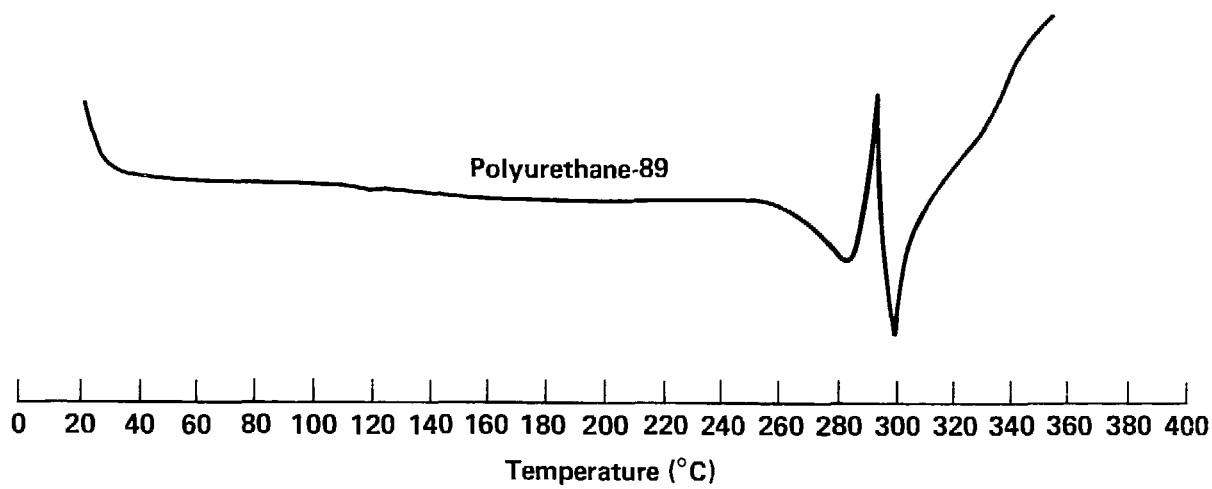

Figure 41. DSCA of polyurethane-89 heated in air at 20°C/min.

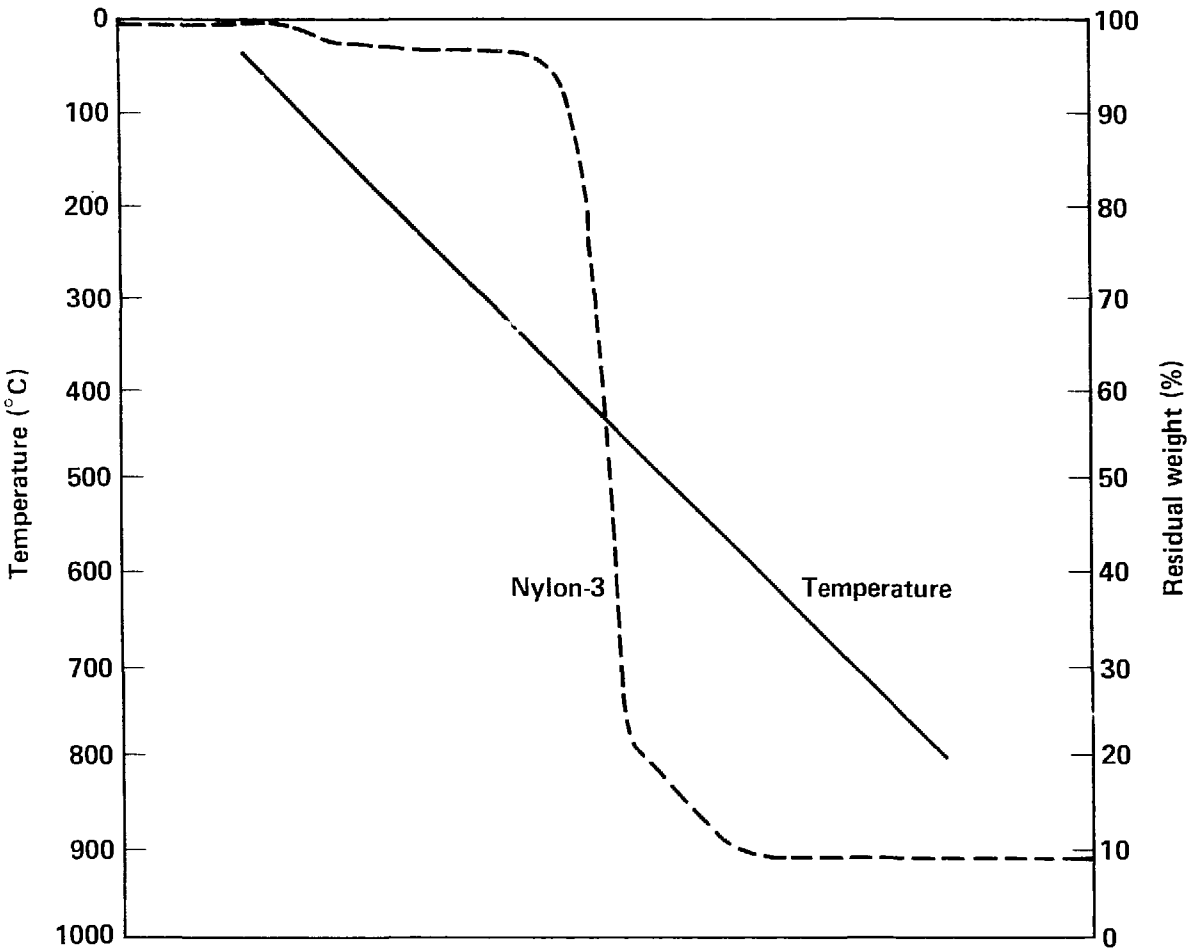

Figure 42. Thermogram of nylon-3 heated in air at 20°C/min.

pyrolysis. Our DSCA study in air showed two endotherms in the first phase (Fig. 45), one at 206°C (which we attribute to melting), and the other starting at 248°C, which we attribute to random bond scission with very little ring or ester-group breakdown. The beginning of the main degradation phase is accompanied by an exotherm that begins at 340°C and is due to ring breakdown, destruction of the ester linkages, and formation of free radicals which recombine to form various aromatic and aliphatic degradation products.

Heating rates between 10 and 40°C/min have no effect on the temperature responsible for initial weight loss (Table 14). However, a heating rate of 80°C/min lowers the temperature responsible for the initial weight loss from 220°C to 100°C. The temperatures leading to initial degradation in the second and third phase of pyrolysis are slightly increased by the higher heating rates. The degradation rates increase substantially in the second phase of pyrolysis with higher heating rates, increase moderately in the third phase of pyrolysis, and remain the same in the initial phase of pyrolysis. There is no char at the end of all pyrolysis runs.

Gas-chromatographic analysis results of the liquid pyrolyzate generated during the second degradation phase and separated on our Carbowax-20M revealed predominantly aromatic compounds [Appendix B (Figs. B17 and B18)]. The gaseous pyrolyzate is presently being analyzed.

Conclusions

Our most practical finding is that all of the insulations we analyzed formed detectable

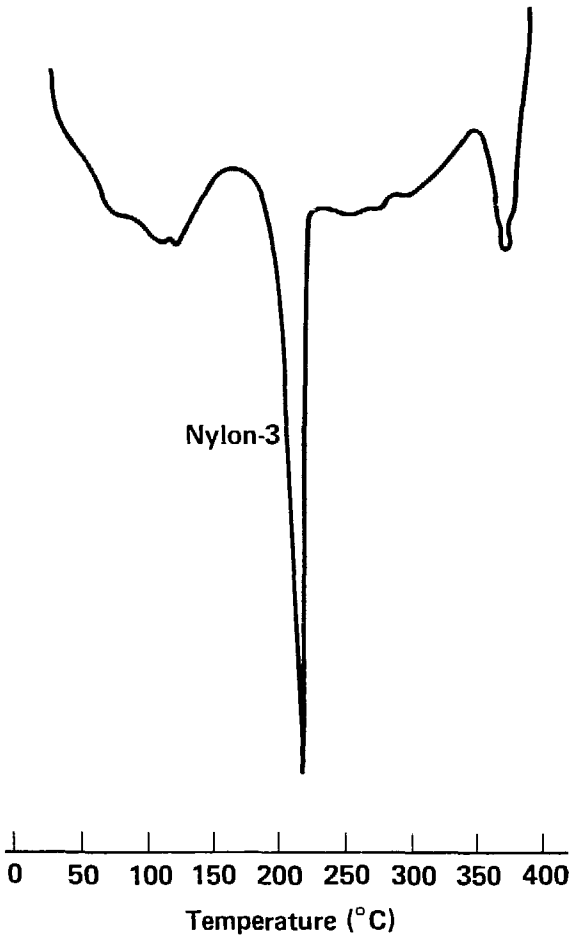

Figure 43. DSCA of nylon-3 heated in air at 20°C/min.

amounts of light hydrocarbons upon smoldering or flaming combustion. These components could be detected in the very early degradation stage of the samples, either heated under controlled laboratory conditions or ignited in our large-scale test cell. Such information is useful for selecting or designing appropriate early warning alarm systems for buildings housing costly equipment.

Results of the gas-chromatographic, mass-spectrometric analysis of the liquid pyrolyzates can be used to isolate those insulations that incorporate flammable plasticizers. The data, however, shows that there are no unique components pertinent to specific insulations that can be of practical value in fire detection.

As stated in our previous reports, the mode of thermal degradation of the insulations is influenced by the composition of the formulations of the insulations. Some plasticizers such as dioctylphthalates will enhance the flammability of the insulations, and, therefore, should be accompanied by flame retardants if used in the insulation.

Production of acidic components is enhanced by higher heating rates. However, higher heating rates do not increase the total acid production. The presence of acid acceptors (e.g., ZnO, MgO, Sb_2O_3 and $CaCO_3$) will influence how much acid is released into the environment.

In general, flame retardants used in the insulations we studied increased charring and decreased the degradation rate during the main phase of pyrolysis.

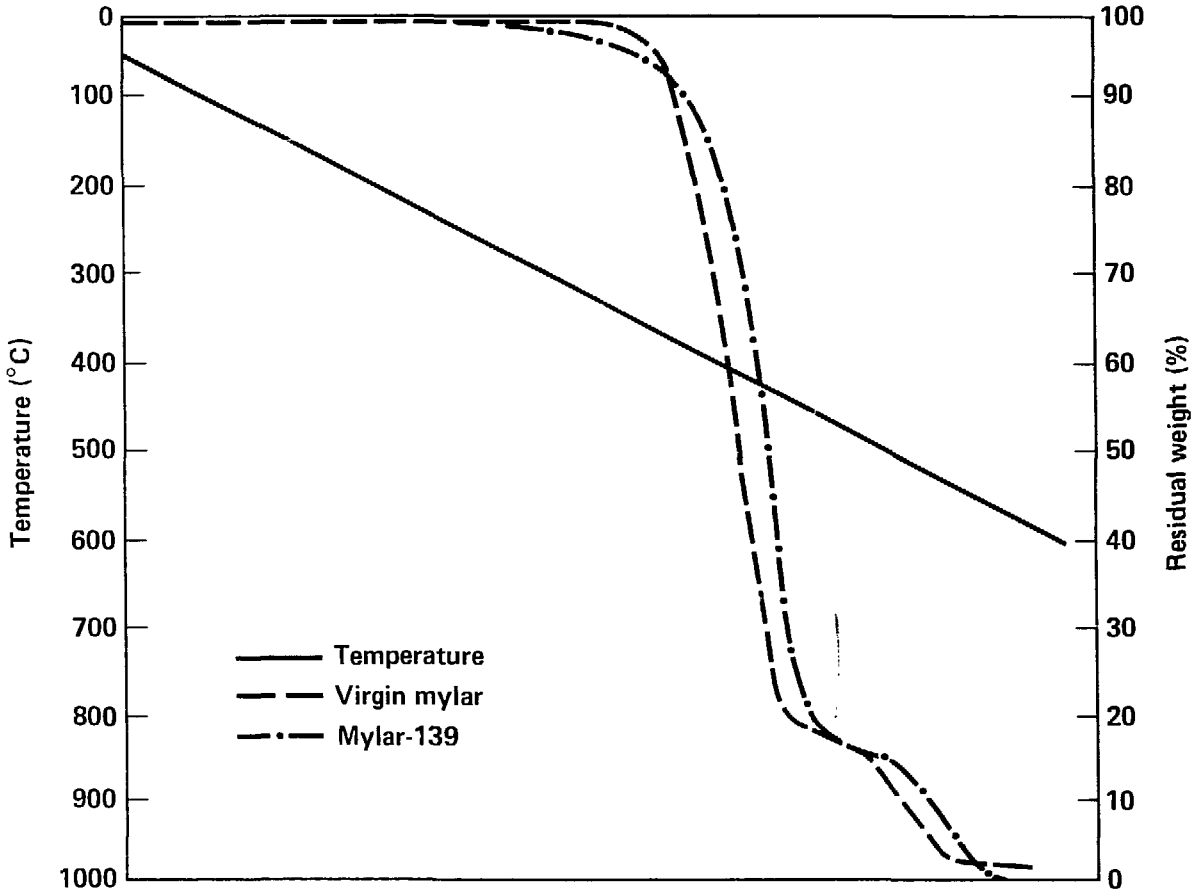

Figure 44. Thermogram of virgin mylar and mylar-139 heated in air at 20°C/min.

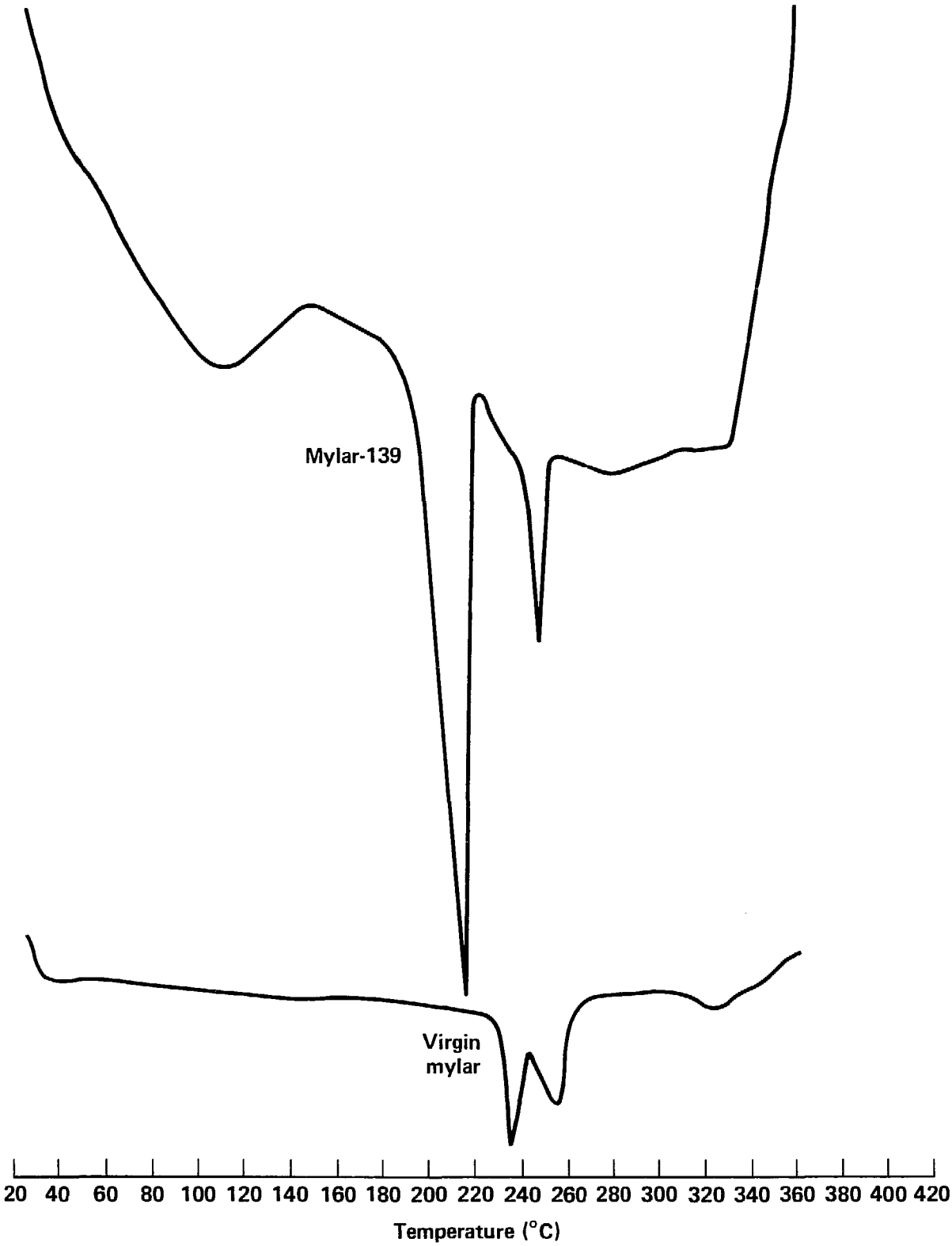

Figure 45. DSCA of virgin mylar and mylar-139 heated in air at 20°C/min.

Fire-Risk Assessment of the TMX-U Magnetic Fusion Experiment

Introduction

Over the course of our study, one major objective has been to develop a protocol to assess fire risk in DOE facilities. This protocol would ultimately integrate all of our experimental and analytical efforts to evaluate potential fire hazards, fire-protection system response, and potential fire damage to such facilities. Research facilities, unlike commercial industrial settings,[13,14] require slightly different rules for assessing fire risk. In research, funds are allocated to obtain information in a timely manner as opposed to an industrial setting where fire-risk assessments are made with regard to some uncertain impact on profit. In high technology research facilities, we measure fire risk relative to the impact on program schedules and budgets in the form of milestone delays and budget increases due to potential fire-related damage. In order to identify the specific nature of fire risk at these facilities, we choose to assess these risks relative to the research program at each facility on an individual experiment, on a Division or Department level, and ultimately at the DOE level.

As described in previous reports, we developed and used the protocol listed in Table 15 to provide a consistent basis for determining various levels of fire protection in DOE-research facilities. In summary, the assessment involves the following steps:

- Defining the potential hazard and magnitude of fire in each critical zone, area or compartment;
- Assessing the reliability and effectiveness of the fire-protection system; and
- Evaluating the interaction of the above two efforts in order to estimate the amount of damage (in terms of programmatic delay and capital loss) to each area.

The Tandem Mirror Experiment-Upgrade (TMX-U) primarily addresses steps 2 and 4 in Table 15. The study is a semi-detailed survey of TMX-U operations covering critical equipment replacement costs, delivery and repair times, operational necessity, and resultant estimated experimental down times.

The following data was provided by knowledgeable operations personnel and represents the best current information as to the potential negative impact on the TMX-U budget and schedule from fire-caused damage.

Facility Description

Figure 46 lists the objectives of the TMX-U experiment and the subsystems necessary to pursue these objectives. Additionally, Fig. 47 illustrates the physical location of these subsystems housed in Building 435. Figure 48 is a simplified representation of hardware and equipment essential to the operation of the experiment.

As indicated in Fig. 46, all subsystems need to be working for the facility to be fully operational. However, contingency workaround plans exist for some of these systems. Given the layout and elevation plans of the experiment building, we needed to identify and evaluate specific areas and compartments of the facility that would have a significant impact on continued progress of the program. One basic assumption was that the experimental program depends only upon equipment availability.

The information summarized in Tables 16 through 18, which list each of the TMX-U subsystems and their primary components, was provided by programmatic personnel responsible for each subsystem. We assumed a loss of these components, and calculated the estimated time delays and associated replacement costs.

In addition, we have noted whether contingency workaround plans and/or spares exist for subsystems and components. The length of programmatic delays must be compared to the experiment's critical path milestones, or CPM, to evaluate their negative impact on the research schedule. Similarly, the expected replacement costs must be weighed against yearly funding levels that might cause delays in additional equipment purchases.

In practice, personnel would develop and use these tables to identify potentially high consequence areas due to their exorbitantly high values and criticality to the continued operation of TMX-U. Once these "critical" areas are identified, a fire-growth model would be used to predict the fire threat and determine the mitigating effects of the fire-protection system. The analytical results describe the fire risk. If it turns out that resulting fire losses are unacceptable due to high operational value (i.e., approaching the larger figures in Tables 16–18), then program management must make the decision to either accept this fire risk or initiate changes to reduce it to an acceptable level.

Table 15. General flow of systems approach to fire risk.

1

DIVIDE BLDG. INTO ZONES

CRITERIA:

A. May Use Fire Protection Zones.
B. Natural Building Boundaries (Walls and Rooms).

2

SELECT CRITICAL AREAS FOR ANALYSIS

CRITERIA:

A. Capital Loss.
B. Programmatic Delay.

3

PERFORM ANALYSES TO DETERMINE FIRE HAZARD AND ZONE

CRITERIA:

A. Fire Growth Analysis.
B. Fire Protection System Analysis.
C. Research into Identified Problem Areas.

4

ASSESS POTENTIAL LOSS IN EACH CRITICAL ZONE

CRITERIA:

A. Programmatic Delay.
B. Capital Loss.

5

ASSESS EXPT. FIRE IMPACT ACCEPTABILITY AND COMPARE EACH ZONE

CRITERIA:

A. LLNL Guidelines.
B. DOE Guidelines.
C. Programmatic Delay.

6

IDENTIFY COST-EFFECTIVE SOLUTIONS TO INCREASE FIRE SAFETY OF FACILITY

CRITERIA:

A. Reiterate Loss Assessment With Recommended Changes.

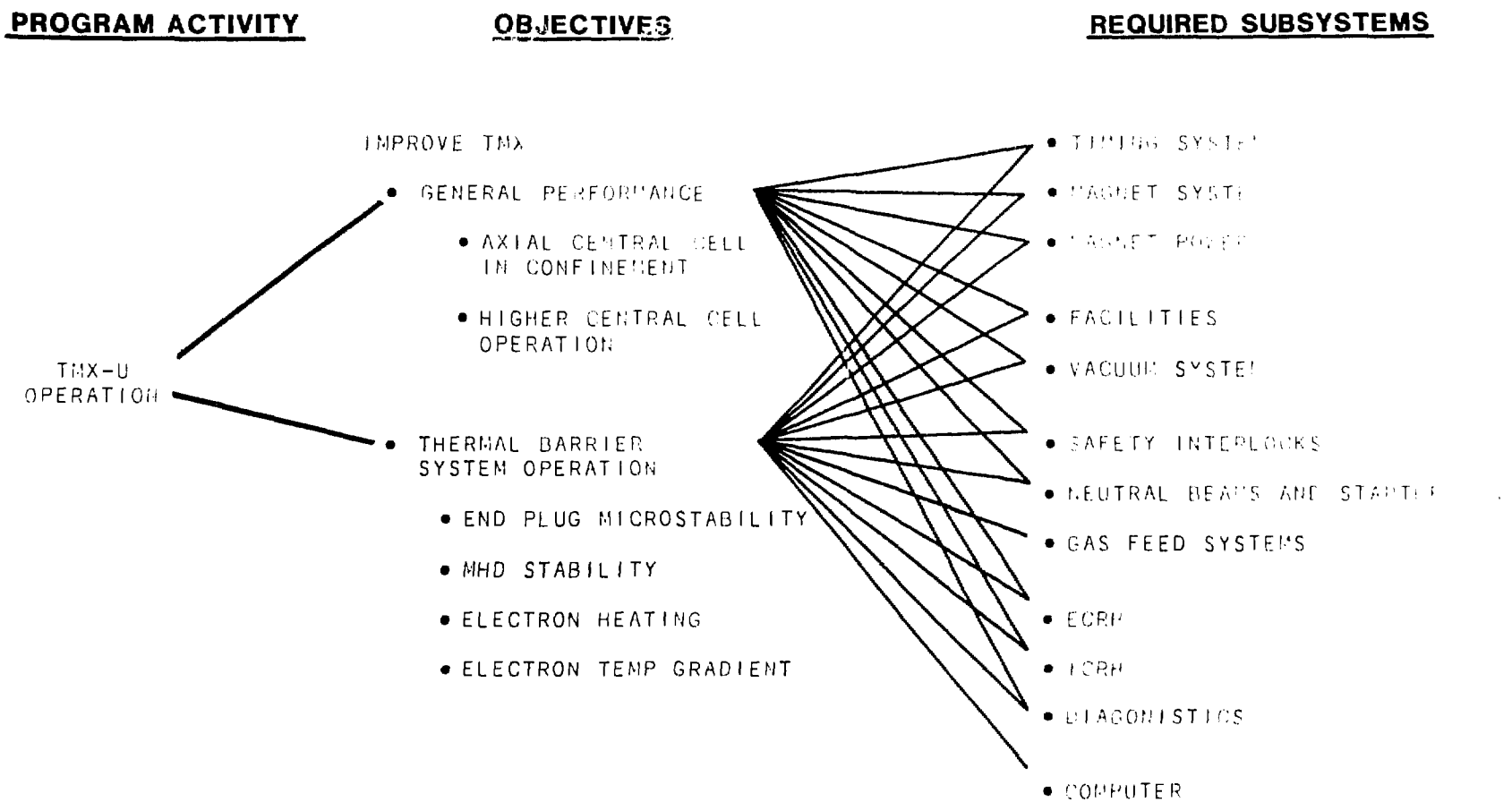

Figure 46. TMX-U objectives and critical subsystems.

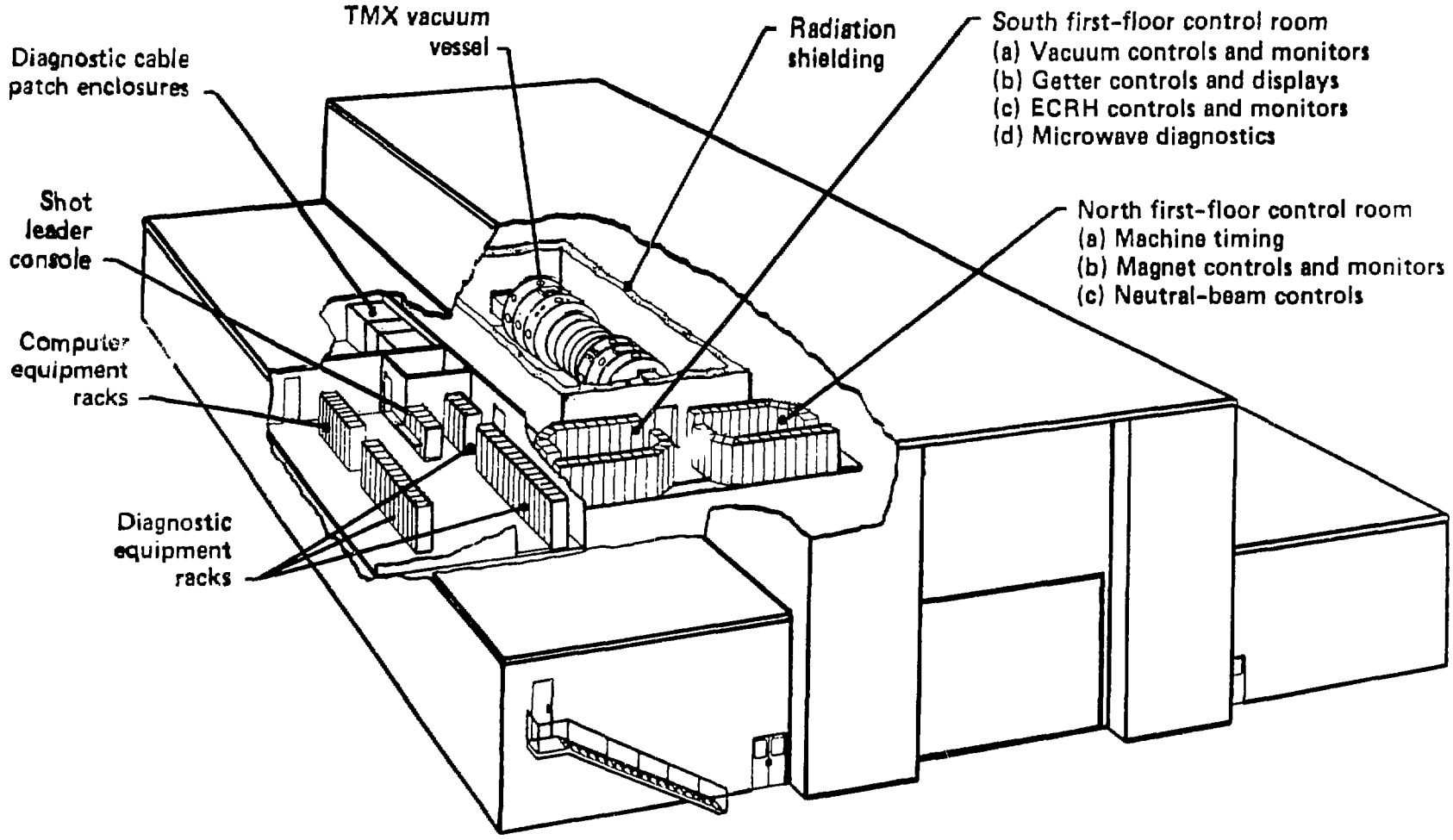

Figure 47. TMX-U experimental facility.

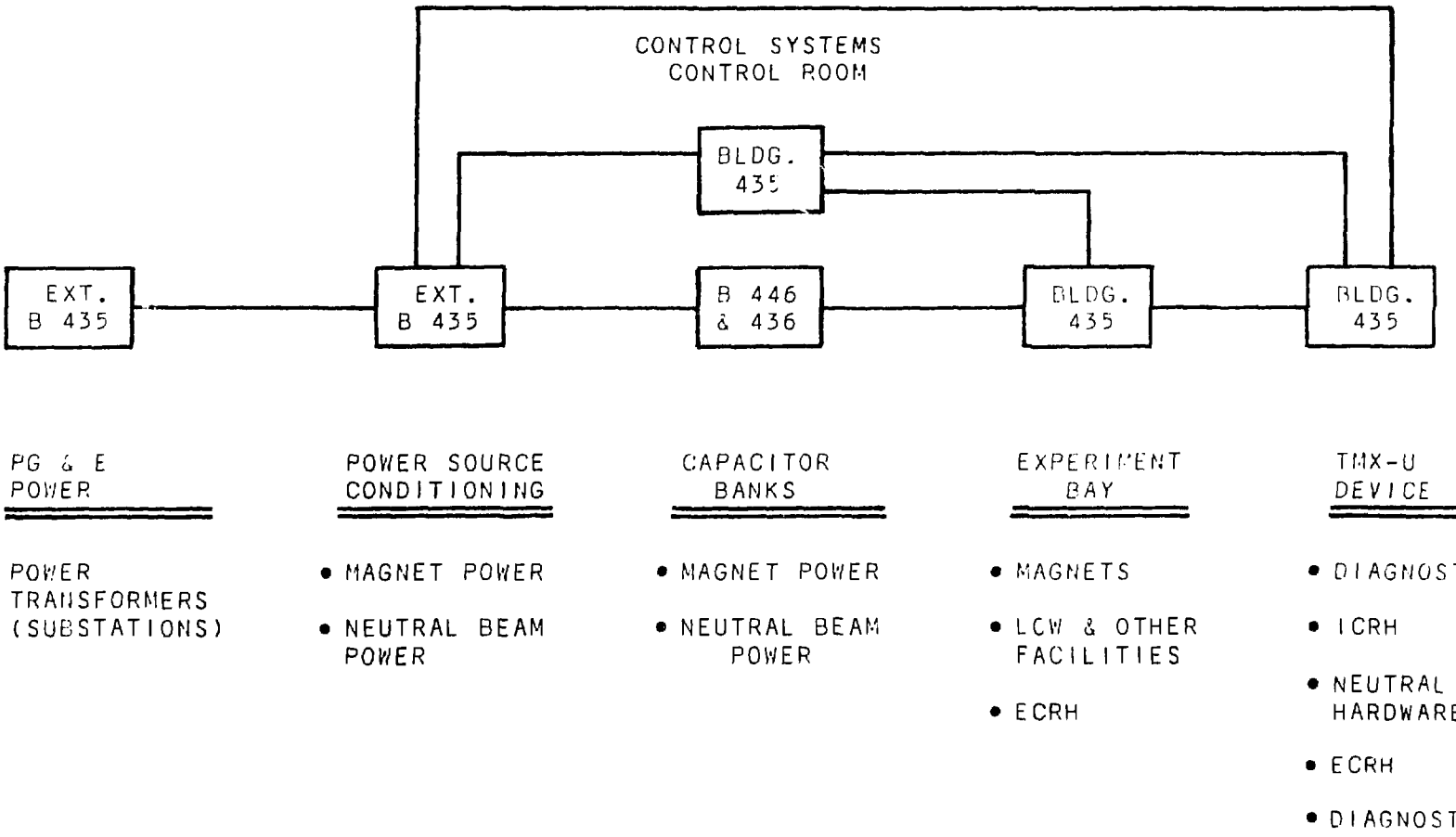

Figure 48. Essential TMX-U subsystems.

Table 16. Survey results of operational readiness for TMX-U (systems 1-4).

Programmatic delay					Replacement cost (1980$) × 10^3			
Least	Expected	Most	Workaround plan (Y/N)	Strategic bldg. containing strategic equipment	Least	Expected	Most	Eqpt. spares or immediate delivery (Y/N)
				1) Supervisory timing system				
8 wks	12 wks	16 wks	Yes	• (HP 9835, camac, buffers, wiring)	40.	50.	60.	Yes
				2) Magnet set subsystem				
7 mos	12 mos	18 mos	No	• end plug (per set)	300.	1500.	1500.	No
3 mos	9 mos	12 mos	No	• transition set (per set)	200.	660.	660.	No
3 mos	6 mos	9 mos	Yes	• central cell	175.	175.	550.	coils exist
				3) Magnet power subsystems				
–	5 mos	–	No	• substation (ea.)(7)	–	90.	–	No
–	5.5 mos	–	No	• pwr supply (ea.)(42)	–	40.	–	No
–	5.5 mos	–	No	• cables (ea. run)(10)	–	7.	–	No
–	1.5 mos	–	No	• controls (set)(1)	–	10.	–	Yes
–	1.5 mos	–	No	• computer (1)	–	10.	–	No
				4) Facilities				
2 days	2 days	3 days		• vacuum valves	200.	250.	300.	No
–	Plant Engr.	–		• cooling water lcw	–	Plant Engr.		–
4 hrs				• power	200.	250.	300.	Y/N (METF)

Table 17. Survey results of operational readiness (systems 5-9).

Programmatic delay					Replacement cost (1980$) × 10^3			
Least	Expected	Most	Workaround plan (Y/N)	Strategic bldg. containing strategic equipment	Least	Expected	Most	Eqpt. spares or immediate delivery (Y/N)
				5) Vacuum Vessel Subsystem				
1 mo	3 mos	6 mos	Yes	• exter. vac. sys.	20.	35.	60.	Partial spares
1.25 mo	1.5 mos	2 mos	No	• vacuum vessel	5.	7.	10.	No
2 mos	5 mos	8 mos	No	• getter system & pwr supplies	55.	90.	170.	No
1 wk	3 wks	5 mos	No	6) Interlocks (ctrl room)	20.	30.	55.	Yes
				7) Neutral beam system				
3 mos	5 mos	7 mos	No	• accel/decc area	360.	480.	540.	No
2 mos	4 mos	6 mos	No	• arc. & fil. area	246.	288.	378.	No
5 mos	7.5 mos	10 mos	No	• capacitor bank 436	560.	752.	960.	No
4 mos	5 mos	6 mos	No	• 1st floor 446	160.	416.	520.	No
2 mos	3 mos	4 mos	No	• control room area	200.	448.	480.	No
				8) Gas feed system				
1 mo	1.5 mos	2 mos		• gas box	10.	16.	36.	No
–	1 mo	–	No	• puffer valves	–	5.	–	No
–	1 mo	–	No	• streaming guns	–	10.	–	No
4.5 mos	6 mos	7.5 mos	Yes	9) ECRH (electro/cyclotr reson. heat) • substation • ac distribution • gyrotrons • wave guides (vessel ext.) • vessel internals	125.	150.	250.	Yes
negligible	12 mos	19 mos	No	• A/C distrib. sub-systems	10K	550.	650.	partial spares

Table 18. Survey results of operational readiness (systems 10-12).

Programmatic delay				Strategic bldg. containing strategic equipment	Replacement cost (1980$) · 10^3			
Least	Expected	Most	Workaround plan (Y/N)		Least	Expected	Most	Eqpt. spares or immediate delivery (Y/N)
				10) ICRH Subsystem (ion cyclotron reson. heating)				
1 mo	2 mos	4 mos	No	• antenna sytem	15.	35.	100.	Yes
3 mos	5 mos	8 mos	Yes	• transmitters	50.	80.	250.	Yes
1 mo	–	3 mos	No	• transmission lines	10.	–	20.	Yes
2 mos	–	4 mos	Yes	• control & das	20.	22.	30.	Yes
				11) System diagnostics				
2 mos	12 mos	18 mos	No	• control/record (no computer)	30.	1400.	2900.	No
0.5 mos	6 mos	10 mos	No	• cable patch area	5.	70.	150.	No
0.5 mos	6 mos	8 mos	No	• diagnostic cnduit	5.	70.	250.	No
1 mo	2 mos	3 mos	No	• record & cent. timing	10.	40.	60.	No
1 mo	4 mos	6 mos	No	• pit equip area	20.	150.	200.	No
0.5 mo	4 mos	6 mos	Yes	• supp. diag. instru.	10.	120.	200.	No
				12) Computer (rm. 2062)				
				• hardware				
3 mos	4 mos	8 mos	redundancy	• data acquisition computer	144K	180K	216K	Yes
3 mos	4 mos	8 mos	redundancy	• data reduction computer	160k	200K	240K	Yes
2 mos	3 mos	6 mos	redundancy	• disc	96K	120K	144K	Yes
1 wk	2 wks	1.5 mos	redundancy	• camac recorders	–	100K	–	Yes
0 mos	6 M	18 M	No	• data (software on disc)				Yes/No

In FY 83, we will perform a complete fire-risk analysis on TMX-U that will include the predicted fire threat in critical areas, the fire-protection system response, and resultant damage. It will be the first validation exercise for the overall risk-assessment methodology.

Observations

The potential loss assessment of the TMX-U fusion experiment produced these observations (Tables 16–18).

- Extensive fire damage to the following subsystems could cause prolonged time delays and exorbitant replacement costs: system diagnostics—control/recording (second level of Building 435); magnet set subsystem—end plugs (central pit, Building 435); neutral beam subsystem (Building 436, Building 446, and control area).
- The primary high value areas are the vessel and control rooms in Bldg. 435.
- There is a notable lack of backup components and workaround plans in Building 435 vessel and control rooms.
- Basically, *all* subsystems are required to pursue both objectives of thermal barrier operation and TMX general-performance improvement.
- More than 50% of expected schedule delay from potential fire damage for all critical subsystems is greater than four months.

The above observations are based *only* on an extensive damage scenario, which should not be confused with the actual fire risk in these areas. As stated earlier, the fire risk cannot be determined without assessing potential damage by predicting the fire threat and the degree of mitigation provided by the fire protection system response. The resultant damage may be minimal, marginal, or very severe and it is this level of risk that management must evaluate.

Conclusions and Future Work

In FY 82 we have continued the validation of our experimental and analytical techniques specified in Fig. 1. Furthermore, we have been orienting our results toward application in preparation for our target completion date in 1985. Our FY 82 conclusions are summarized below.

Large-Scale Vertical Cable Burns

The performance of six large-scale cable burns in FY 82 provided preliminary validation of the test apparatus. Results of the experiments indicated that:

- It is difficult to achieve a sustained ignition with a 20 kW ignition source;
- After ignition, rate of flamespread is very slow;
- Rates of heat release were low and slow to peak;
- The low heat-release rates appeared to be due to the cable diameter (1.25 cm to 2.54 cm), the large percentage of conductor, and the packing density.

In FY 83 we will continue to use the protocol we developed in 1982 to confirm these observations. And, in the future, we will be evaluating the effect of varying ignition source strength, airflow, cable composition (i.e., multiconductor vs solid copper, etc.), and cable diameter.

Small-Scale Ease-of-Ignition Experiments

The most important finding from this series of experiments was the development of a testing protocol to evaluate the effects of physical and chemical cable properties on susceptibility to ignition. This protocol will be used in FY 83 in an attempt to develop a means to predict a cable's time to ignition without having to perform a test on it.

Fire Modeling

The problems which surfaced in the 1981 series were rectified in the 1982 model burns. Furthermore, a number of modifications and improvements to the experimental setup and parameters were implemented. Data contained in Table 10 are semi-equilibrium values. These data will be used to rate preliminary models and establish criteria for FY 83 tests. In fact, we will use the same fuels in 1983 tests as we did in FY 82 tests, but we will vary the following parameters: fire location in test cell, ventilation input and output locations (high, low; low, high, etc.), and location of fire on the floor and above the floor. These experiments will add to our growing data base of fire model validation data.

Fire Chemistry

This year's experiments employed higher heating rates and produced the useful DSCA and TGA results listed below:

- Laboratory results of thermal and chemical analysis can be used effectively to infer how a material will react in a real fire environment.
- Faster heating rates used in thermal gravimetric studies correspond to conditions found in a real fire environment (large-scale experiments).
- The mode of thermal degradation of the insulations is influenced by the composition of the formulations of the plastic insulations.
- Production of acidic components is enhanced by higher heating rates. However, higher heating rates do not increase the total acid production.
- The presence of acid acceptors (e.g., $CaCO_3$) influences how much acid is released into the environment.
- Flame retardants used in the insulations studied increased charring and decreased the rate of degradation in the main phase of pyrolysis and therefore the rate of production of HCl.
- All insulations studied form detectable amounts of light hydrocarbons in the early stages of degradation, both in laboratory-scale and large-scale burns. These light hydrocarbons could possibly serve as signatures for early warning detection systems.

Fire-Risk Analysis

We continued to develop the components necessary to an overall fire-risk assessment technique during FY 82. Analysis of the LLNL TMX-U experiment produced the most detailed programmatic and budgetary information to date. The fire-modeling effort is at a point where we should be able to apply it to the TMX-U critical spaces in FY

83. Furthermore, the reliability of fire-protection systems can be easily calculated from our previously completed studies. The interaction of these major components, along with an assumed level of fire-protection effectiveness, will produce a predicted level of damage. Evaluation of resulting loss from fire will yield fire risk in these spaces.

References

1. H. K. Hasegawa, N. J. Alvares, A. E. Lipska, H. W. Ford, and D. G. Beason, *Fire Protection Research for Energy Technology Projects: FY 79 Yearend Report*, Lawrence Livermore National Laboratory, Livermore, California, UCID-18902 (1981).
2. H. K. Hasegawa, N. J. Alvares, A. E. Lipska, H. W. Ford, S. Priante, and D. G. Beason, *Fire Protection Research for Energy Technology: FY 80 Yearend Report*, Lawrence Livermore National Laboratory, Livermore, California, UCRL-53179 (1981).
3. H. K. Hasegawa, N. J. Alvares, A. E. Lipska-Quinn, D. G. Beason, K. L. Foote, and S. J. Priante, *Fire Protection Research for Energy Technology: FY 81 Yearend Report*, Lawrence Livermore National Laboratory, Livermore, California, UCRL-53179-81 (1982).
4. E. E. Zukoski, K. Kubota, and B. Cetegen, *Entrainment in Fire Plumes*, U.S. Dept. of Commerce, National Bureau of Standards, Washington, D.C., NBS-GCR80-294 (1980).
5. *IEEE Standard for Type Test of Class IE Electric Cables, Field Splices, and Connections for Nuclear Power Generating Stations*, the Institute of Electrical and Electronics Engineers, New York, New York, 1974.
6. L. Orloff, *Simplified Radiation Modeling of Pool Fires*, Factory Mutual Research, Norwood, Mass., FMRC J.I. No. OE1EO.BU-1 (1980).
7. N. Alvares and K. Foote, *Contrast Between Natural and Experimentally Controlled Fires in Forced Ventilation Enclosures*, Lawrence Livermore National Laboratory, Livermore, CA, UCRL-88588 (1983).
8. H. Steckler, National Bureau of Standards, Gaithersburg, Maryland, private communication (1982).
9. C. F. Cullis and M. M. Hirschler, *The Combustion of Organic Polymers*, International Series of Monographs on Chemistry, Clarendon Press, Oxford, p. 129 (1981).
10. A. Holmstrom and E. M. Sorvik, "Thermal Degradation of Polyethylene in a Nitrogen Atmosphere of Low Oxygen Content III Structural Changes Occurring in Low Density of Polyethylene at Oxygen Contents Below 1.2%," *Journal of Applied Polymer Science* **18**, 779 (1974).
11. K. Ashida, F. Yamauchi, M. Katoh, and T. Harada, *Advanced Urethane Science Technology* **3**, 130 (1974).
12. H. E. Stepniozka, *Industrial Engineering Chemical Products Research Development* **12**, (1) 29 (1973).
13. G. Ramachandran, "Statistical Methods in Risk Evaluation," International Symposium on Fire Risk Evaluation (1979), ISBN 91-7144-138-7.
14. C. L. Farmer, "A Probabilistic Risk Analysis Technique With Applications to Enclosure Fires," International Symposium on Fire Risk Evaluation (1979), ISBN 91-7144-138-7.

Appendix A.
Mass-Balancing Equations

MASS BALANCE

$$\text{Mass}_{in} = \frac{1.176 * (300) * 742}{(\text{Temp}_{in} + 273)\,760}\,(\text{Inlet Air})(1.03)$$

$$\text{Mass}_{out} = -\frac{1.176 * (300) * 742}{(\text{Temp}^{a}_{out} + 273)\,760}\,43\sqrt{\frac{\text{diff pressure (Pa)}}{\text{density exit air}}}$$

$$\text{Mass}_{net} = \text{Mass}_{in} + \text{Mass}_{out} + \text{Fuel}_{in}$$

$$O_{2in} = 0.23\,(\text{mass}_{in})$$

$$O_{2out} = O_{2net} - O_{2in}$$

MAJOR SPECIES

$$O_{2net} = -(J1^{b} * CO_{2net}) + (J2^{b} * CO_{net})$$

$$CO_{2net} = 0.0152\,(\%\ CO^{a}_{2})\,(\text{mass}_{out})$$

$$CO_{net} = 0.0096\,(\%\ CO) * (\text{mass}_{out})$$

$$CH_{4net} = 5.52 \times 10\text{m}^{-7}\,(\text{ppm } CH_4)\,(\text{mass}_{out})$$

$$H_2O_{net} = (J3^{b} * CO_{2net}) + (J4^{b} * CO_{net})$$

ATOMIC BALANCE

$$\text{Carbon} = (Z1^{b} * \text{Fuel}_{in}) + 0.27\,(CO_{2net}) + 0.43\,(CO_{2net})$$

$$\text{Hydrogen} = (Z2^{b} * \text{Fuel}_{in}) + 0.11\,(H_2O_{net}) + 0.25\,(CH_{4net})\,0.75\,(CH_{4net})$$

$$\text{Oxygen} = (Z3^{b} * \text{Fuel}_{in}) + O_{2net} + 0.89\,(H_2O_{net})\,0.73\,(CO_{2net}) + 0.57\,(CO_{net})$$

$$\text{Mass} = \text{Fuel}_{in} + O_{2net}\,(CO_{2net} + CO_{net} + CH_{4net} + H_2O_{net})$$

ENERGY BALANCE

$$Q_{in} = 0.00102\,(\text{Temp}_{in} + 273)\,(\text{Mass}_{in})$$

$$Q_{out} = 0.00109\,(\text{Temp}_{out} + 273)\,(\text{Mass}_{out})$$

$$Q_{net} + Q_{in} + Q_{out}$$

$$Q_{Fire} = -V1^{b} * (J1^{b} * CO_{2net}) + (J2^{b} + CO_{2net})$$

$$Q_{wall} = -(Q_{net} + Q_{fire})$$

---

[a] Time delayed.
[b] Values change with fuel type.

Appendix B.
Fire Chemistry Experiment Data

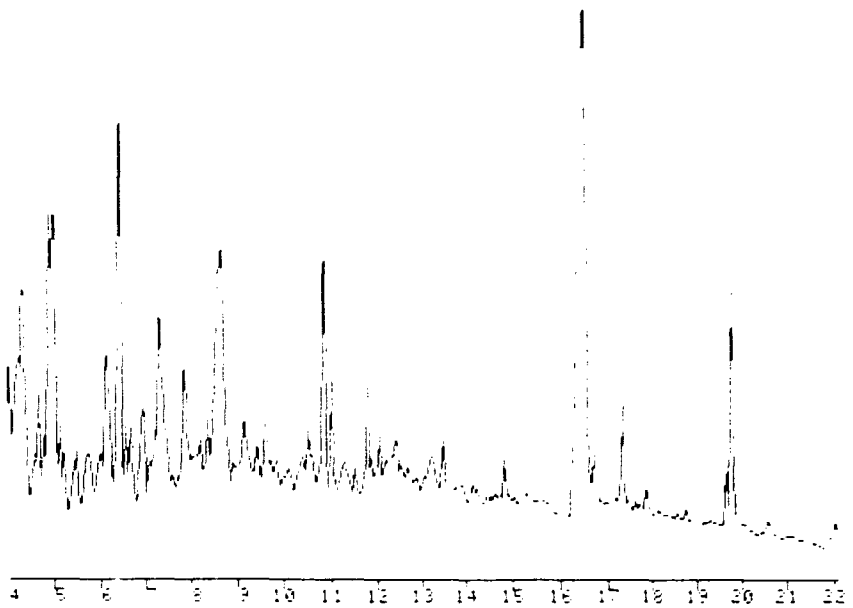

T_R	COMPOUND
4.2	6-methyl-1-heptanol cis-3-hexene
4.3	3-ethyl-2-hexen-1-ol
4.4	1,2-dichloro-2-methylpropane
4.6	2,5-dimethyl-trans-3-hexane
4.7	2-methyl-1-pentadecene
5.0	2,3-dimethylhexane, 2-phenylheptadecane
5.5	1-chloro-heptadec-6-ene
5.7	3,7-dimethyl-1-octanol
6.1	thujyl alcohol
6.4	1,1-dichloroacetone
7.0	octyl acetate
7.9	isooctyl alcohol
8.7	2-dimethylaminocyclohexanone
9.2	hexacosanol-1
9.6	octadecanol-1
10.9	undecylenaldehyde
11.0	citronylproprionate
16.5	phthalic anhydride
17.4	benzoic acid
17.8	benzidine
19.6	phenanthrene
19.8	n-butylphthalate

Figure B1. Pyrolyzate of PVC-3 generated in air in tube pyrolyzer during the main region of degradation. Separation was performed on Carbowax-20M fused silica capillary column.

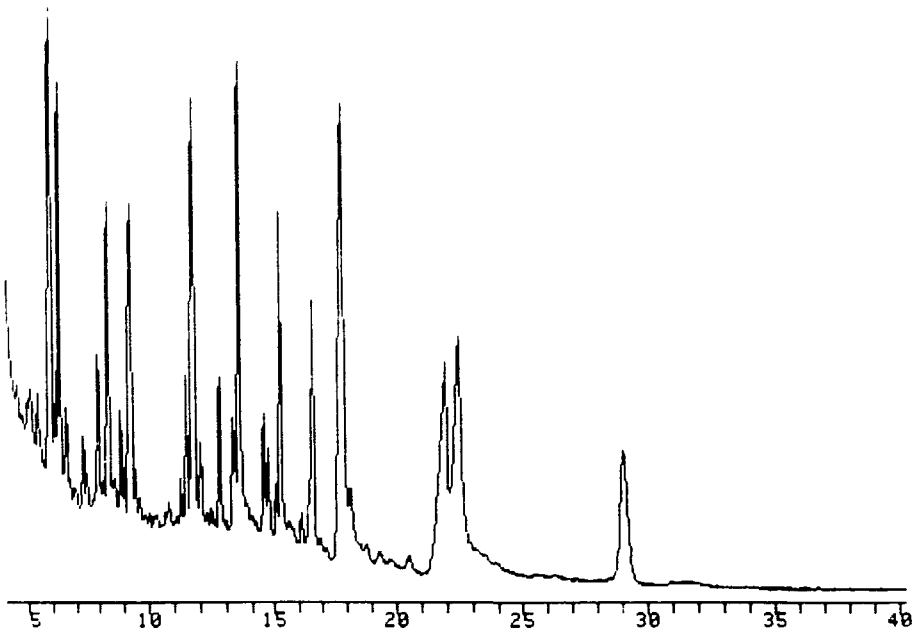

T_R	COMPOUND
5.1	2-ethyl-N-methyl pyrolidine
5.4	2-acetophenone
6.0	3-cholorodecane
6.3	naphthalene
7.3	methyl laurate
8.4	2,6-ditertiary butyl-p- cresol
8.9	biphenyl
9.3	2,6-di-T-butyl-1,4-benzoquinone
11.4	methyl hexadecanoate
12.0	fluorene
12.7	1-hexacosene
13.3	methylstearate
13.6	lauric acid
14.5	n-octadecanitrile
15.1	anthracene or phenanthrene
15.3	myristic acid
16.3	decanoic acid
17.8	palmitic acid
21.9	stearic acid
22.2	dioctylphthalate
29.0	3,3,4,4-tetramethyl-2,2-diphenoxyethane

Figure B3. Pyrolyzate of PVC-104 generated in air in tube pyrolyzer during the main region of degradation separated on Carbowax-20M.

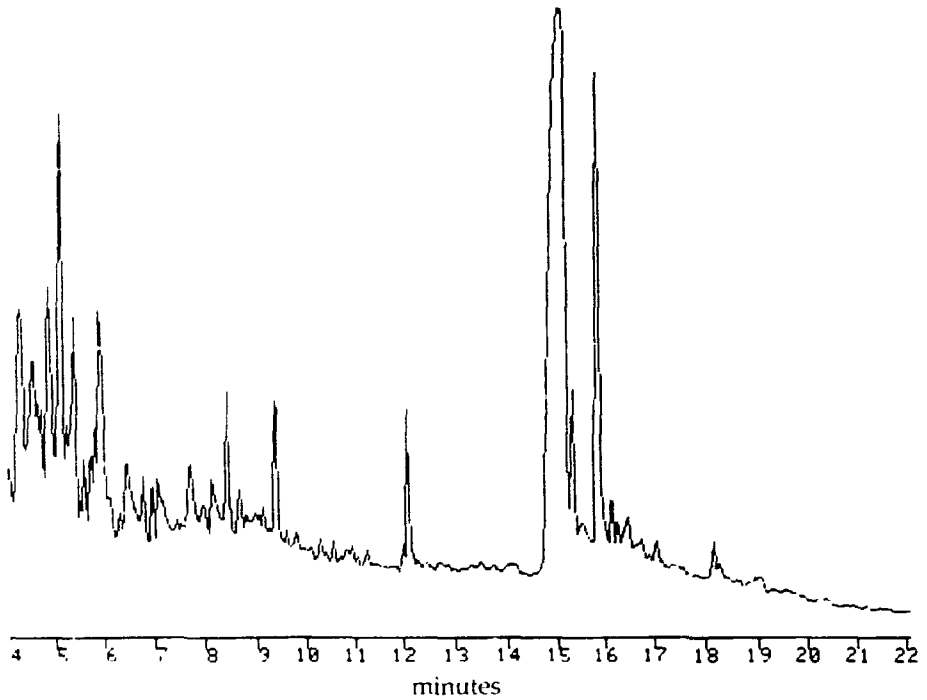

T_R	COMPOUND
4.3	*0-isobutylhydroxylamine*
4.5	1-decanol
4.9	1-chlorotetradecane
5.1	hexyl vinyl ether
5.4	n-heptane
5.6	unidentified
8.1	n-decyl ether
9.4	naphthalene
12.1	phenol
15.1	phthalic anhydride
15.9	benzoic anhydride
18.1	*phthalic acid*
18.2	*phenanthrene*

Figure B2. Pyrolyzate of PVC-78 generated in air in tube pyrolyzer during the main region of degradation separated on Carbowax-20M.

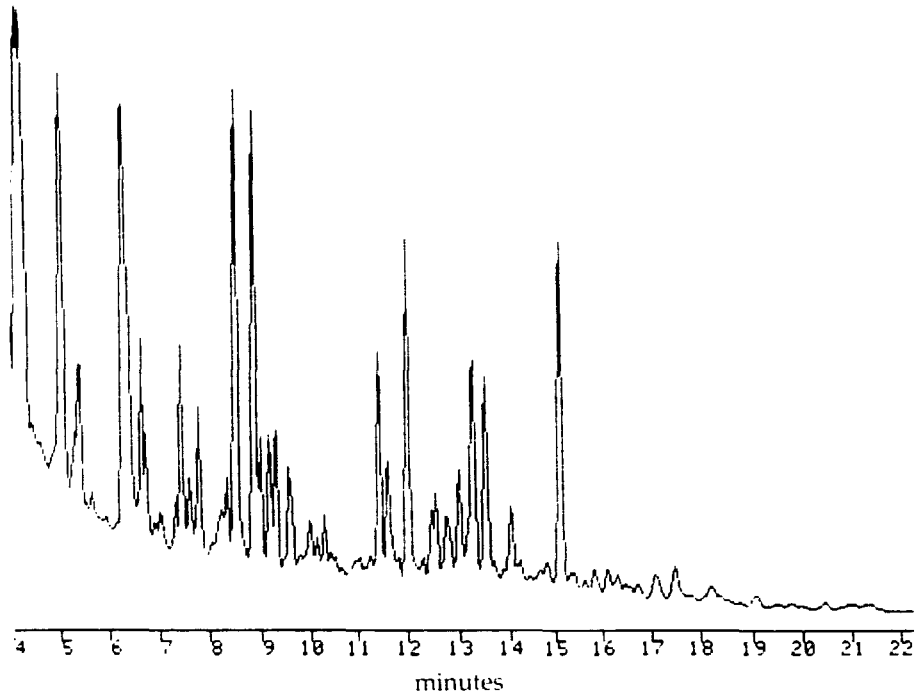

T_R	COMPOUND
4.2	benzaldehyde
5.1	1-methyl-1h-indene
5.4	acetophenone
6.3	azulene
6.7	naphthalene
7.5	1-methylnaphthalene
7.6	dioctyladipate
7.9	2-methylnaphthalene
8.4	2,6-ditertiary butyl-p-cresol
8.5	methyl-1-indene
8.9	biphenyl
9.2	2-methylbiphenyl
9.3	cinnamaldehyde
9.6	biphenylene
10.3	0-xylene
11.5	diphenylmethane
12.0	fluorene
12.6	5-phenyl-1,3-cyclohexadiene
12.8	benzoic acid
13.0	diphenylethylene, 1,1-diphenylethene
13.6	9,10-dihydrophenanthrene
14.0	1,2 diphenylethylene
15.1	phenanthrene, anthracene
17.1	3-phenylcinnoline
17.5	2-phenylnaphthalene
24.7	2-benzylnaphthalene
25.5	2-methylpyrene
33.1	2,3,4-tetrahydrotriphenylene

Figure B4. Pyrolyzate virgin PVC generated in air in tube pyrolyzer during the main region of degradation separated on Carbowax-20M capillary column.

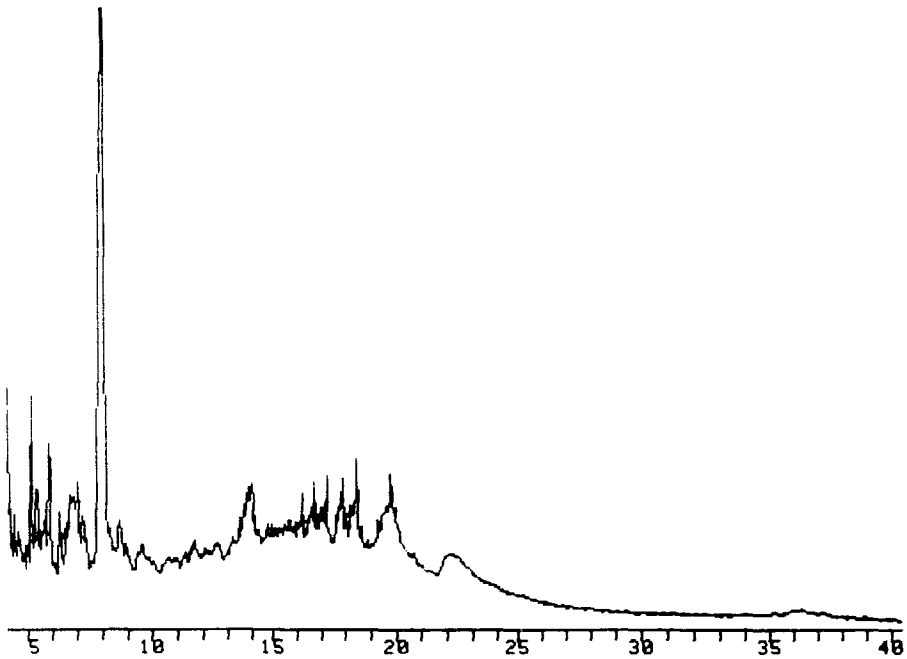

T_R	COMPOUND
4.2	o-chlorotoluene
5.2	phenylcyclopropane
5.4	o-chloroethylbenzene
8.1	chloroprene dimer
8.8	5,6-benzobicyclo(2,2,1) hept-2-ene
17.9	4,4'-dimethoxystilbene

Figure B5. Pyrolyzate of virgin Neoprene generated during the main phase of pyrolysis and separated on SE-54.

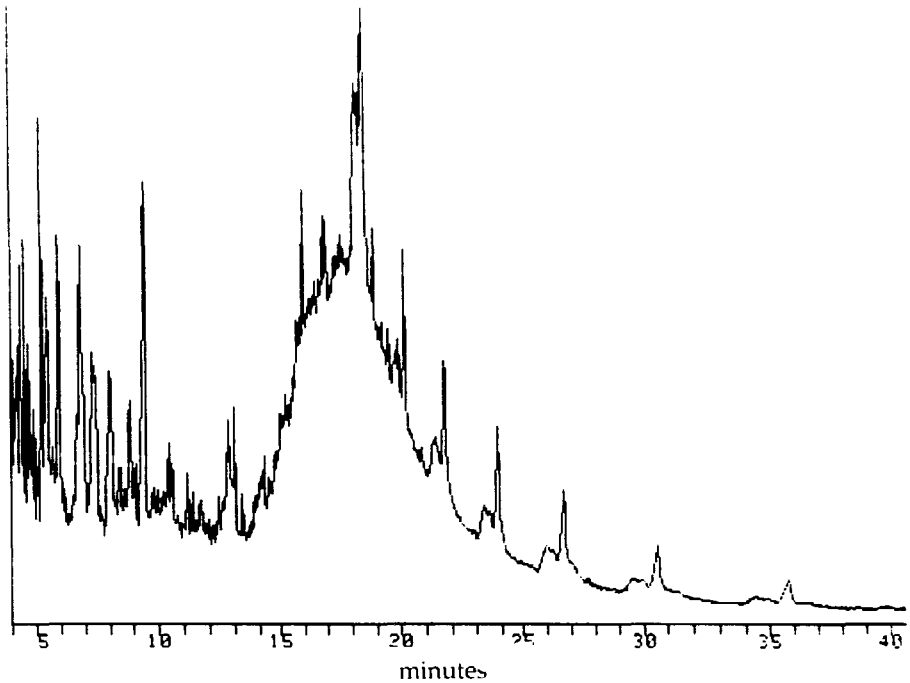

T_R	COMPOUND
4.4	1,2 dimethylcyclohexene
4.6	2-n-hexyl-n-methyl pyrolidine
4.8	propylbenzene
5.3	3-chlorocyclohexene and methylstyrene
5.5	o-chloroethylbenzene
6.0	x-chloro-o-xylene
6.9	methylallylbenzene
8.9	1-methylnaphthalene and di-n-amylphthalate
9.5	3,3,6-trimethyl-1-indanone
12.8	1-allylnaphthalene
18.6	phenyl-B-naphthylamine
20.2	bis (3,5,5-trimethyl hexyl) adipate
21.8	di-nor-dodecyl ether
23.9	x-dodecylcyclohexanol
26.8	squalene

Figure B6. Pyrolyzate of Neoprene 007 generated during the main phase of pyrolysis and separated on SE-54.

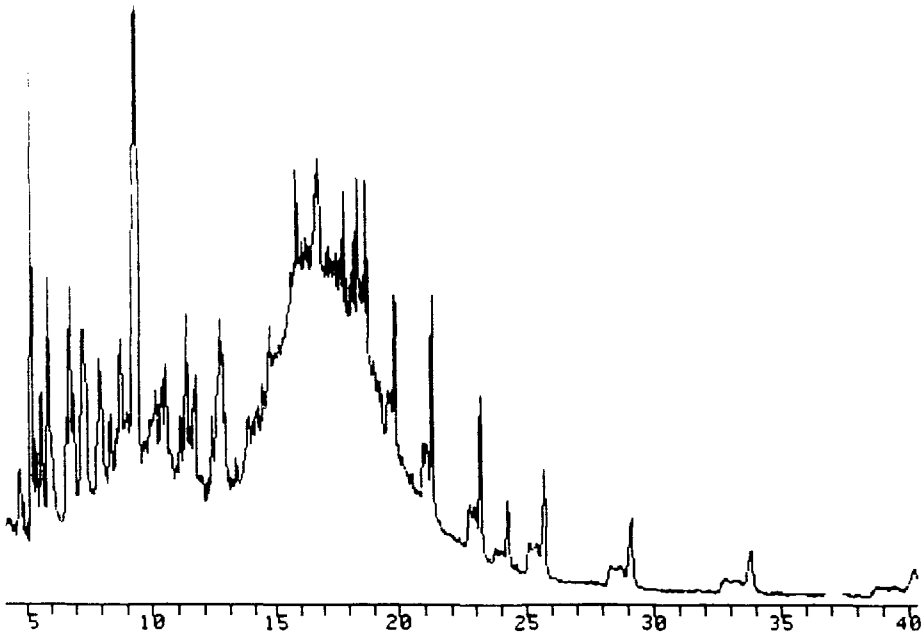

Γ_R	COMPOUND
5.2	o-methylstyrene
5.6	o-cresol
5.9	p-cresol
6.8	5-methyl indan
7.3	naphthalene
8.8	1-methyl naphthalene
9.5	7-hydroxy-5,6-benznorbornene
	1,5,8-trimethyl-1,2,3,4-tetrahydronaphthalene
11.7	4-methyl-2,6-di-tert-butylphenol
12.7	1-allylnaphthalene
16.8	7-ethylbenz(A)anthracene
19.9	squalene
24.3	dioctylphthalate

Figure B7. Pyrolyzate of Neoprene 435 generated during the main phase of decomposition and separated on SE-54 capillary column.

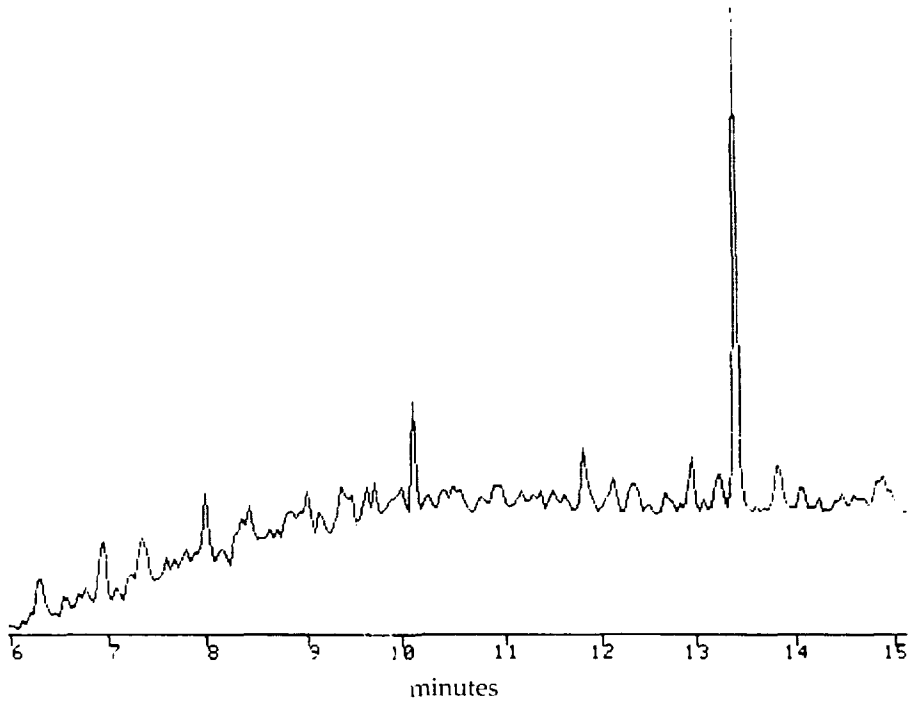

T_R	COMPOUND
6.0	17-pentatriacontene
6.4	hexadecanol
7.1	2,3,4-trimethyl-4,5-methylene-tetradecane
8.1	2-(2-octyldecyl)-cis-bicyclo-(3,3)octane
10.2	2,4-dimethylquinoline
11.9	3-ethyl-5-(2-ethylbutyl)-octadecane
13.0	2-linoleyl-1,3-diac tin
13.5	xanthane

Figure B8. Pyrolyzate from rubber-12 generated in TGA furnace during the main phase of degradation and separated on Carbowax-20M capillary column.

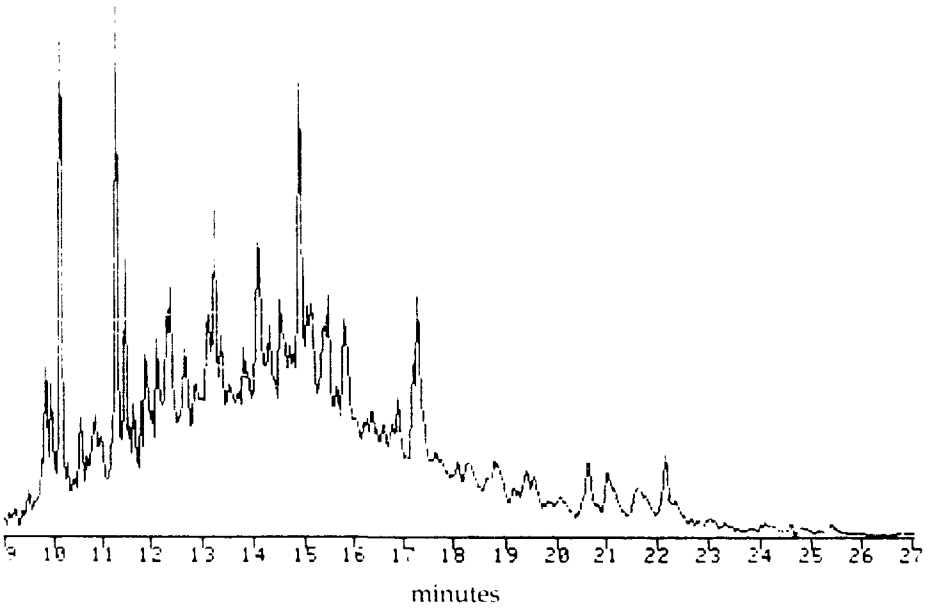

T_R	COMPOUND
9.9	3-methylbiphenyl
10.2	2,4-dimethylquinoline
11.4	1,3-diphenylpropane
11.6	2,4'-dimethylbiphenyl
11.9	phthlide
12.0	alpha-hydroxy-toluic acid
12.5	2-methyltridecane
13.3	heptacosane
14.2	nor-pentacosane
15.0	n-hexatriacontane
15.6	nonylphenol
15.8	3-ethyl-5(2-ethylbutyl) octadecane
17.3	palmitic acid
20.7	triphenyl
22.2	dioctylphthalate

Figure B9. Pyrolyzate from rubber-138 generated in TGA furnace during the main phase of degradation and separated on Carbowax-20M capillary column.

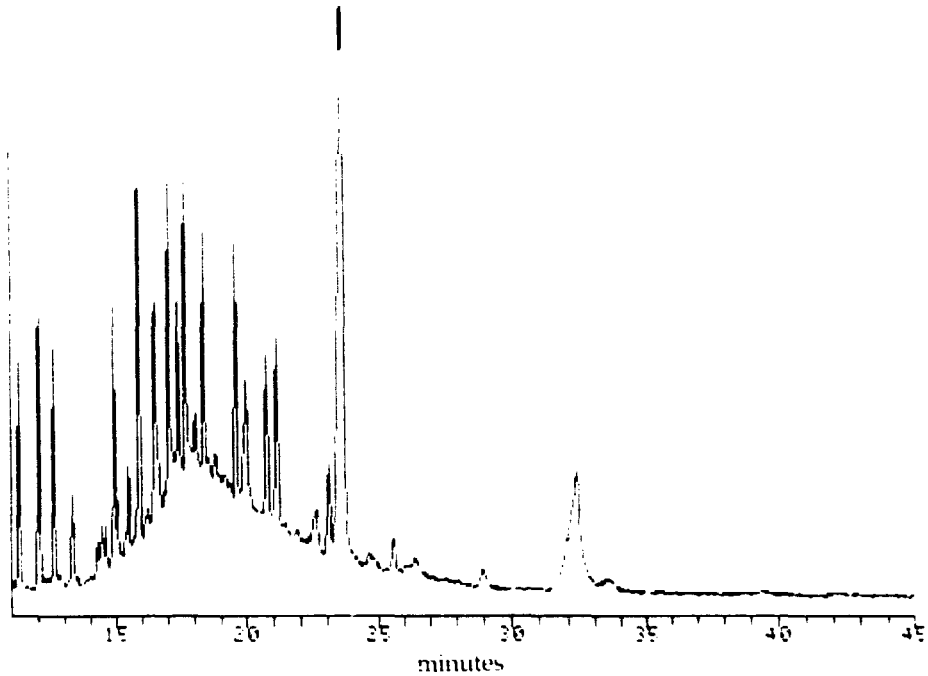

T_R	COMPOUND
12.2	nor-decyl thiol norbutyrate
12.8	tri-n-nbutyl phosphate
13.5	2,5-dihydroxybenzoic acid
15.1	butyl-0 -phthalate
15.7	nor-triocontane
16.0	butyl(butoxycarbonyl)methyl phthalate
16.7	palmitic acid
17.3	1,10-bis(1-decahydronaphthyl)decane
17.6	11-N-decyldocosane
18.6	octadecane
19.8	n-tricosane
20.3	n-butyl-0-phthalate
21.0	dioctyl adipate
21.4	hexatriacontane
23.8	dioctylphthalate
32.4	tetracosanol

Figure B10. Thermal degradation products of rubber-138 generated in the large-scale test cell and separated on SE-30 fused silica capillary column.

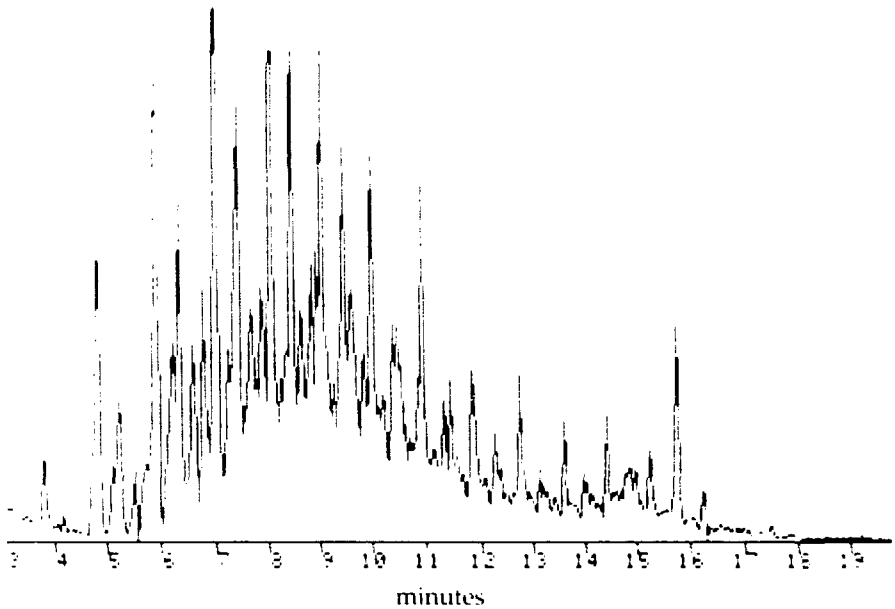

I_R	COMPOUND
3.8	1-hexadecene
4.9	1-octadecene
5.3	1,12-tridecadiene
6.0	heptacosanol
6.4	linoleic acid
6.6	oleic acid
6.8	1-dotriacontanol
7.1	1,12- tridecadiene
7.7	2-hexanal
7.9	1-undecyne
8.1	1-dotriacontanol
8.5	oleyl alcohol
9.5	2-cis-9-octadecenyloxy ethanol
10.1	octadecanol-1
10.5	2D-methyl-1-octen-7-ol
11.0	1-docosene
11.9	1,7-dicyclopentyl-4-(3prim-cyclopentypropyl)-heptane
12.8	hexadecanol
13.6	heptadecanyl acetate
15.3	1-docosanol

Figure B11. Pyrolyzate of virgin polyethylene generated during the main phase of degradation and separated on Carbowax-20M.

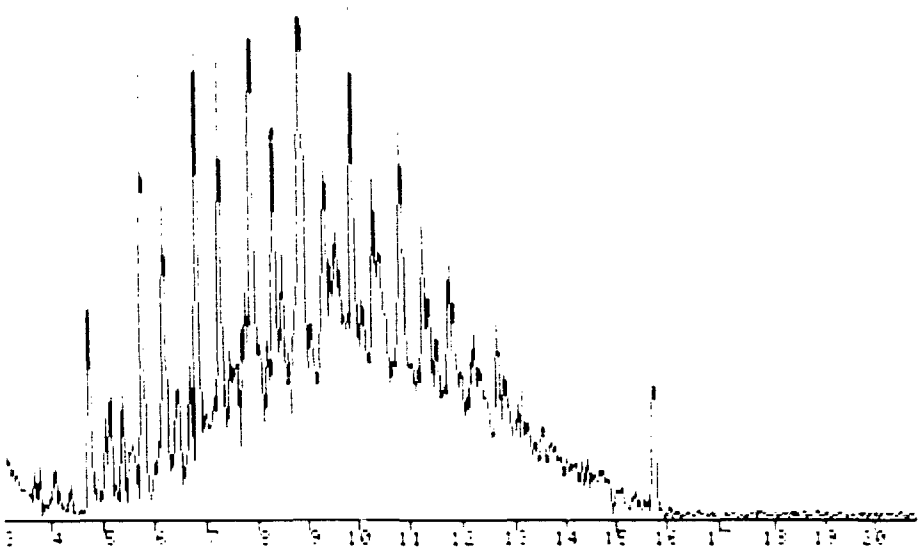

T_R	COMPOUND
4.7	hexadecanol-1
5.9	1-hexadecene
6.3	1,4-dicyclopentylbutane
6.9	2L-methyl-dodecanol-1
7.4	tridecanol
8.0	octadecanol-1
8.4	octadecanal
9.0	tetradecanol
9.4	oleyl alcohol
10.9	heptadecanyl acetate
11.3	1-N-amylcyclohexene-1
12.7	hexadecanol

Figure B12. Pyrolyzate from polyethylene 77 generated during the main phase of pyrolysis in a TGA furnace and separated on Carbowax-20M column.

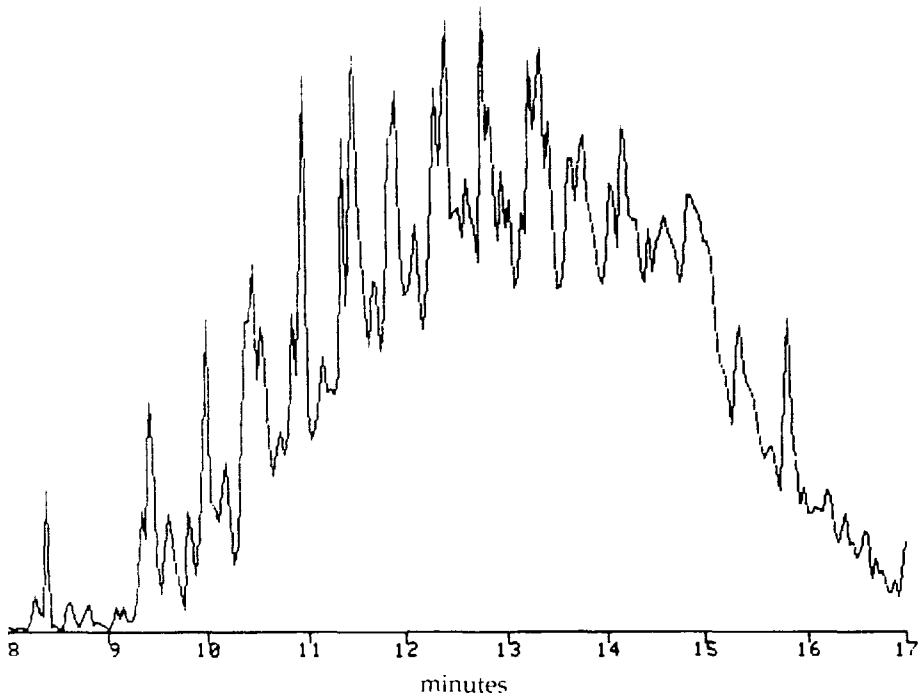

T_R	COMPOUND
8.5	cis-hexahydroindane
9.5	tricyclo (5,2,1,0:2,6:)decan-3-ol
10.1	1,12-tridecadiene
10.5	spiro (5,6) dodecane
11.1	methyl-9,12-hexadecadienoate
11.5	methyl C_9C_{15} octadecadienoate
12.0	1-dodecyne
12.5	thujyl alcohol
12.8	methyl linoleate
13.9	7,7-dimethyl-3-methylen-bicyclo-(3,1,1)heptane
14.2	methyl heptadeca-5,8,11-trienoate
15.0	di-n-butylphthalate
15.4	1,4-dihydroxy-2(1H)-quinolone

Figure B13. **Pyrolyzate of polyethylene-95 generated in TGA furnace during the main phase of degradation and separated on Carbowax-20M capillary column.**

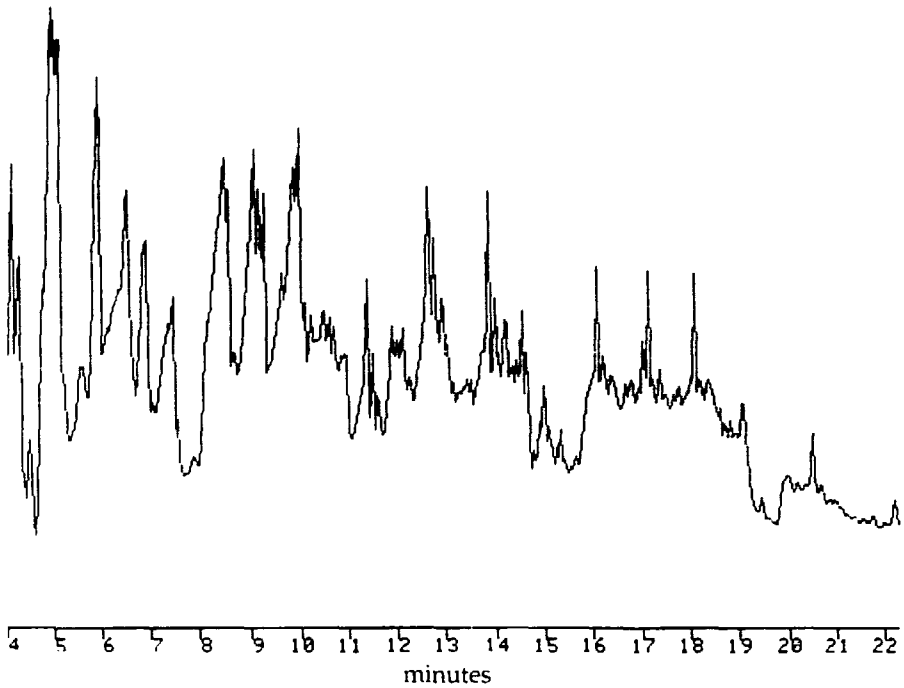

T_R	COMPOUND
4.6	1,2,4-trimethylbenzene
6.6	trans-3-methyl-2-[illegible]enyl methyl ether
9.3	hexahydrofarnesol
12.0	4-ethyldicyclohexylmethane
12.1	ascaridole

Figure B14. Pyrolyzate from virgin polypropylene generated in TGA furnace during the main phase of degradation and separated on Carbowax-20M capillary column.

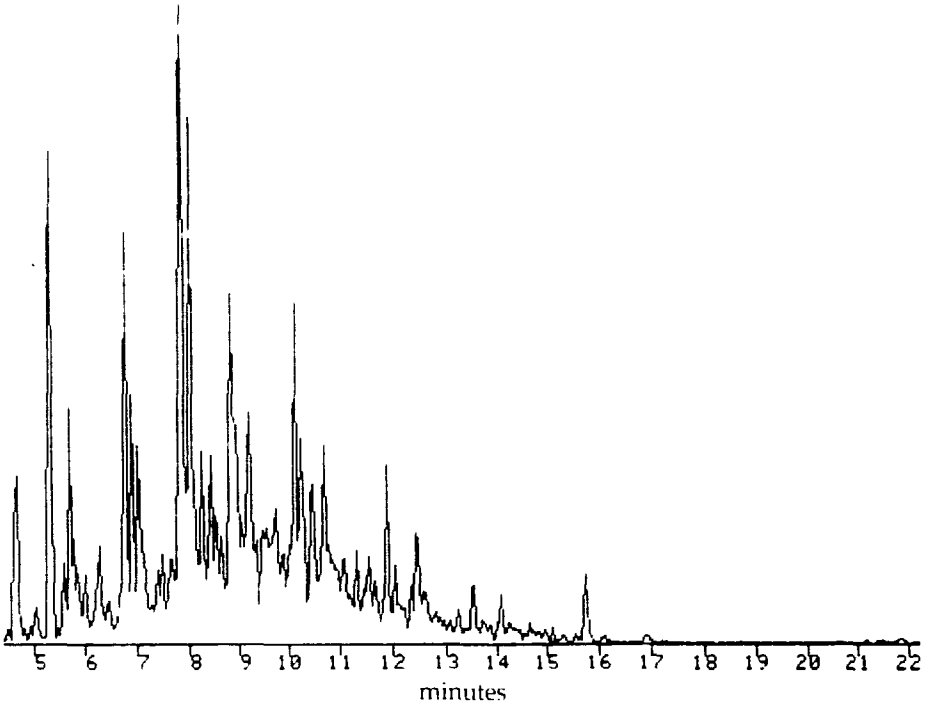

T_R	COMPOUND
4.7	trans-3,4-dimethyl-3-hexen-2-one
5.4	4-methylpent-3-enoic acid
5.8	2-t-butylcyclobutanone
6.8	isobutylcyclopentane
7.1	methyl tert butyl acrolein
7.9	6-methyl-5-hepten-2-one
8.0	1,3-diaminocyclohexane
8.3	5-hexen-2-one
8.9	4-methyl-pent-4-en-2-one
9.3	nona-3-ene-2-one
10.2	3,4-epoxy-2-hexanone
10.5	2,4-xylenol
10.8	hexadecanol
11.9	cis-2,5-dimethyl-tetrahydrofuran
12.5	2,5-dimethyl-2-hexene

Figure B15. Pyrolyzate from propylene-90 generated in TGA furnace during the main phase of degradation and separated on Carbowax-20M capillary column.

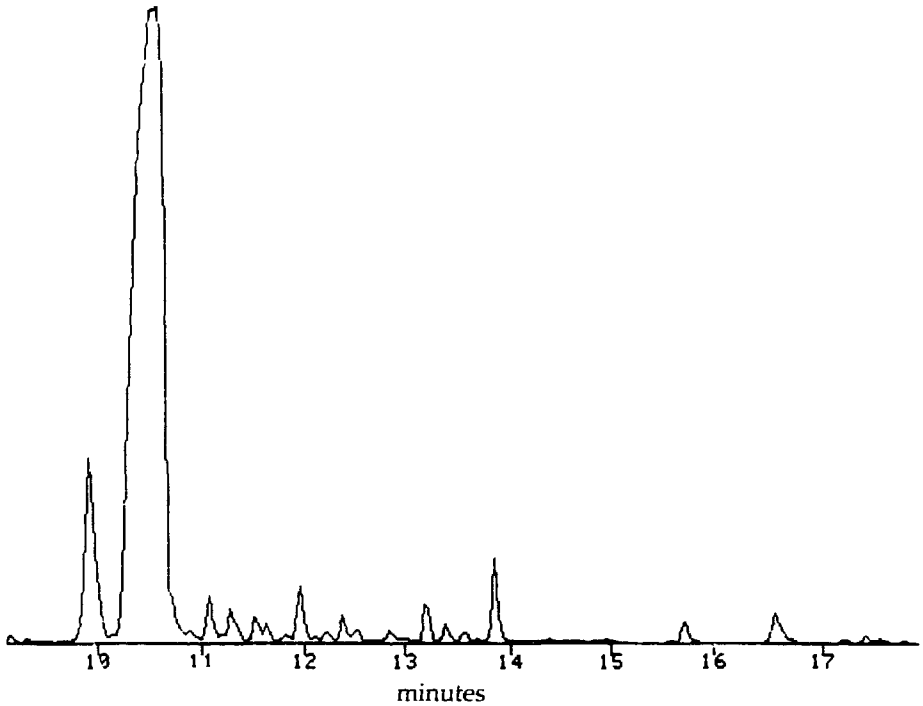

T_R	COMPOUND
10.0	2,3-dimethylpyrimide-4-one
10.6	1-hexene
11.1	5-methyl-2-pyridone
11.3	4,6,6-trimethyl-δ-valerolactone
12.0	e-caprolactam
13.9	1-methylimidazole
15.7	1-methylbutyl isobutyrate
16.6	ethyl-(1', 3'-dimethlybutyl)amine
21.1	methyl-succinic acid
22.6	cyclododecane

Figure B16. Pyrolyzate of nylon insulation generated in TGA furnace and separated on Carbowax-20M capillary column.

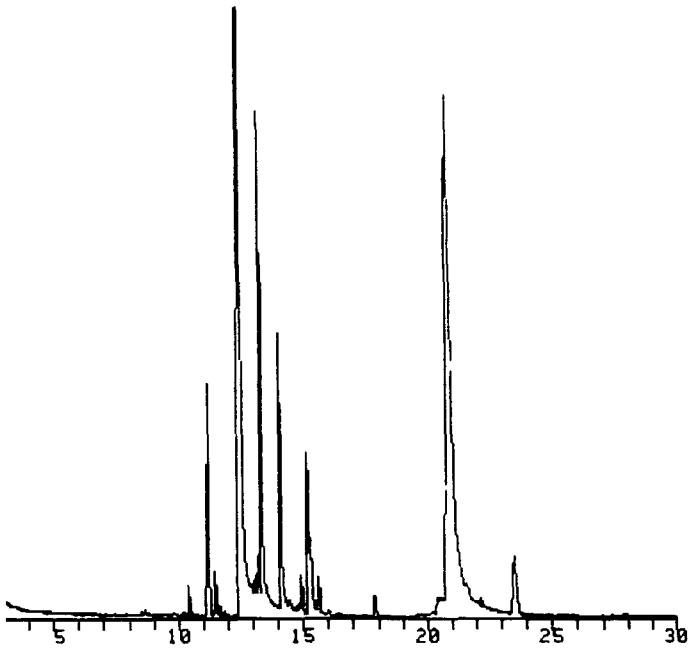

T_R	COMPOUND
12.5	benzoic acid
13.4	methyl benzoate
14.2	ethyl benzoate
15.2	isobutyl cinnamate
20.9	isopropyl phthalate
23.6	phenyl benzoate

Figure B17. Pyrolyzate from virgin mylar generated in TGA furnace during the main phase of degradation and separation on carbowax 20M column.

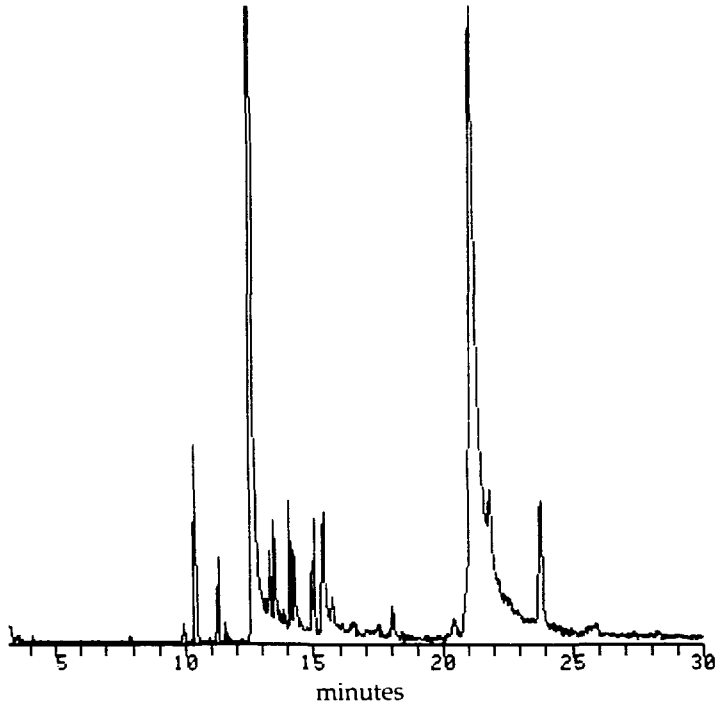

T_R	COMPOUND
10.5	caprolactam
12.6	benzoic acid
13.5	methyl benzoate
15.4	isobutyl cinnamate
21.2	isopropyl phthalate
23.9	phenyl benzoate

Figure B18. Pyrolyzate from mylar #139 generated in TGA furnace during the main phase of degradation and separation on Carbowax 20M column.